National Renewable Energy Laboratory
A national laboratory of the U.S. Department of Energy
Office of Energy Efficiency & Renewable Energy
Innovation for Our Energy Future

Ultra-High Efficiency Multijunction Cell and Receiver Module, Phase 1B: High Performance PV Exploring and Accelerating Ultimate Pathways

Final Subcontract Report
13 May 2005 – 10 December 2008

R. R. King
Spectrolab, Inc.
Sylmar, California

Subcontract Report
NREL/SR-520-47602
March 2010

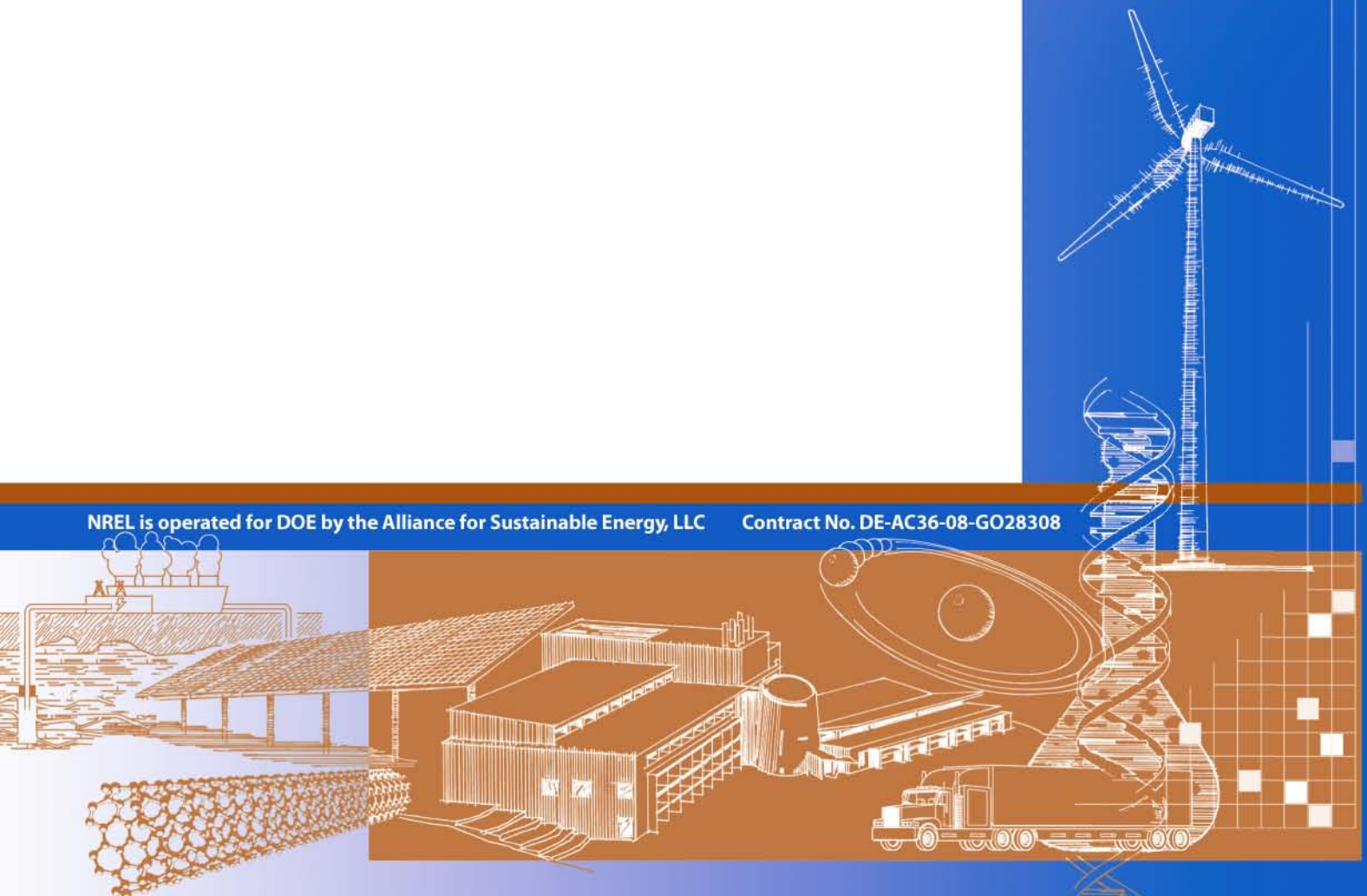

NREL is operated for DOE by the Alliance for Sustainable Energy, LLC Contract No. DE-AC36-08-GO28308

Ultra-High Efficiency Multijunction Cell and Receiver Module, Phase 1B: High Performance PV Exploring and Accelerating Ultimate Pathways

Final Subcontract Report
13 May 2005 – 10 December 2008

R. R. King
Spectrolab, Inc.
Sylmar, California

NREL Technical Monitor: F. Eddy
Prepared under Subcontract No. ZAT-4-33624-12

Subcontract Report
NREL/SR-520-47602
March 2010

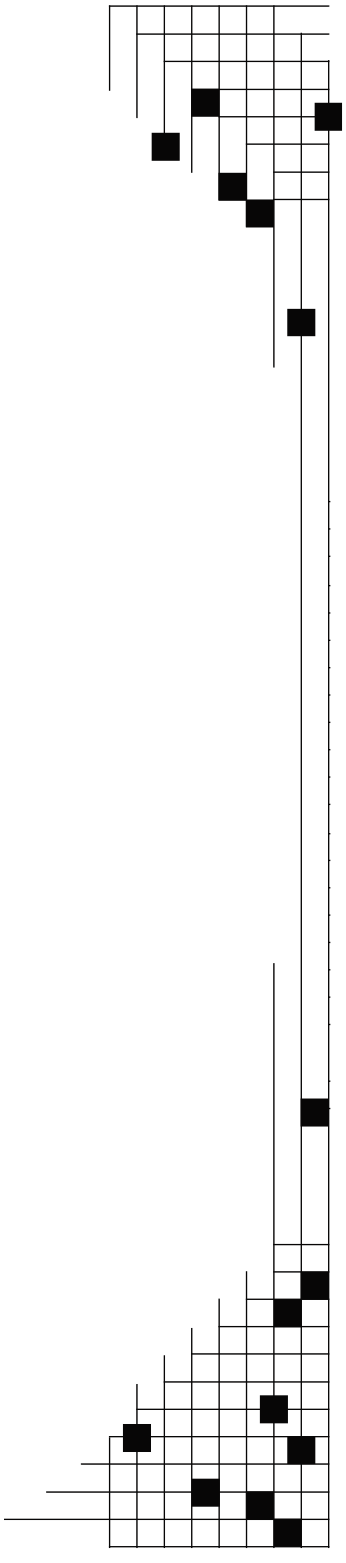

National Renewable Energy Laboratory
1617 Cole Boulevard, Golden, Colorado 80401-3393
303-275-3000 • www.nrel.gov

NREL is a national laboratory of the U.S. Department of Energy
Office of Energy Efficiency and Renewable Energy
Operated by the Alliance for Sustainable Energy, LLC

Contract No. DE-AC36-08-GO28308

Table of Contents

1 Introduction 1

1.1 Program Overview 1

2 Concentrator Cell Technology Development 3

2.0 Introduction 3
2.1 Cell Development Progress Report 1 7
2.2 Cell Development Progress Report 2 14
2.3 Cell Development Progress Report 3 19
2.4 Cell Development Progress Report 4 21
2.5 Cell Development Progress Report 5 26
2.6 Cell Development Progress Report 6 28
2.7 Cell Development Progress Report 7 32
2.8 Cell Development Progress Report 8 34
2.9 Cell Development Progress Report 9 38
2.10 Cell Development Progress Report 10 47
2.11 Cell Development Progress Report 11 56
2.12 Cell Development Progress Report 12 57
2.13 Cell Development Progress Report 13 61
2.14 Cell Development Progress Report 14 64
2.15 Cell Development Progress Report 15 81

3 Receiver Package Technology Development 103

3.0 Introduction 103
3.1 Receiver Development Progress Reports 1-4 104
3.2 Receiver Development Progress Reports 5-8 114

4 Summary 117

5 References 121

Acknowledgements 123

1 Introduction

1.1 Program Overview

The High Performance Photovoltaics (HiPerf PV) research program at Spectrolab spanned 7 years, beginning in Aug. 2001 and ending in Dec. 2008, and was the main pathfinder research program for developing high-efficiency terrestrial concentrator solar cells and receivers at Spectrolab for many years when the efficiency and cost potential of these new types of cells were far from certain. In this time period, at the beginning of concentrator photovoltaics (CPV) development at Spectrolab, the CPV cell market did not exist, there were no CPV cell products, and the promise of CPV technology was just a vision shared by a few at Spectrolab and the National Renewable Energy Laboratory (NREL). The funding of the NREL HiPerf PV program at Spectrolab by NREL and the U.S. Department of Energy (DOE) was critical to the development of this nascent technology at a crucial time. Multijunction III-V solar cells are now by far the dominant type of cell used in terrestrial concentrator photovoltaics, due to the cost benefits conferred by their very high efficiencies. Indeed, there has been an explosion of interest and financial investment in CPV, and a proliferation of CPV system manufacturers in recent years, in large part enabled by the emergence of the high-efficiency multijunction concentrator cells that were the subject of NREL HiPerf PV program at Spectrolab.

There are two primary objectives in concentrator photovoltaics research and development that the NREL/Spectrolab HiPerf PV program was designed to achieve. The first objective is to develop ultra-high efficiency concentrator multijunction cells, in recognition of the tremendous leveraging effect that cell efficiency has on all area-related costs of the overall concentrator PV system. The second objective is to develop a robust concentrator cell receiver package, enabling the reliable operation of concentrator cells in high concentration modules.

1.2 Program Administration

The NREL/Spectrolab HiPerf PV program was divided into two phases: Phase 1A, from 2001 to 2004 (Subcontract NAT-1-30620-01), and Phase 1B, from 5/13/2005 to 12/10/2008 (Subcontract ZAT-4-33624-12). Phase 1A, entitled "High Efficiency, Low Cost III-V Concentrator PV Cell & Receiver Module," was summarized in an earlier final report at the end of that phase of work. Phase 1B (Exploring and Accelerating Ultimate Pathways), entitled "Ultra-High-Efficiency Multijunction Cell and Receiver Module," is summarized in this final report.

For the first parts of the program, from 2001 to 2006, the HiPerf PV program at Spectrolab had two co-Principal Investigators, reflecting the dual emphasis on high-efficiency concentrator cell development, and on robust concentrator receiver package development. Richard King was co-PI responsible for high-efficiency cell development, and Raed Sherif was co-PI in charge of concentrator receiver package development. Beginning in 2006 to the end of the program in 2008, the emphasis of the program shifted to focus on cell development, so the program had only one PI in that time frame (R. King).

Raed Sherif was Program Manager, handling administrative and programmatic aspects of the HiPerf PV program from 2001 to 2006, and Richard King was Program Manager of the HiPerf PV program from 2006 to the program end in 2008. Spectrolab would like to thank Martha Symko-Davies, Bob McConnell, and Fannie Posey-Eddy at NREL for their leadership and encouragement as NREL Technical Monitors over the course of the HiPerf PV program at Spectrolab. A special acknowledgement is goes out to Martha Symko-Davies for her vision and energy in her role to launch the HiPerf PV program, and to make that high-efficiency concentrator PV research was an important part of the NREL HiPerf PV research portfolio. The organization chart at the end of the HiPerf PV program is shown in Fig. 1.1 below.

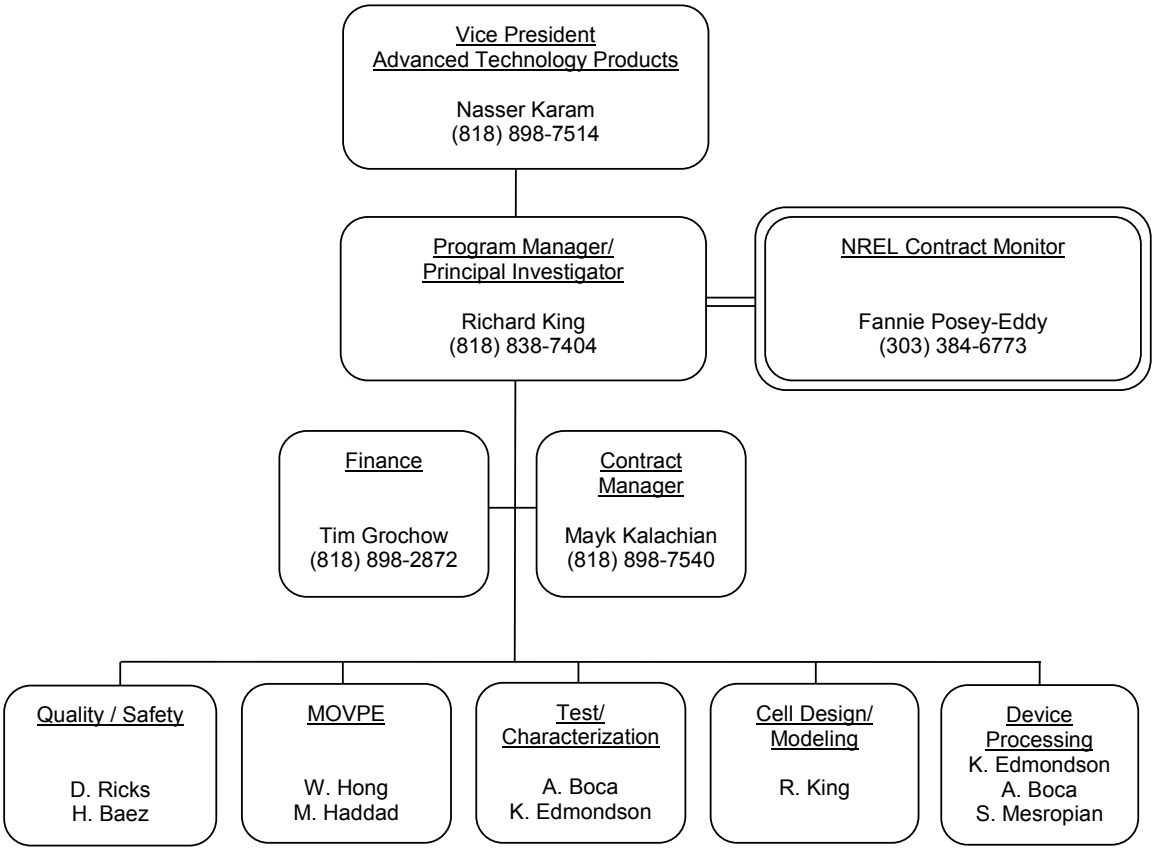

Fig. 1.1 Organization chart for the NREL/Spectrolab HiPerf PV program as of the end of the program.

2 Concentrator Cell Technology Development

2.0 Introduction

Advances made in the science and technology of terrestrial concentrator solar cells and receivers in the NREL/Spectrolab HiPerf PV program are divided in two areas in this report: Concentrator Cell Technology Development, and Receiver Package Technology Development. In each section, the technical development made is described in chronological order, in a summary of the technical sections of progress reports from the beginning to end of Phase 1B of the program: "Ultra-High-Efficiency Multijunction Cell and Receiver Module." A full list of references is given at the end of the report, and for convenience, the references cited in each section are also listed at the end of the section

Some of the key results in terrestrial concentrator cell technology in this program include:

A major program milestone, demonstration of solar cells with 41% efficiency, was met with the attainment of 40.7% conversion efficiency in a Spectrolab experimental metamorphic terrestrial concentrator cell in 2006. As described in King et al., *Appl. Phys. Lett.*, 2007 [1], this was the first solar cell of any type to reach over the 40% efficiency milestone. This efficiency result was independently confirmed as a world record by NREL.

Spectrolab received the R&D 100 Award for 2007, for its development of the metamorphic multijunction solar cell described in the last paragraph with up to 40.7% efficiency, in the High Performance Photovoltaics (HiPerf PV) program funded by NREL. NREL kindly nominated Spectrolab for the award.

Near the same time as the 40.7% metamorphic multijunction cell result was achieved, an experimental lattice-matched 3-junction terrestrial concentrator cell with 40.1% efficiency [1] was also produced by Spectrolab in the HiPerf PV program, a record for lattice-matched photovoltaic cells. This 40.1%-efficient lattice matched cell result was independently confirmed at NREL. Thus, although metamorphic multijunction cells have the highest efficiencies to date, lattice-matched cells are close behind. Another experimental metamorphic 3-junction cell produced by Spectrolab also reached 40.1% efficiency [18], as independently confirmed at NREL.

Prior to the 40.7% metamorphic and 40.1% lattice-matched record multijunction cell efficiencies above, Spectrolab achieved record cell efficiencies with 39.0% lattice-matched and 38.8% metamorphic 3-junction concentrator cells [4] in the NREL HiPerf PV program, which in turn broke the previous record efficiencies, also held by Spectrolab and established in the HiPerf PV program, for 37.3% lattice-matched and 36.9% metamorphic concentrator cells [2], which broke the still earlier Spectrolab record efficiency of 35.2% for a lattice-matched terrestrial concentrator cell [3]. Thus Spectrolab's work in the NREL HiPerf PV program was responsible for a high rate of advancement of the state-of-the-art in photovoltaic cell efficiency, sustained over many years, leading to the dominance of III-V multijunction cell technology in concentrator PV systems today, and contributing significantly to the rapid rise of the concentrator PV industry in recent years.

The efficiency benefits of high-band-gap, disordered GaInP top cells and wide-band-gap tunnel junctions under the terrestrial solar spectrum at high concentration were developed and demonstrated by Spectrolab in Phase 1A of the HiPerf PV program, for both metamorphic and lattice-matched 3-junction terrestrial concentrator cells, enabling the efficiency advances described above.

A large range of concentrator cell parameters were evaluated experimentally in multiple cell builds, including:

- differing types of wide-band-gap tunnel junctions
- different top subcell band gaps, and GaInP top subcell group-III sublattice disordering
- amount of current mismatch or J-ratio
- amount of lattice mismatch in metamorphic cells
- layer structure to reduce dislocation density in active cell regions resulting from the metamorphic buffer
- layer structure to result in high peak tunneling current density in tunnel junctions for high light intensities
- growth parameters in the metamorphic buffer layers
- subcell doping levels and doping profiles
- AR coating type
- gridline spacing and grid configuration
- gridline width and gridline definition process
- concentrator cell size, and
- other semiconductor device design parameters contributing to the high experimental concentrator cell efficiencies achieved in the program, and helping to establish high-efficiency terrestrial concentrator cell processes for mass production, for implementation in commercial concentrator PV systems.

A general multijunction solar cell modeling program was developed to calculate efficiency of cells with up to 10 subcells as a function of subcell band gap, concentration ratio, cell temperature, and other parameters [7]. The ideal efficiency limited by radiative recombination can be calculated, as well as efficiency including the effects of series resistance and metal grid shadowing, and the efficiency normalized to experimental concentrator cell results.

Four-junction (4J) terrestrial concentrator cells were modeled to determine the predicted efficiency as a function of subcell band gap, and 4J GaInP/ AlGaInAs/ GaInAs/ Ge concentrator cells were built and tested with efficiencies up to 35.7% in early prototype cells [7].

The energy production values of 3J, 4J, 5J, and 6J terrestrial concentrator cells were modeled and contrasted for varying sun angle over the course of the day, and for varying current balance among subcells in high-voltage, low-current device designs [7].

A large cell build was carried out incorporating high-efficiency cell structures (HECS) in lattice-matched as well as metamorphic multijunction cells, comparing the effects of HECS and metamorphic materials in high-efficiency terrestrial concentrator 3- and 4-junction cells.

Upright metamorphic GaInAs subcells were grown and characterized in terms of their band-gap-voltage offset, $(E_g/q) - V_{oc}$, with lattice mismatch to the Ge substrate up to 1.6% for 23%-In GaInAs with 1.1-eV band gap.

Inverted metamorphic (IMM) GaInAs subcells were grown and characterized in terms of band-gap-voltage offset, and by cathodoluminescence and electron-beam-induced current (EBIC) measurements, out to a high lattice mismatch of 3.1% with respect to Ge for 44%-In GaInAs, with a band gap of 0.84 eV [17]. The dislocation density and recombination activity at a single dislocation was characterized as a function of subcell composition and lattice mismatch [17].

Inverted lattice-matched (ILM) cells such as inverted GaInP and inverted 1%-In GaInAs cells were grown and characterized, for incorporation into inverted metamorphic terrestrial concentrator multijunction cells.

Inverted metamorphic (IMM) GaInP/ 1%-In GaInAs/ 30%-In GaInAs 3-junction terrestrial concentrator cells were grown and processed, with tunnel junctions working well at over 80 suns for early prototype devices.

Single-junction component cells of high-efficiency 3-junction concentrator cells were built and tested at Spectrolab, representing a wide range of J-ratios for optimizing performance under fresnel lenses in actual field operating conditions. These single-junction component cells (also called "isotype" cells) were delivered June 19, 2008, for field testing at Amonix in their fresnel lens concentrator system, satisfying the deliverable associated with Task 30 of the revised statement of work for Spectrolab's HiPerf PV program with NREL.

High-efficiency 3-junction terrestrial concentrator cells were built and tested at Spectrolab, targeting improved efficiency and energy production under real-world operating conditions in the field in fresnel lens concentrator PV systems. Fifty (50) of these cells were delivered August 21, 2008, for field testing at Amonix in their fresnel lens concentrator system, satisfying the deliverable D3.7 associated with Task 31 of the revised statement of work for Spectrolab's HiPerf PV program with NREL. These high-efficiency Spectrolab cells have since been incorporated into a high-efficiency fresnel lens demonstration module by Amonix, for testing at NREL.

References – Section 2.0

[1] R. R. King, D. C. Law, K. M. Edmondson, C. M. Fetzer, G. S. Kinsey, H. Yoon, R. A. Sherif, and N. H. Karam, "40% efficient metamorphic GaInP / GaInAs / Ge multijunction solar cells," *Appl. Phys. Lett.*, Vol. 90, No. 18, 183516, 4 May 2007.

[2] R. R. King, C. M. Fetzer, K. M. Edmondson, D. C. Law, P. C. Colter, H. L. Cotal, R. A. Sherif, H. Yoon, T. Isshiki, D. D. Krut, G. S. Kinsey, J. H. Ermer, Sarah Kurtz, T. Moriarty, J. Kiehl, K. Emery, W. K. Metzger, R. K. Ahrenkiel, and N. H. Karam, "Metamorphic III-V Materials, Sublattice Disorder, and Multijunction Solar Cell Approaches with Over 37% Efficiency," *Proc. 19th European Photovoltaic*

Solar Energy Conference, Paris, France, June 7-11, 2004 (WIP-Munich, Munich, Germany, 2004), ISBN 3-936-338-14-0, ISBN 88-89407-02-6, pp. 3587-93.

[3] R. R. King, C. M. Fetzer, P. C. Colter, K. M. Edmondson, D. C. Law, A. P. Stavrides, H. Yoon, G. S. Kinsey, H. L. Cotal, J. H. Ermer, R. A. Sherif, K. Emery, W. Metzger, R. K. Ahrenkiel, and N. H. Karam, "Lattice-Matched and Metamorphic GaInP/ GaInAs/ Ge Concentrator Solar Cells," *Proc. of the 3rd World Conference on Photovoltaic Energy Conversion*, Osaka, Japan, May 11-18, 2003, pp. 622-625.

[4] R. R. King, D. C. Law, C. M. Fetzer, R. A. Sherif, K. M. Edmondson, S. Kurtz, G. S. Kinsey, H. L. Cotal, D. D. Krut, J. H. Ermer, and N. H. Karam, "Pathways to 40%-Efficient Concentrator Photovoltaics," *Proc. 20th European Photovoltaic Solar Energy Conf.*, Barcelona, Spain, June 6-10, 2005, pp. 118-123.

[7] R. R. King, R. A. Sherif, D. C. Law, J. T. Yen, M. Haddad, C. M. Fetzer, K. M. Edmondson, G. S. Kinsey, H. Yoon, M. Joshi, S. Mesropian, H. L. Cotal, D. D. Krut, J. H. Ermer, and N. H. Karam, "New Horizons in III-V Multijunction Terrestrial Concentrator Cell Research," *Proc. 21st European Photovoltaic Solar Energy Conference and Exhibition*, Dresden, Germany, Sep. 4-8, 2006 (Munich, WIP-Renewable Energies, 2006) (ISBN: 3-936338-20-5), pp. 124-128.

[18] R. R. King, D. C. Law, K. M. Edmondson, C. M. Fetzer, G. S. Kinsey, H. Yoon, R. A. Sherif, D. D. Krut, J. H. Ermer, P. Hebert, P. Pien, and N. H. Karam, "Multijunction Solar Cells with Over 40% Efficiency and Future Directions in Concentrator PV," *Proc. 22nd European Photovoltaic Solar Energy Conference*, Milan, Italy, Sep. 3-7, 2007, pp. 11-15.

2.1 Cell Development Progress Report 1

In the area of cell development, three major approaches were pursued: lattice-matched (LM), metamorphic (MM), and mechanically stacked (MS). Development over the first quarter included some work in all three areas. The majority of the epitaxial research occurred in the metamorphic area, while there has been some work initiated at the cell level for the other two areas. This section will discuss the lattice-matched and metamorphic monolithic approaches. Further discussion of the mechanically stacked approach is given in sections 2.1.3 and 2.1.4.

2.1.1 Lattice-Matched Cell Development

In lattice-matched device work, technologies developed in the NREL HiPerf PV program and others allow a terrestrial concentrator 3-junction cell to be achieved with a high-bandgap (~1.9-eV) GaInP top subcell, lattice-matched to the $Ga_{0.99}In_{0.01}As$ middle subcell. Earlier cell builds in the NREL HiPerf PV program, showed the clear advantage of a high-bandgap (hi-Eg) top subcell in terrestrial concentrator GaInP/ GaInAs/ Ge 3-junction cells under the terrestrial solar spectrum. Examples of this high-efficiency technology include the record 37.3%-efficient lattice-matched 3-junction cell [2] at 175 suns (17.5 W/cm^2) concentration under the standard AM1.5D, low-AOD solar spectrum for concentrators, and the record 32.0%-efficient lattice-matched one-sun cell [3] with 4 cm^2 area, under the standard AM1.5G spectrum for one sun (0.100 W.cm^2).

A fairly large cell build of 685 1 x 1 cm^2 and 1.5 x 1.5 cm^2 dual-ohmic cells of this type with a high-bandgap (hi-Eg) top subcell, designed for 300-500 suns concentration, was completed. As expected from earlier builds, 3-junction cells with the hi-Eg top cell condition gave higher performance than the low-bandgap (lo-Eg) top cell condition built as controls, in initial testing of bare cells under X-25 simulator at 1-sun AM1.5G conditions. Figure 1 shows the efficiency distribution for each population.

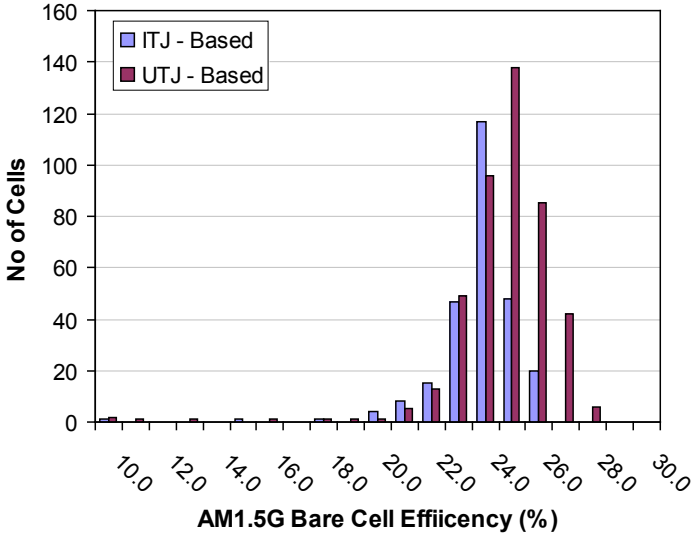

Fig. 2.1.1 Bare cell efficiency at AM1.5G, 1-sun distribution for 685, 1 x 1 and 1.5 x 1.5 cm^2 terrestrial cells with low-bandgap (CITJ) and high-bandgap (CUTJ) GaInP top subcells.

As shown in this figure, the median of the hi-Eg (CUTJ, or UTJ-based) cells is approximately higher by 1% absolute than the (CITJ, or ITJ-based cells). As seen in earlier experimental terrestrial concentrator cell runs in the HiPerf PV program, this gain is due to the increase in open-circuit voltage, resulting from the higher bandgap of the GaInP top cell, as seen in Fig. 2.1.2.

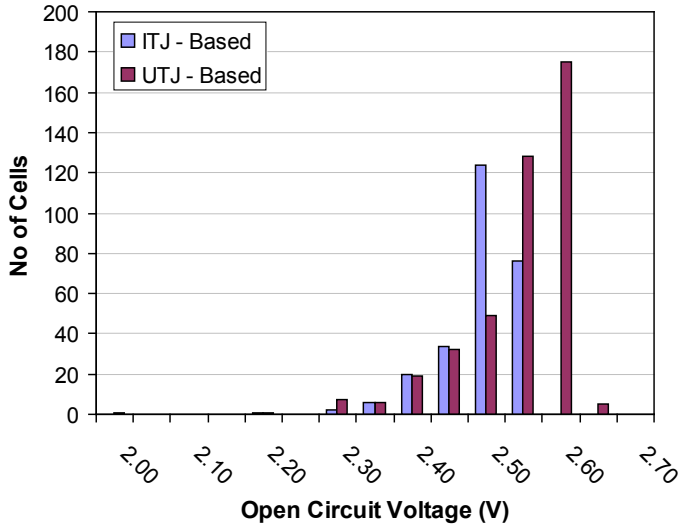

Fig. 2.1.2 Bare cell open circuit voltage at 1-sun AM1.5G conditions for 685, 1 x 1 and 1.5 x 1.5 cm^2 terrestrial cells based on lo-Eg (CITJ) and hi-Eg (CUTJ) GaInP top subcells.

The majority of hi-Eg cells show a peak V_{oc} between 2.60V and 2.65 V, while the lo-Eg cells show a similar peak between 2.50 and 2.55 V. The hi-Eg cells measure 65 mV higher on average than the lo-Eg cells in this build, consistent with results seen on earlier experimental terrestrial concentrator cell builds.

In the present build, the 1 x 1 cm^2 cells showed lower performance than the 1.5 x 1.5 cm^2 cells in both efficiency and open-circuit voltage,

2.1.2 Metamorphic Cell Development

One of the major areas of epitaxial development in this quarter has been the metamorphic (MM) approach. In this approach the top two subcells are grown intentionally mismatched in atomic lattice constant to the Ge subcell. As previously described, this results in a more optimal splitting of the solar spectrum and thus higher efficiencies are possible with this approach than the lattice-matched (LM) GaInP/Ga(In)As/Ge 3J cell. In particular our research efforts have focused on a cell with 8%-In content in the middle GaInAs subcell. This gives epitaxial layers with 0.5% mismatch to the Ge subcell. So the composition of the middle cell layers is $Ga_{0.92}In_{0.08}As$ and the composition of the top subcell layers, lattice-matched to the middle subcell layers, is $Ga_{0.44}In_{0.56}P$. Previous results include the record 36.9% efficiency [2] at 308

suns under the AM1.5D, low-AOD spectrum, and 31.3% efficiency [3] at 1-sun AM1.5G conditions.

Previous results have shown outstanding performance for the MM GaInAs subcell, while the $Ga_{0.44}In_{0.56}P$ to subcell is been more challenging, particularly in the open-circuit voltage as compared to lattice-matched technologies. This is as expected since the open-circuit voltage is highly sensitive to the defects propagating upward from the metamorphic buffer layers. The best method of tracking the performance is to use the band gap to open-circuit voltage offset [1,2,4]: $W_{oc} = (E_g/q) - V_{oc}$. A lower band-gap-voltage offset indicates fewer Shockley-Read-Hall recombination sites, fewer crystal dislocations, and higher crystal quality. GaInAs single junction cells exhibit an offset of 400 to 450 mV, with the lowest point being at the lattice matched conditions. This offset has been observed to hold for metamorphic $Ga_{1-x}In_xAs$ on Ge to approximately 35% indium content [4]. For GaInP cells, the offset is slightly higher, ranging from 450 to 550 mV. To date, metamorphic GaInP cells have exhibited a 550 mV offset. Recent metamorphic cells appear to have overcome this discrepancy in band-gap-voltage offset. Figure 2.1.3 shows a comparison between quick process 2J cells of previous MM $Ga_{0.44}In_{0.56}P/Ga_{0.92}In_{0.08}As$ cells on Ge, LM $Ga_{0.51}In_{0.49}P/Ga_{0.99}In_{0.01}As$ cells, and recent MM cells. The quick process alters the offset from the values shown above to somewhat lower values. On this scale, previous 2J MM cells had an average offset of 454 mV, while the LM offset ranges from 380 mV to 450 mV with an average of 410 mV. The recent result for the metamorphic averages 409 mV, essentially equivalent to the average band-gap-voltage offset for lattice-matched 2J cells. The cells presented as the best MM cells to date in Fig. 2.1.3 are from the same epitaxial run that produced the concentrator cell record 36.9% efficiency. That means that we would expect a slight voltage increase for metamorphic cells over previous builds. That in turn would produce a slightly higher performance than the record 36.9% cell.

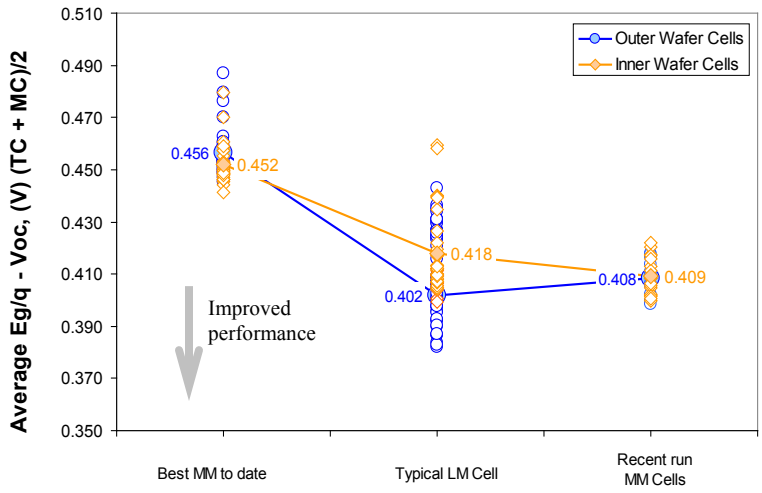

Fig. 2.1.3 Comparison of the average bandgap voltage offset $W_{oc} = (E_g/q) - V_{oc}$ averaged for both top cell and middle cell together for previous metamorphic 8%-In, lattice-matched, and recent 8%-In MM cells. Lower values indicate improved performance.

There are still many other tasks to accomplish before demonstrating the next increase in fully-processed metamorphic cell light I-V performance at concentration. The significant task of translating improved quick-process cell performance to full-process concentrator cells has begun. We have established a matrix of experiments (for lattice-matched and metamorphic structures) covering a wide range of top/middle cell ratios, wide-band-gap and narrow-band-gap top cells, and 3 different types of AR coatings, and are planning a new metal patterning mask with many different cell sizes and varying metal grid coverage fraction, in order to reach the program efficiency goals.

2.1.3 Mechanically-Stacked Multijunction Cell Development

Figure 2.1.4 shows the light I-V (LIV) results of a GaInP/GaAs 2J cell mechanically stacked on a Si cell from SunPower Corp., from Spectrolab's previous mechanical stack research effort under Phase 1A of the NREL HiPerf PV program. The top 2J GaInP/GaAs subcell assembly had an efficiency of 24.9% and the bottom Si subcell had an efficiency of 2.9% measured under the AM1.5G (0.1000 W/cm^2, 25°C) spectrum for a total efficiency of 27.8%, as previously reported.

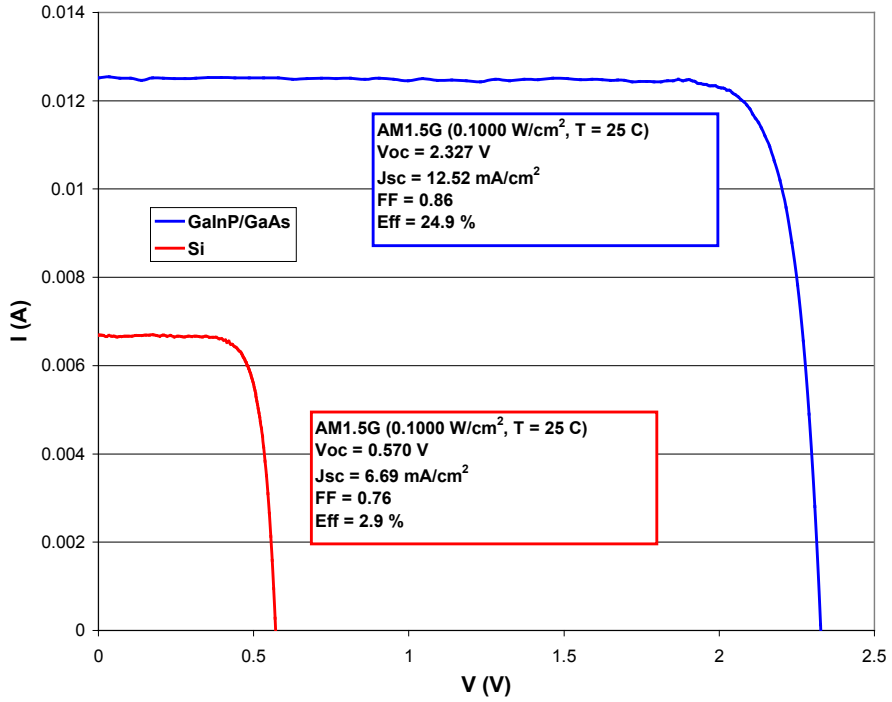

Fig. 2.1.4 LIV curves for GaInP/GaAs 2J cell mechanically stacked on GaSb bottom cell as previously reported.

From this previous effort, it was realized that absorption losses in the GaAs substrate were contributing to the lower than expected performance of the Si subcell. GaAs substrates with lower doping will have higher transmission of light through the wafer into the bottom cell, thereby increasing overall stack efficiency.

Fig. 2.1.5 shows the measured transmission of a high- and low-doped n-type GaAs substrate with an anti-reflective coating (AR) on both sides. The AR coating was optimized to maximize the current in the wavelength range of the bottom subcell (>900 nm) without sacrificing the current available for the GaInP/GaAs top subcells (350-890 nm). The bottom subcell could consist of a Si or GaSb subcell or other subcell combination (InGaAs/InP). The figure shows the improvement in transmission through the substrate.

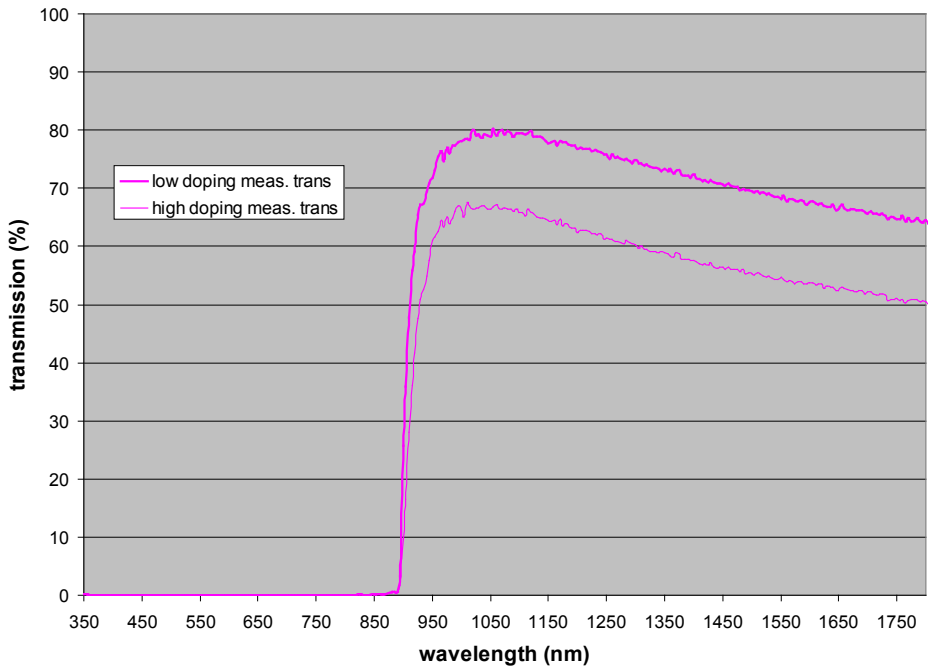

Fig. 2.1.5 Improved IR transmission for an n-type GaAs substrate with AR coating on both sides.

From the measured reflectance and transmission curve of the AR coated substrate, the absorptance (A = 1 - T - R) can be calculated. The results of integrating the absorptance, reflectance, and transmission curves with the AM1.5D, low-AOD (0.1000 W/cm^2) solar spectrum in the range of 350-1800 nm are shown in Table 2.1.1 below to quantify the expected improvement of the new GaAs substrates in terms of percent available current density. The 350-1800 nm wavelength response range for a GaSb cell is shown in the table. GaSb cells could be used for example in GaInP/GaAs//GaSb cells, with a GaInP/GaAs cell mechanically stacked on GaSb.

Table 2.1.1 Percent of light in the AM1.5D, low-AOD spectrum transmitted or absorbed in a GaAs wafer with low or high bulk doping, and AR coating on both sides, in the 350-1800 nm wavelength response range for a GaSb bottom cell.

wafer doping	% transmitted (350-1800 nm)	% absorption (350-1800 nm)
low	34.27	54.70
high	27.70	62.10

This amounts to a 7.4% absolute or ~12% relative reduction in absorptive losses in the substrate due to free carrier absorption. This improvement adds ~ 4 mA/cm^2 of current density available for the bottom subcell to collect by reducing substrate absorption loss out to 1800 nm in this calculation.

As a starting point for new work, it was found that the original cells had a low J-ratio of ~0.92 when integrated with the AM1.5D, low-AOD spectrum. Additionally, the cumulative top cell and middle cell current is only ~77% of the available current density expected in the wavelength range of 350-950 nm for the GaInP/GaAs top subcells.

Better current balancing in the top and middle subcells was achieved in recent mechanical stack runs by adjusting MOVPE growth parameters. Preliminary data from a calibration run indicates a J-ratio from 1.0 to 1.04 for the AM1.5D, low-AOD spectrum at the quick-process level.

The design of these mechanical stack cells require front and back wafer processing, and require much care and handling. Initial attempts on cell processing requiring front and back AR and metallization were unsuccessful. After a number of process alterations, we have developed a fairly robust processing scheme for mechanical stack cells.

As mentioned above, the AR coatings have been optimized for increased transmission while also minimizing reflection losses in the top two subcells. Additional improvements could be made to the AR coating by using an alternative AR stack and/or using MgF_2.

2.1.4 Mechanical Stack Cells for JX Crystals

Spectrolab was subcontracted by JX Crystals to build and deliver high efficiency 2J GaInP/GaAs subcells on GaAs for stacking on GaSb bottom subcells. The mechanical stack cells utilize a mesa structure with both positive and negative contacts accessible from the front side and positive contact on the backside of the cell. Figure 2.1.6 shows an example 2J GaInP/GaAs prototype cell with leads recently delivered to JX Crystals. The cell size is 7.5 mm x 7.5 mm with an aperture area of 0.25 cm^2.

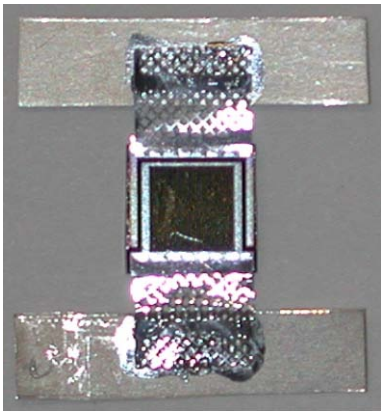

Fig. 2.1.6 GaInP/GaAs 2J Spectrolab cell with interconnects ready for mechanical stacking. Both 'n' and 'p' contacts are accessible from the front.

References – Section 2.1

[1] R. R. King, D. C. Law, K. M. Edmondson, C. M. Fetzer, G. S. Kinsey, H. Yoon, R. A. Sherif, and N. H. Karam, "40% efficient metamorphic GaInP / GaInAs / Ge multijunction solar cells," *Appl. Phys. Lett.*, Vol. 90, No. 18, 183516, 4 May 2007.

[2] R. R. King, C. M. Fetzer, K. M. Edmondson, D. C. Law, P. C. Colter, H. L. Cotal, R. A. Sherif, H. Yoon, T. Isshiki, D. D. Krut, G. S. Kinsey, J. H. Ermer, Sarah Kurtz, T. Moriarty, J. Kiehl, K. Emery, W. K. Metzger, R. K. Ahrenkiel, and N. H. Karam, "Metamorphic III-V Materials, Sublattice Disorder, and Multijunction Solar Cell Approaches with Over 37% Efficiency," *Proc. 19th European Photovoltaic Solar Energy Conference*, Paris, France, June 7-11, 2004 (WIP-Munich, Munich, Germany, 2004), ISBN 3-936-338-14-0, ISBN 88-89407-02-6, pp. 3587-93.

[3] R. R. King, C. M. Fetzer, P. C. Colter, K. M. Edmondson, D. C. Law, A. P. Stavrides, H. Yoon, G. S. Kinsey, H. L. Cotal, J. H. Ermer, R. A. Sherif, K. Emery, W. Metzger, R. K. Ahrenkiel, and N. H. Karam, "Lattice-Matched and Metamorphic GaInP/ GaInAs/ Ge Concentrator Solar Cells," *Proc. of the 3rd World Conference on Photovoltaic Energy Conversion*, Osaka, Japan, May 11-18, 2003, pp. 622-625.

[4] R. R. King, D. C. Law, C. M. Fetzer, R. A. Sherif, K. M. Edmondson, S. Kurtz, G. S. Kinsey, H. L. Cotal, D. D. Krut, J. H. Ermer, and N. H. Karam, "Pathways to 40%-Efficient Concentrator Photovoltaics," *Proc. 20th European Photovoltaic Solar Energy Conf.*, Barcelona, Spain, June 6-10, 2005, pp. 118-123.

2.2 Cell Development Progress Report 2

2.2.1 J-Ratio Study/Optimization for Terrestrial Solar Spectra

As mentioned in Progress Report 1, a large matrix of both lattice-matched and metamorphic cells cell designs has been grown, fabricated and characterized to the quick-process (QP) level. The purpose of this matrix is to capitalize on the improvements made in cell performance, especially metamorphic cell improvements, and also to control the sensitivity of current matching for different input spectra. The main variable was the J-ratio (top-cell J_{sc} to middle-cell J_{sc} ratio). Most of the other parameters such as the sheet rho, top cell band gap, and tunnel junction type were held constant at different J-ratios, although there are run splits which vary these parameters at a constant J-ratio as well. These wafers will be processed with a new concentrator mask set, the EC-01 (Experimental Concentrator 01) mask set with a wide range of concentrator cell sizes and grid spacings. When fully characterized, this cell build will provide information on a large parameter space, from which to choose the optimum design for a given concentration ratio and incident spectrum.

The wafers were grown with the following QP J-ratio targets under the AM0 spectrum: 1.07, 1.12, 1.16, 1.20, and 1.24, in order to achieve a range of J-ratios approximately centered on unity for the AM1.5D, low-AOD terrestrial concentrator spectrum. Quantum efficiency (QE) measurements were carried out on QP cells to determine the J-ratio, and J-ratio offsets to the AM0, AM1.5G, AM1.5D (old version), and AM1.5D, low-AOD solar spectra were calculated, although the AM1.5D, low-AOD is the targeted spectrum for cell optimization.

Figure 2.2.1 below shows the target J-ratio (Jt/Jm) in black squares and the measured QP J-ratio in blue diamonds for AM0. In most cases the QP J-ratio is within a few points of the target for a given cell design. The red closed circles indicate the J-ratio predicted for the AM1.5D, low-AOD spectrum for non-AR coated cells. The quantum efficiency is closely tied to the transmission of the AR films. Once the cells are AR-coated, the J-ratio should be near unity for maximum efficiency. Run splits will explore the effect of the different AR coatings on QE and J-ratio.

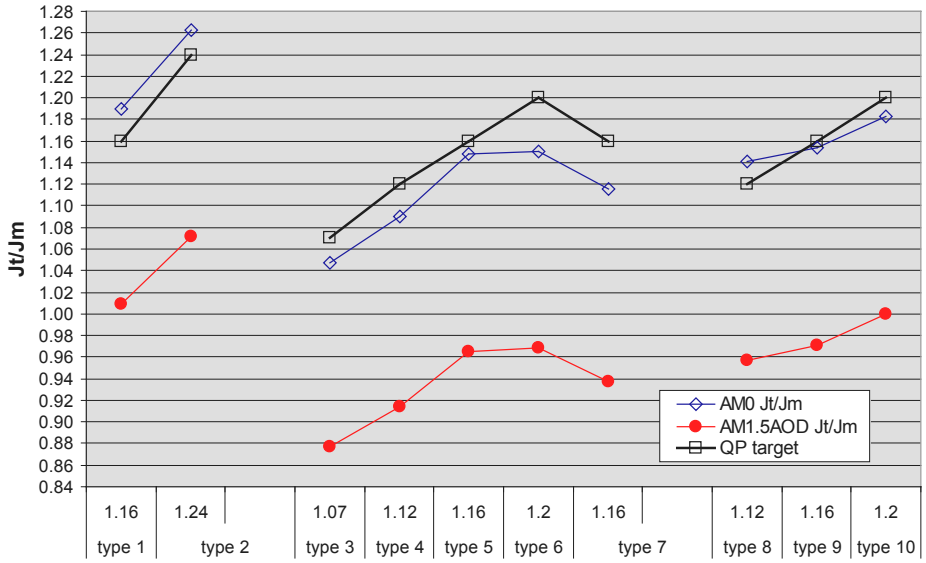

Fig. 2.2.1 Jt/Jm for lattice-matched cell designs.

Preliminary efficiency projections were calculated based on the QP voltage and FF, along with the J_{sc} from spectral response. The projections show that at 1 sun, the efficiencies are expected to be from 31 to 33% for lattice-matched cells, and 27 to 31% for metamorphic cells under the AM1.5D, low-AOD spectrum. The highest performing cells will be tested under high concentration.

Figure 2.2.2 shows the external quantum efficiency of a hi-Eg top cell and a lo-Eg top cell design with the same J-ratio. From the figure, a difference of ~76 meV is evident between the top cells, also the hi-Eg top cell has a thicker base to compensate lower current density resulting from higher Eg. The V_{oc} difference is ~127 mV. The middle cell QE becomes more square in shape as the top cell base thickness is increased. Once coupled with the AR coating, the QE for the middle cell will approach 100%.

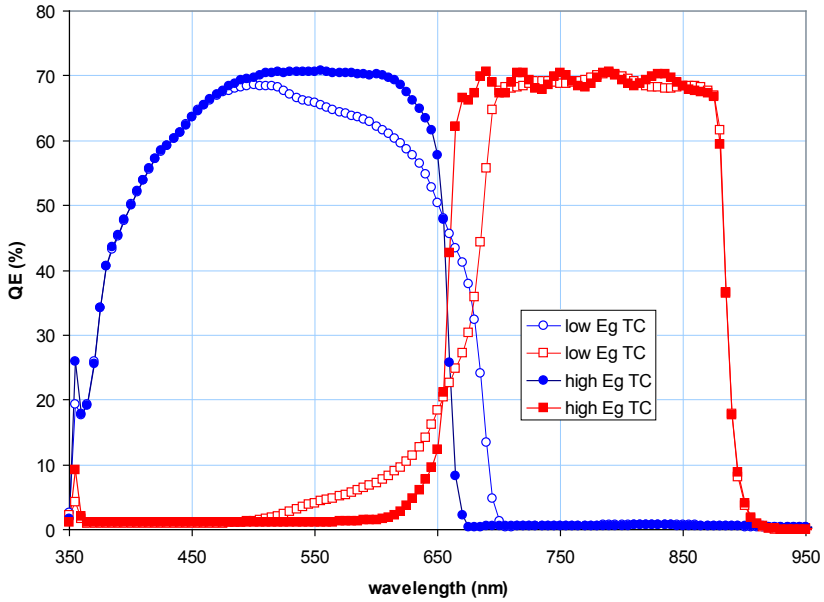

Fig. 2.2.2 Quantum efficiency of a high-band-gap (hi-Eg) and low-band-gap (lo-Eg) solar cell.

As described in [1,2,4], the average offset between the sum of subcell band gaps and the V_{oc} is an indication of material quality, with lower values indicative of higher crystal quality. From calculations based on quick-process cell QE data, the approximate average (Eg/q)-V_{oc} offset for lattice-matched cells is ~390-420 mV. The offset for the metamorphic cells is only slightly higher at ~ 420-450 mV. These measurements will be verified with full process data, but are consistent with previous QP results.

2.2.2 Full Process Cell Data Results

A batch of solar cells that are 1.5 cm x 1 cm with single busbar were grown and fabricated. These cells had some design features that are similar to the designs planned for the upcoming HiPerf PV build. Quantum efficiency (QE) measurements were performed on some of the full process (FP) cells to characterize the effect of the different J-ratios on the current matching for the AM1.5D, low-AOD spectrum.

Figure 2.2.3 shows the QP AM0 target J-ratio (black open squares) and the average QP AM0 J-ratio (blue open diamonds) helping to characterize the differences in cell structures for the six runs. The QP data was also convoluted with the AM1.5D, low-AOD spectrum (filled orange diamonds) to confirm current matching. QE data from four FP cells from each run are shown convoluted with the AM0 (light blue open squares) and AM1.5D, low-AOD (red filled triangles) spectra. The average J-ratio of the four cells is shown as well. Full processed cells have additional processing and are AR-coated. As is evident from the chart, the additional processing and AR coating lowers the J-ratio from the QP values.

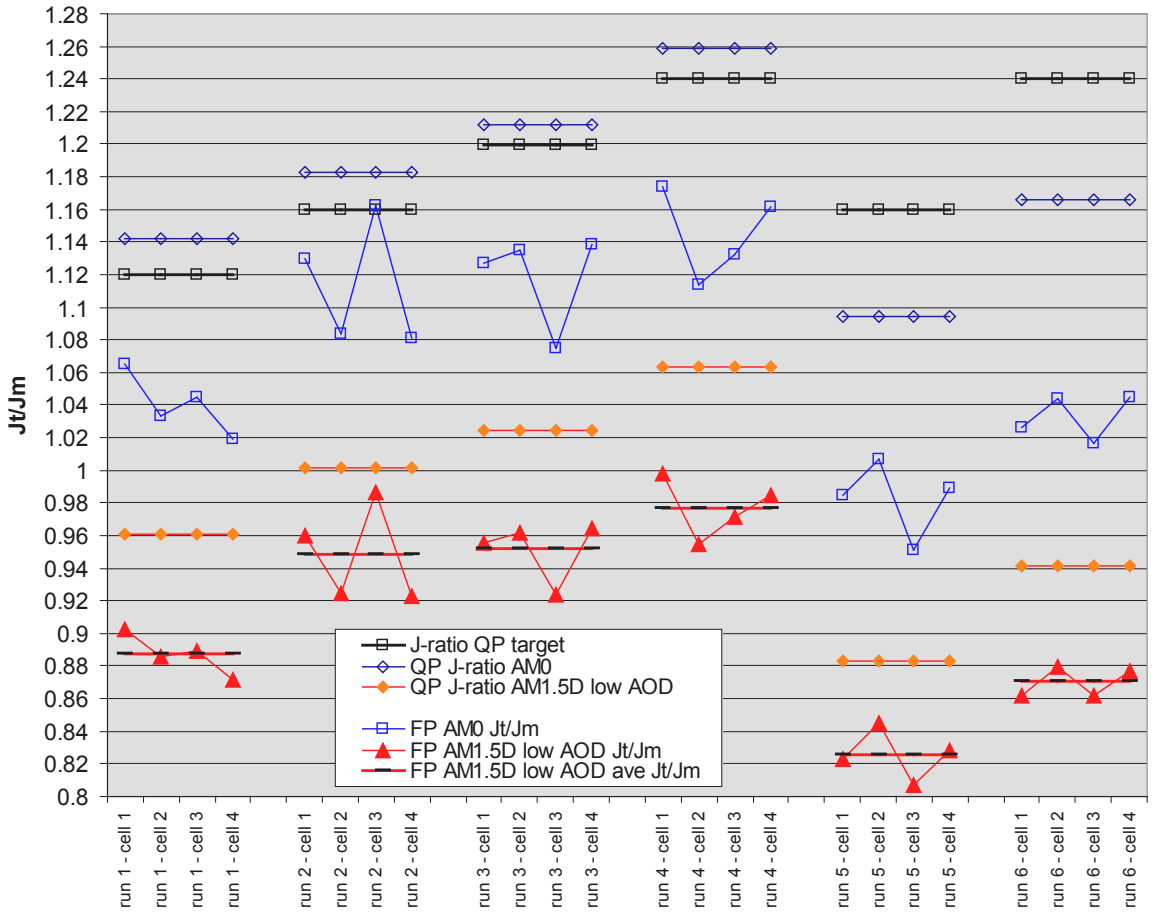

Fig. 2.2.3 Target and actual J-ratio of 1.5 cm x 1 cm cells.

2.2.3 Experimental Concentrator 01 (EC-01) Photomask Design

A new photomask set, called the experimental concentrator 01 (EC-01) mask set, is currently being designed. The experimental concentrator mask will have a number of different cell sizes and gridline pitches optimized for concentrations from ~250X to ~2000X. The cell aperture sizes range from 0.8 cm x 1.0 cm to as small as 0.2 cm x 0.2 cm. The mask will utilize different gridline designs, such as linear gridlines between two busbars and gridlines in a staggered chevron pattern, with varying line spacings. The targeted gridline width is in the range of 12-15 microns. The mask is sectioned into 4 quarters; a representative schematic of the mask is shown in Fig. 2.2.4. Diagnostic features are also included on the mask, to permit determination of sheet resistance, contact resistance, and grid metal resistance, as well as test structures for DLTS, tunnel junction measurement, and reflectivity. This new mask set will be used for the upcoming J-ratio cell build described above.

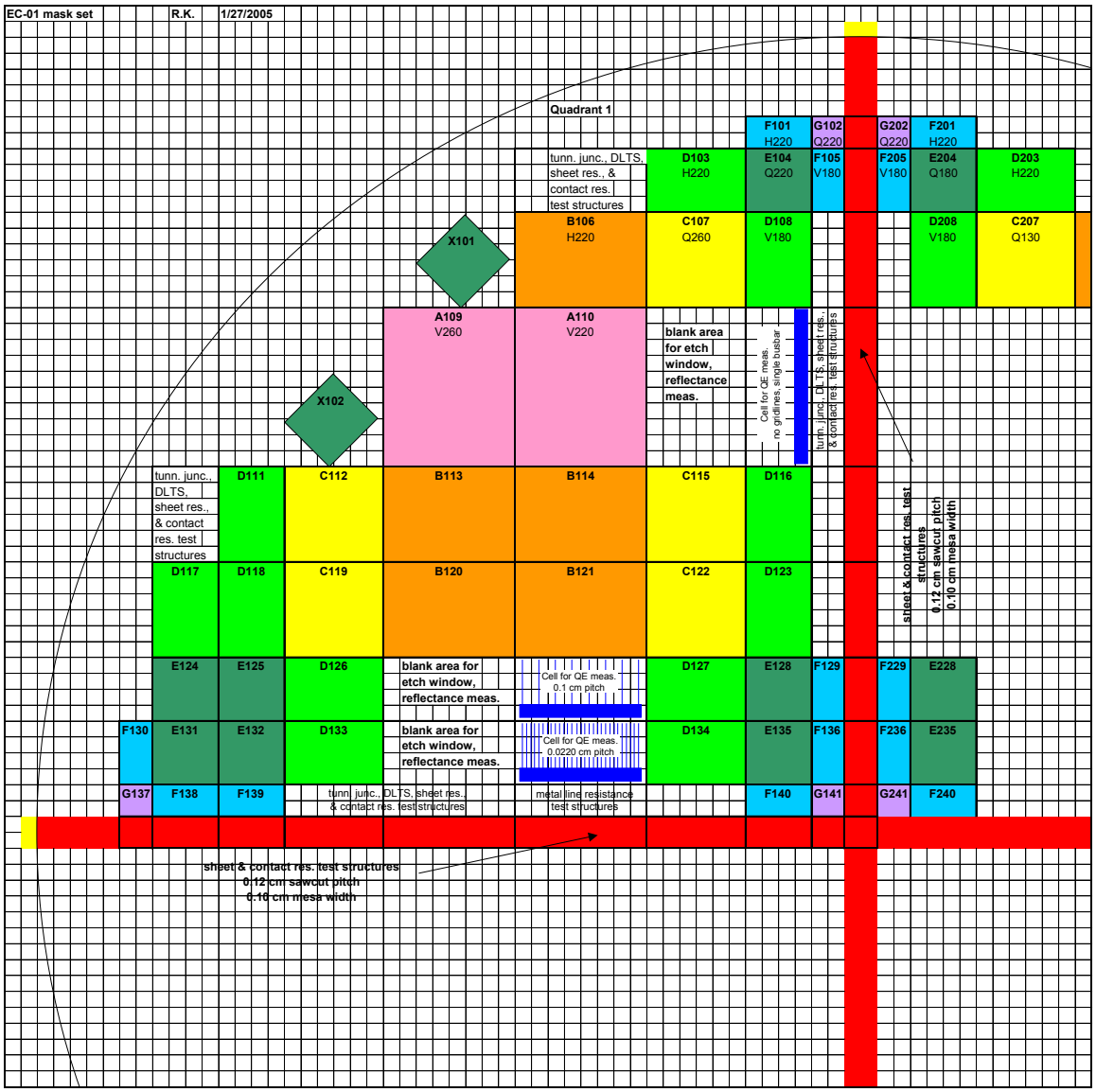

Fig. 2.2.4 Schematic of New Spectrolab Experimental Concentrator 01 (EC-01) Photomask.

2.3 Cell Development Progress Report 3

2.3.1 EC-01 Concentrator Cell Build

A number of build splits were included in the Experimental Concentrator 01 (EC-01) cell build starting late February 2005. Upon receiving the wafers from MOVPE, the wafers were staged in groups based on processing similarity. The run splits include: metamorphic (MM) and lattice-matched (LM) 3-junction cells, ordered and disordered GaInP top cell material, 3 different AR coat designs, various tunnel junction designs, and a wide range of current ratio (J-ratio) between top and middle cells, metallization coverage fraction, and cell size.

An initial build was processed in advance of the main build in order to check process compatibility with the new photomask. Two different processes were used for the metal layer: one used a conventional liftoff process, and the other used an image reversal process. The advantage of the conventional liftoff is that narrower gridlines may be possible, though this is not clear. The major disadvantage of the conventional liftoff process is a much longer liftoff time, especially for terrestrial cell designs that have a high pitch density. Most cells had a 6 um or 8 um as-designed gridline width. A number of different AR coatings were used in the build splits. The cells are electrically isolated on the wafer during the cell process. Light I-V (LIV) and quantum efficiency (QE) measurements were carried out on cells on whole wafers.

Figure 2.3.1 shows a completely processed wafer from the EC-01 build. The variety of cell sizes and designs can be seen. The center-to-center grid spacing, or pitch, is optimized for a wide range of concentrations, from approximately 200 to 2000X.

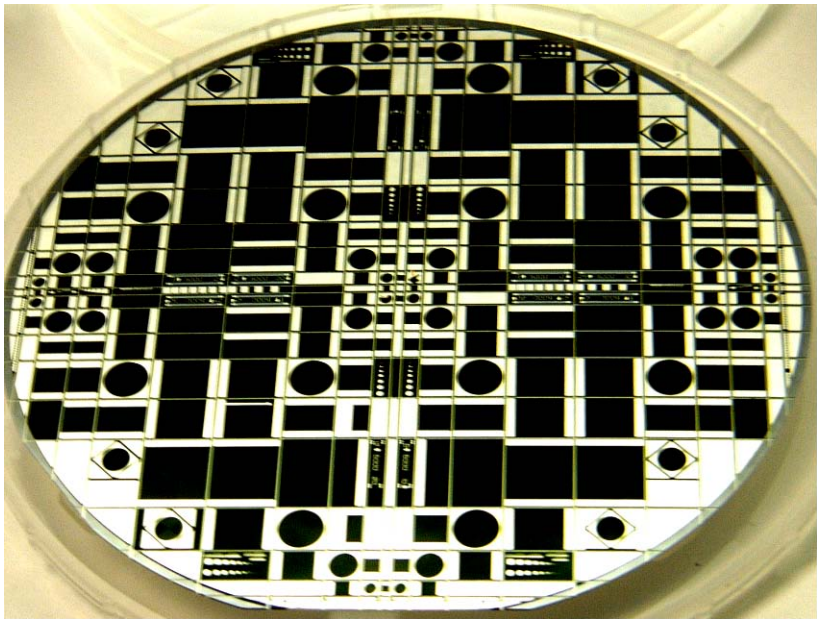

Figure 2.3.1 Wafer from the EC-01 Experimental Concentrator Cell Build.

Figure 2.3.2 shows some of the test structures designed into the wafer. There are a number of test patterns indicated by the red circle for determining sheet, line and contact resistivity. The contact resistance becomes more important at higher concentration. The magenta circle indicates other test structures for probing tunnel junctions, capacitance, dark I-V, etc. The blue circle indicates areas free of metal for reflectivity measurements of the active area. The reflectance field is adjacent to cells designed for spectral response measurements with a low and high pitch density. Additional transmission line measurement (TLM) and test patterns along the top and bottom of the wafer are indicated with the green circle. This will permit checking the uniformity of certain parameters across the wafer. As seen in the photos, most of the cells are designed with two busbars. The cells are tested under high concentration with one current probe per busbar and one voltage probe.

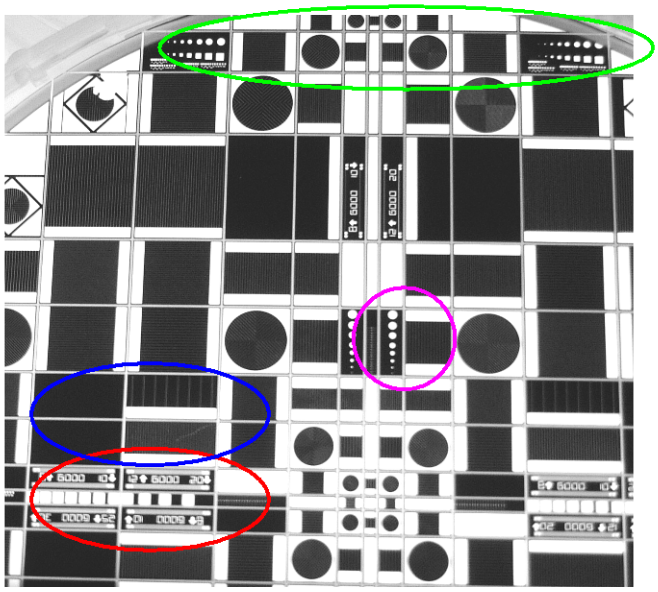

Figure 2.3.2 Test patterns designed into the EC-01 mask

2.4 Cell Development Progress Report 4

2.4.1 EC-01 Concentrator Cell Build

Based on preliminary measurements of very high-efficiency, Spectrolab sent some of the cells from the EC-01 concentrator cell build to the Device Characterization Lab at NREL for independent verification. The few cells tested have yielded a world record efficiency of 39.0% (236 suns, AM1.5D, low-AOD spectrum, 25°C), the highest conversion efficiency yet measured for a photovoltaic device. V_{oc} is 3.089 V at this incident intensity, and J_{sc}/intensity is 0.1431 A/W, both substantially improved in comparison to the previous record cell of a similar design, with 37.3% efficiency. These results will be described in more detail in the paper: "Pathways to 40%-Efficient Concentrator Photovoltaics," R. R. King, D. C. Law, C. M. Fetzer, R. A. Sherif, K. M. Edmondson, S. Kurtz, G. S. Kinsey, H. L. Cotal, D. D. Krut, J. H. Ermer, and N. H. Karam, *20th European Photovoltaic Solar Energy Conference*, 6-10 June 2005, Barcelona, Spain [4]. The light I-V data for the new record cell, as independently confirmed by NREL, are shown in Fig. 2.4.1.

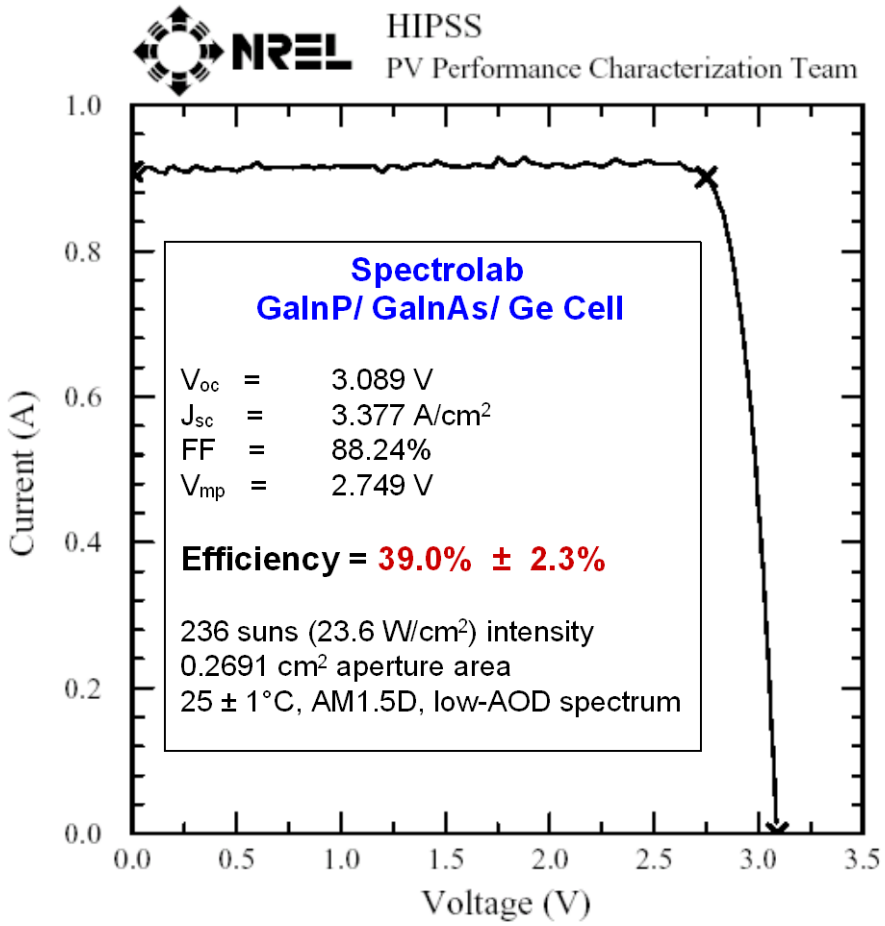

Fig. 2.4.1 Light I-V curve of world-record solar cell built at Spectrolab, and independently confirmed at NREL.

The 39.0%-efficient cell is a lattice-matched 3-junction GaInP/ GaInAs/ Ge cell structure. Metamorphic cells from the EC-01 cell build also have very high efficiencies, up to a value of 38.8% for the limited number of cells measured. Because of the small cell sizes and number of experimental run splits in the EC-01 cell build, there are literally thousands of cells in this build, and a major factor that limits evaluation of the experiments in this build is the difficulty in measuring this quantity of cells. It is quite likely that there are yet higher efficiency cells in the build that have not yet been tested. The results of cell characterization and analysis of the experimental run splits in the build point the way to further potential efficiency improvements. Based on these successes, we are optimistic that we will be able to reach 40% efficiency soon.

2.4.2 Series Resistance Power Losses

Because of the interest in using triple-junction cells under ultra-high concentration conditions (above 1000 suns), we decided to investigate the performance and stability of these cells in this concentration regime. As the concentration level increases, the tunnel junction stability, in particular, becomes important, not to mention the challenges associated with cooling of the cells and of maintaining tracking accuracy. However, the benefit to going to ultra-high concentration is obvious: the solar cell cost (which currently represents about 25% of the system cost at concentration of 500X) becomes smaller.

Figure 2.4.2 shows gridline optimization modeling for cells at 3 levels of concentration: 1000X, 3000X, and 5000X. In the ultra-high concentration regime, the impact of front-metal contact resistance becomes very important as shown in Fig. 2.4.3.

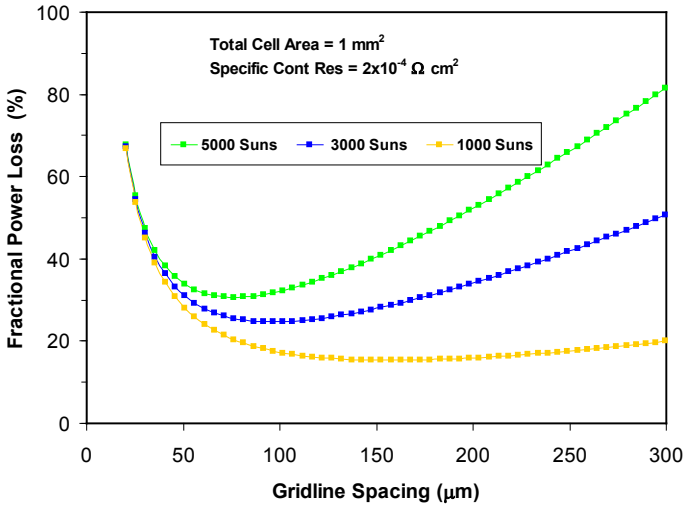

Fig. 2.4.2 Gridline pitch optimization for a 1 mm^2 3J cell.

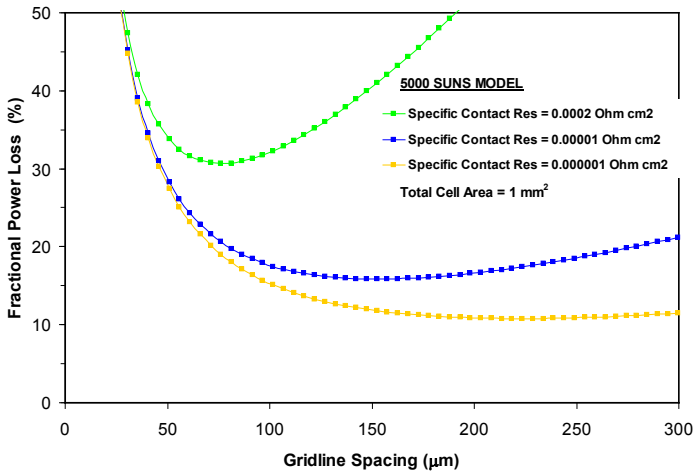

Fig. 2.4.3 Impact of front-metal contact resistance on fractional power loss at 5000X.

The data in Fig. 2.4.2 suggest that the gridline spacing should be about 200 microns for 1000 suns. The cell performance is fairly insensitive for gridline spacing between 150-300 microns. At concentration of 3000 suns, the optimum grid spacing is about 100 microns, and the dependence on the gridline spacing becomes stronger. At 5000 suns, the optimum spacing drops to about 75 microns and any slight deviation from that causes a larger drop in cell performance.

The quantum efficiency for the 3J cells used in this study is shown in Fig. 2.4.4. Light I-V data for a 1-mm^2 concentrator, measured using the high-intensity pulsed solar simulator (HIPSS) is presented in Fig. 2.4.5 and in Table 2.4.1. The corresponding data for the 4-mm^2 cell is shown in Fig. 2.4.6 and in Table 2.4.2.

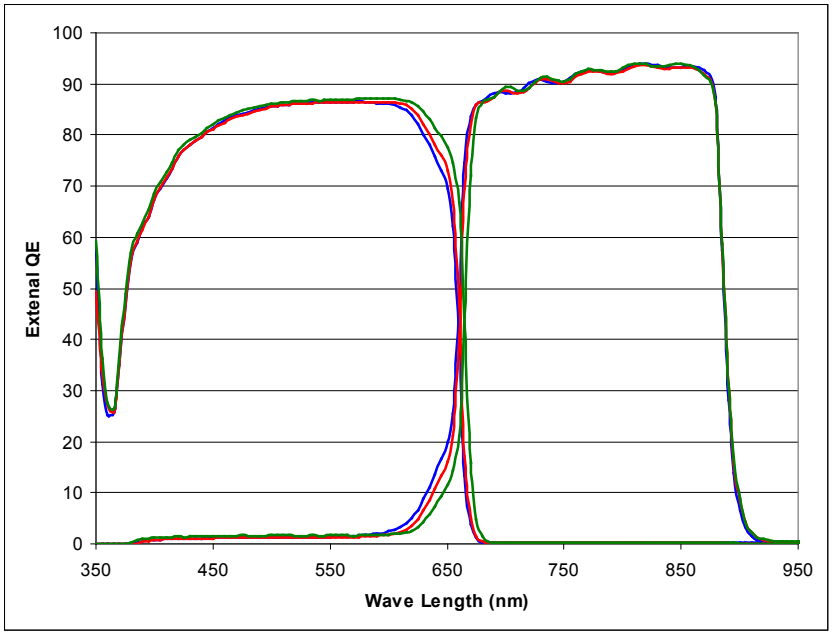

Fig. 2.4.4 External quantum efficiency of the 3J cells used in this study.

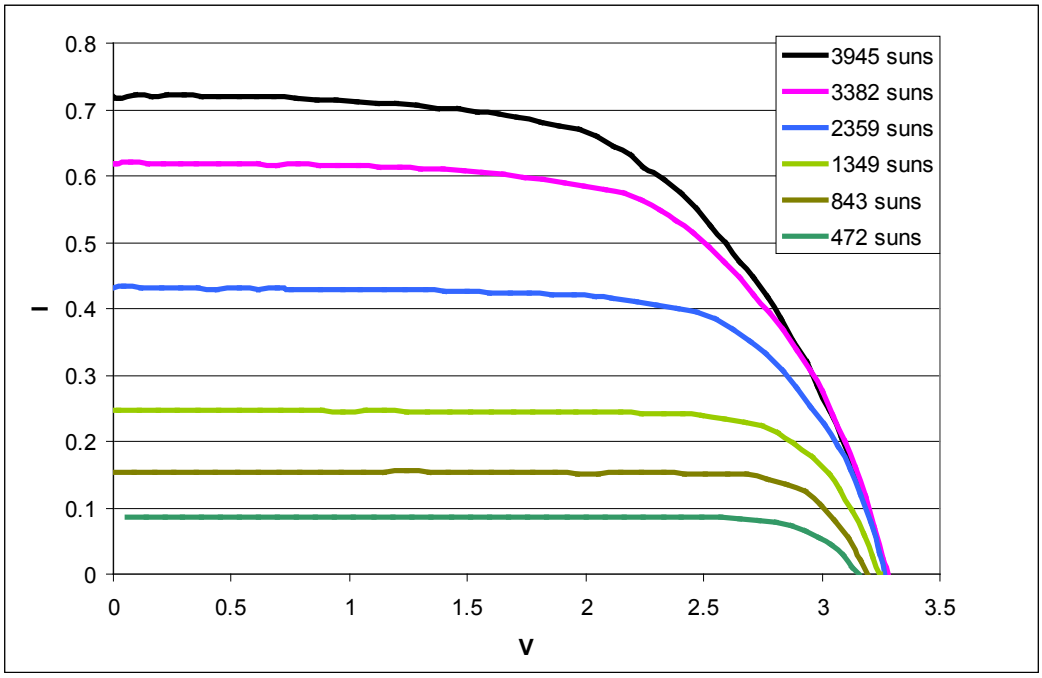

Fig. 2.4.5 HIPSS data for the 1-mm^2 cell, at concentrations of 400 suns up to 4000 suns.

Table 2.4.1 HIPSS data for the 1-mm^2 concentrator cell.

Concentration	Voc	FF	Power	Efficiency.
472 suns	3.153	0.819	0.223W	34.8%
843	3.190	0.814	0.401	34.99%
1349	3.245	0.764	0.613	33.43%
2359	3.267	0.695	0.982	30.59%
3382	3.278	0.625	1.268	27.59%
3945	3.271	0.585	1.383	25.78%

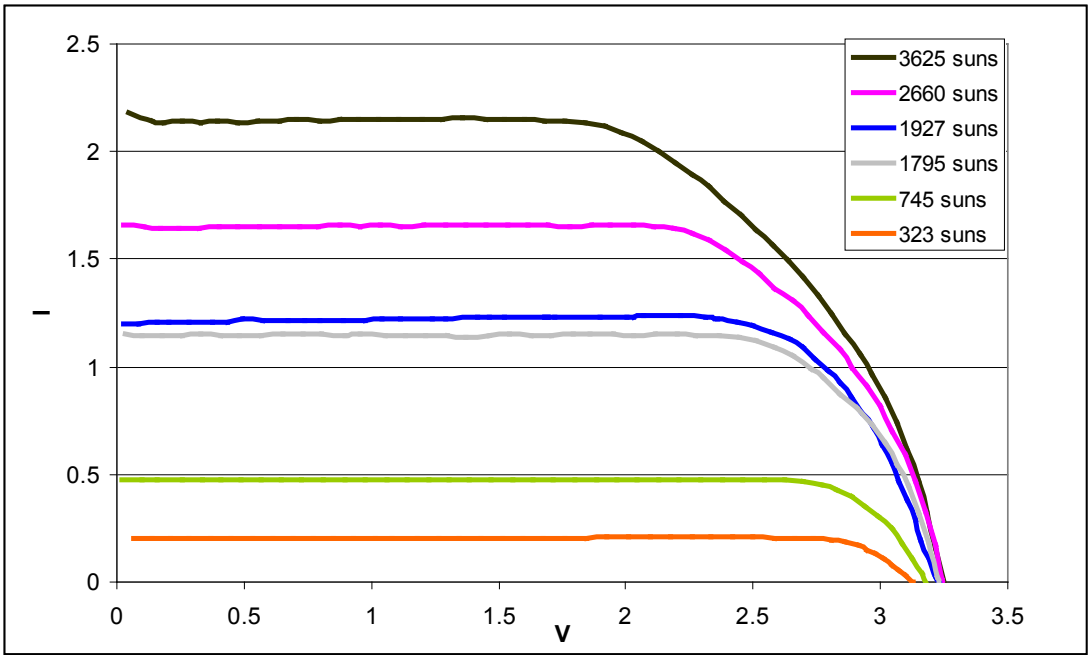

Fig. 2.4.6 HIPSS data for the 4-mm^2 cell, at concentrations of 320 suns up 3620 suns.

Table 2.4.2 HIPSS data for the 2mm x 2mm concentrator cell size.

Concentration	Voc	FF	Power	Efficiency
323 suns	3.127	0.854	0.553	35.99%
745	3.178	0.828	1.259	35.49%
1795	3.230	0.759	2.825	33.07%
1927	3.228	0.750	2.995	32.64%
2660	3.245	0.667	3.697	29.19%
3625	3.248	0.567	4.281	24.81%

The cells used in this study had an approximately 200-micron center-to-center gridline spacing (gridline pitch). This explains the drop in the fill factor due to high I^2R losses in the concentration range of 2000X and above for which these metal grids were not optimized. Significantly, the data show stable tunnel junction performance at extremely high solar concentrations.

References – Section 2.4

[4] R. R. King, D. C. Law, C. M. Fetzer, R. A. Sherif, K. M. Edmondson, S. Kurtz, G. S. Kinsey, H. L. Cotal, D. D. Krut, J. H. Ermer, and N. H. Karam, "Pathways to 40%-Efficient Concentrator Photovoltaics," *Proc. 20th European Photovoltaic Solar Energy Conf.*, Barcelona, Spain, June 6-10, 2005, pp. 118-123.

2.5 Cell Development Progress Report 5

2.5.1 Metal Gridline Profile and Shadowing

Optical gridline measurements were performed on a number of wafers from the EC-01 experimental concentrator cell build, that yielded record-efficiency 39.0% cells as described above. The optical measurements of gridline width to determine grid shadowing were complicated by the difficulty of resolving the base of the gridline due to optical effects. Cells B214 and B213 were measured on representative wafers from each lot. Three gridlines were sampled on each cell, at the left edge (LE), in the middle (M), and at the right edge (RE) of the cell. Initial observations indicate a range of gridline spreading values, due to variation in process detail. We have identified which process steps are most likely to cause excessive spreading and have established process parameters to try in order to reduce gridline spreading on future runs.

Secondary electron microscopy (SEM) photos were taken to confirm the optical data. Fig. 2.5.1 is a SEM image of a gridline on cell B214. SEM images and optical measurements were used together to determine gridline shape and spreading during processing, to develop processes that minimize gridline obscuration.

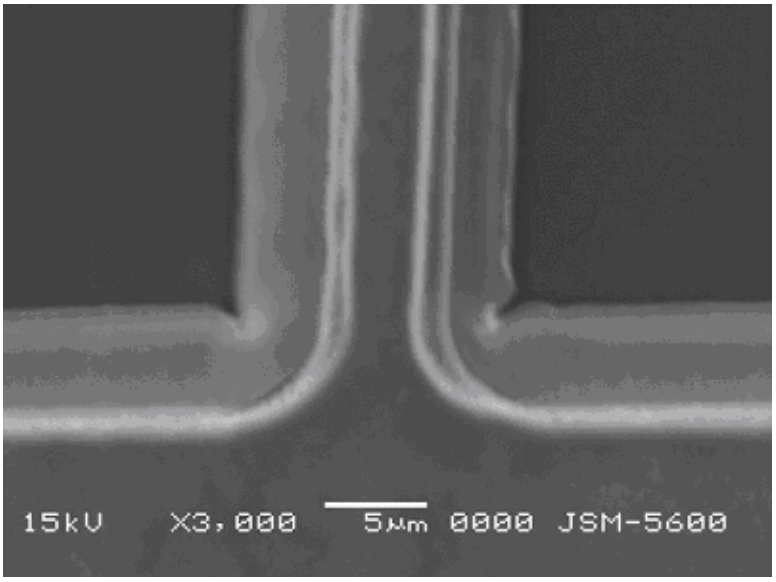

Fig. 2.5.1 SEM of a gridline on cell B214 from the EC-01 build.

As mentioned earlier, there are a number of transmission line measurement (TLM) test patterns for determining the sheet resistance of the top layer of the GaInP top cell, and specific contact resistance between the metal gridlines and the cap. Fig. 2.5.2 shows a schematic of the TLM pattern used for this measurement. Each metal pad is 900 µm× 900 µm and is shown by the inner squares. The metal pad is centered on top of a square mesa Ga(In)As cap. The cap is approximately 50 microns wider on each side than the metal square, and is shown by the outer squares in Fig. 2.5.2.

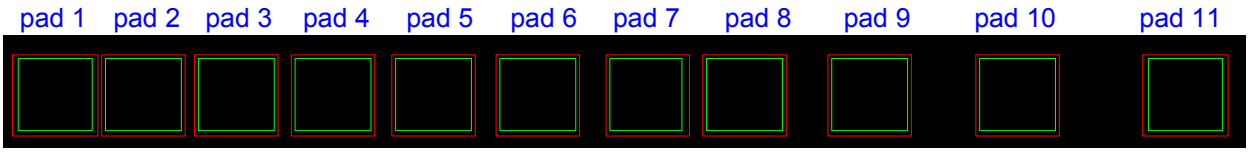

Fig. 2.5.2 TLM pattern for determining sheet resistance and specific contact resistance on wafers from the EC-01 cell build.

The test methodology consists of a current-voltage sweep between two pads, from –1 to +1V or –0.5 to +0.5V for most of the measurements. The I-V sweep has very linear behavior indicating good ohmic contact. The resistance (V/I = R) is calculated for each I-V set and an average resistance is calculated. The zero bias point is omitted from the average R. The contact resistance is then calculated by calculating the slope of R vs. pad spacing. Multiplying the slope by the pad width (0.0900 cm) yields the sheet resistance.

Figure 2.5.3 below shows an example set of TLM data. The TLM data were measured on both the left and right hand side of the wafer. The chart shows that the sheet resistance is quite uniform in this dimension. Two lattice-matched and two metamorphic wafers were measured in the first round of TLM measurements. In this measurement set, the measured sheet rho is higher than the nominal values by 10 to 50%.

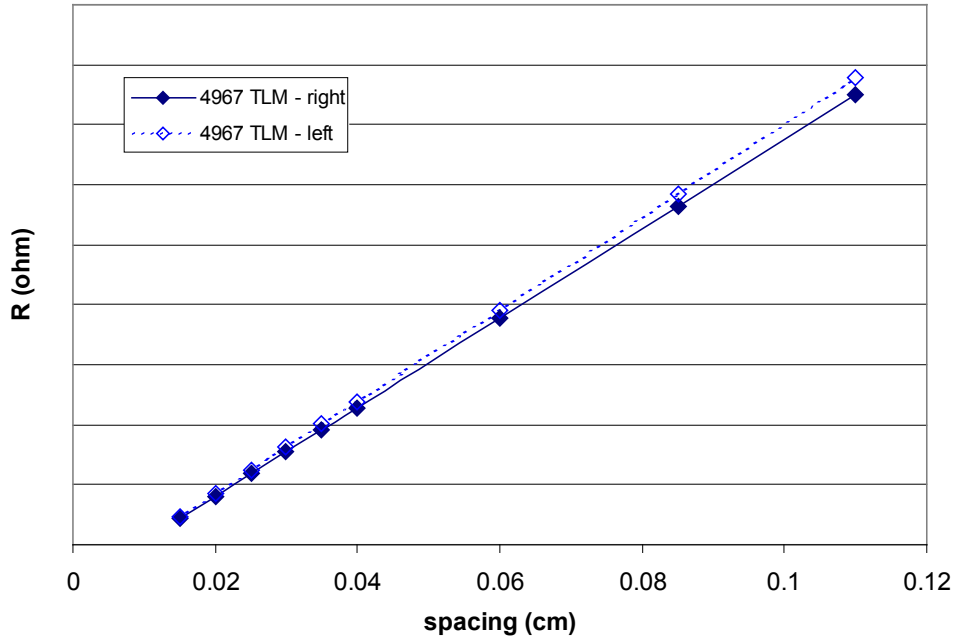

Fig. 2.5.3 Measured resistance vs. TLM pad spacing used to measure sheet resistance for the EC-01 concentrator cell build.

2.6 Cell Development Progress Report 6

2.6.1 EC-01 Concentrator Cell Build Experimental Run Splits

The high-efficiency terrestrial concentrator cell Build #1 using the EC-01 mask (Experimental Concentrator mask 1) contains a number of run splits from which much can be learned about the mechanisms controlling efficiency of multijunction concentrator solar cells. This is the run that yielded the present record 39%-efficient solar cell, a lattice-matched cell, and also the present record-efficiency metamorphic cell with 38.8% at 241 suns, independently confirmed for the AM1.5D, low-AOD spectrum, essentially reaching parity with highest efficiency lattice-matched cell yet demonstrated. The measured dependences of V_{oc}, fill factor, and efficiency on incident intensity are shown in Fig. 2.6.1.

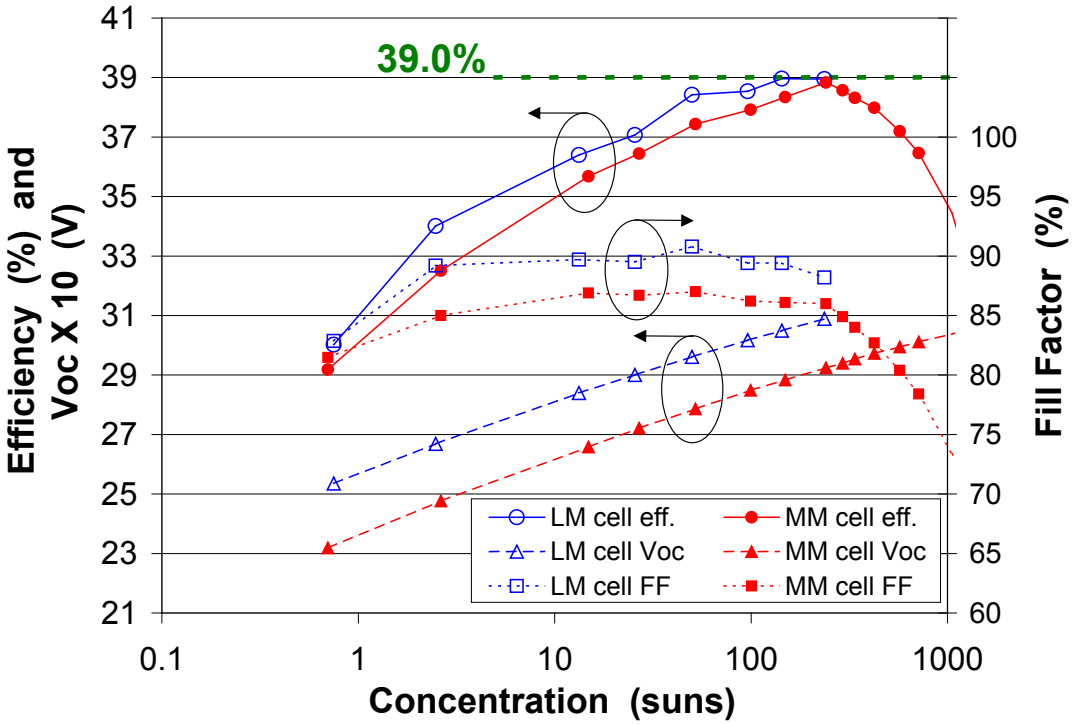

Fig. 2.6.1 Measured open-circuit voltage, fill factor, and cell efficiency as a function of light concentration incident on the cell (1 sun = 0.100 W/cm^2, AM1.5D, low-AOD spectrum), for record efficiency lattice-matched and metamorphic terrestrial concentrator solar cells, reaching 39.0% and 38.8% efficiency, respectively.

Some example device measurements from this build are given in this report. High-throughput electrical and optical characterization of the cells in this build, and of concentrator cells in general, remains one of the most critical needs for large-scale experimentation and manufacturing of concentrator solar cells. These challenges arise: because of the very large numbers of small concentrator cells that are typically produced from a single wafer; because of the need to test at high concentrations (~500x) to simulate typical concentrator cell operating conditions, and since these are multijunction cells; because of the need to control and balance

the spectra incident on each subcell of the multijunction stack. Development of rapid, accurate, and inexpensive cell testing for multijunction concentrator solar cells is a key opportunity and one of the highest priorities for advancing the field of concentrator PV, because of its ability to dramatically accelerate the rate of experimental research on solar cell device structures, and because of its direct effect on the cost of manufacturing large quantities of small concentrator cells.

Figure 2.6.2 shows the cumulative current density plotted versus J-ratio for full-process lattice-matched and metamorphic concentrator cells from EC-01 Build #1. The cumulative current density is defined as the sum of the short-circuit current densities in the top subcell (GaInP) and middle subcell (GaInAs) of a 3-junction cell, found by integrating the measured external quantum efficiency for each subcell with respect to the standard AM1.5D, low-AOD terrestrial concentrator solar spectrum. In a well-current-balanced 3-junction cell, the current density of the cell that can be achieved is roughly half of the cumulative current density, so it is important to maximize this quantity. The cumulative current density can be seen to increase as the J-ratio climbs, and as more and more current is photogenerated in the GaInP top cell. One cause of this phenomenon is that as an increasing fraction of the available light is absorbed in the top cell, a smaller fraction needs to pass through the tunnel junction and other layers with parasitic absorption mechanisms between the top and middle subcells. So the less light that passes through these regions with non-ideal carrier collection probability, the higher the overall cumulative current. Metamorphic cells have a more rapid rise in cumulative current with J-ratio, perhaps indicating that the layers between subcells have more parasitic absorption in the metamorphic case than for lattice-matched cells.

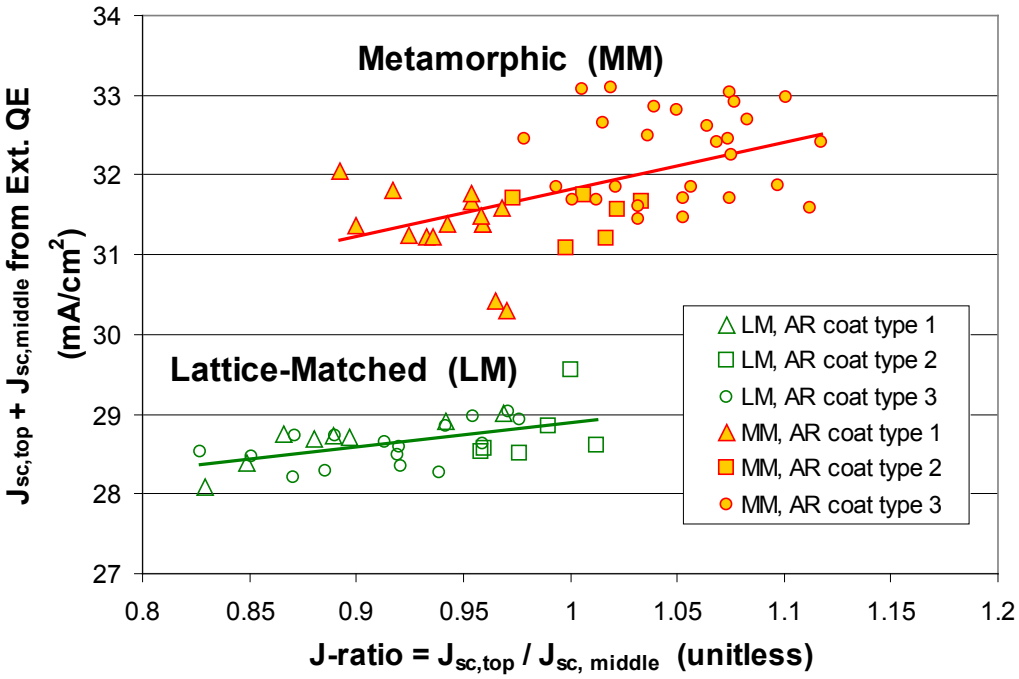

Fig. 2.6.2 Cumulative current density for full-process lattice-matched and metamorphic concentrator solar cells, as a function of J-ratio, for 3 different types of anti-reflection (AR) coating.

The effect of the AR coating type can be seen from Fig. 2.6.2. For metamorphic cells, AR coating type 3 increases the J-ratio, and also increases the cumulative current beyond that expected from the J-ratio increase. The beneficial effect of AR coating 3 is more muted in the case of lattice-matched cells.

Figures 2.6.3 and 2.6.4 show examples of light I-V screening measurements on full-process metamorphic EC-01 Build #1 cells. These are continuous-illumination (as opposed to pulsed) light I-V measurements, made using an X25 solar simulator calibrated with 2 cm x 2 cm metamorphic reference cells that have nearly the same spectral response as the metamorphic subcells of the 3-junction cells under test. Beam divergence and thermal considerations limit the maximum intensity that can be achieved with these steady-state light I-V measurements to ~100 suns, depending on the requirements for uniform spot size. Although the low intensity is a drawback, steady-state light I-V measurements have the powerful advantages of allowing good control over the spectral balance of light on the top and middle subcells, as well as avoiding the transient effects that can cause problems with pulsed light sources.

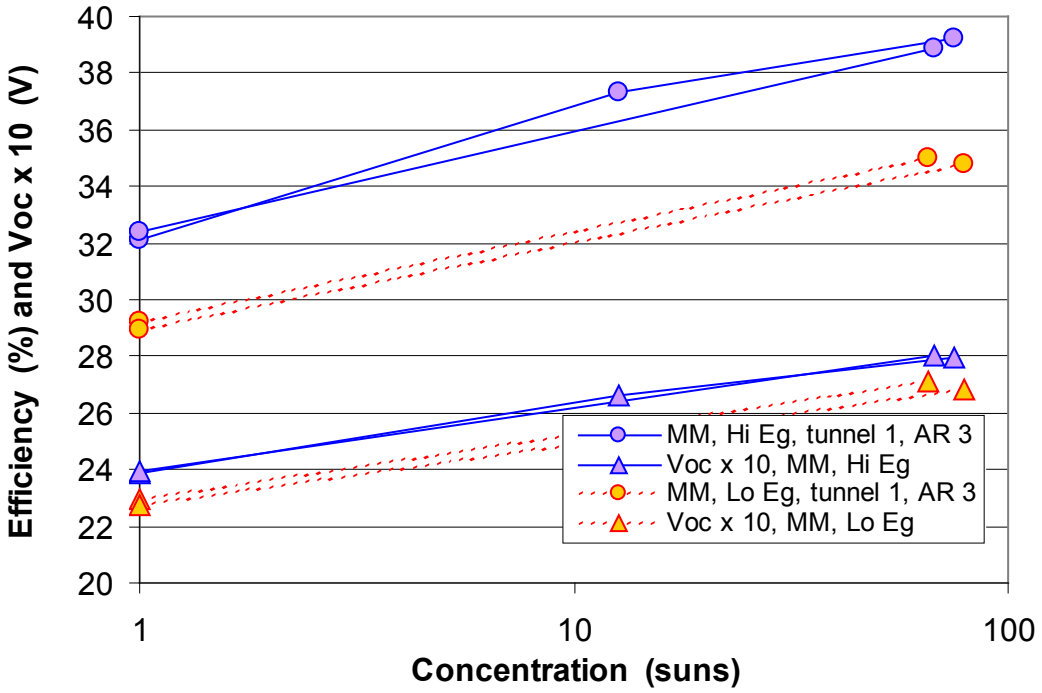

Fig. 2.6.3 Efficiency and open-circuit voltage from light I-V cell screening measurements made with a steady-state light source as a function of concentration, for full-process metamorphic 3-junction concentrator solar cells, with high-band-gap (hi-Eg) and low-band-gap (lo-Eg) experimental conditions for the lattice-mismatched GaInP top cell.

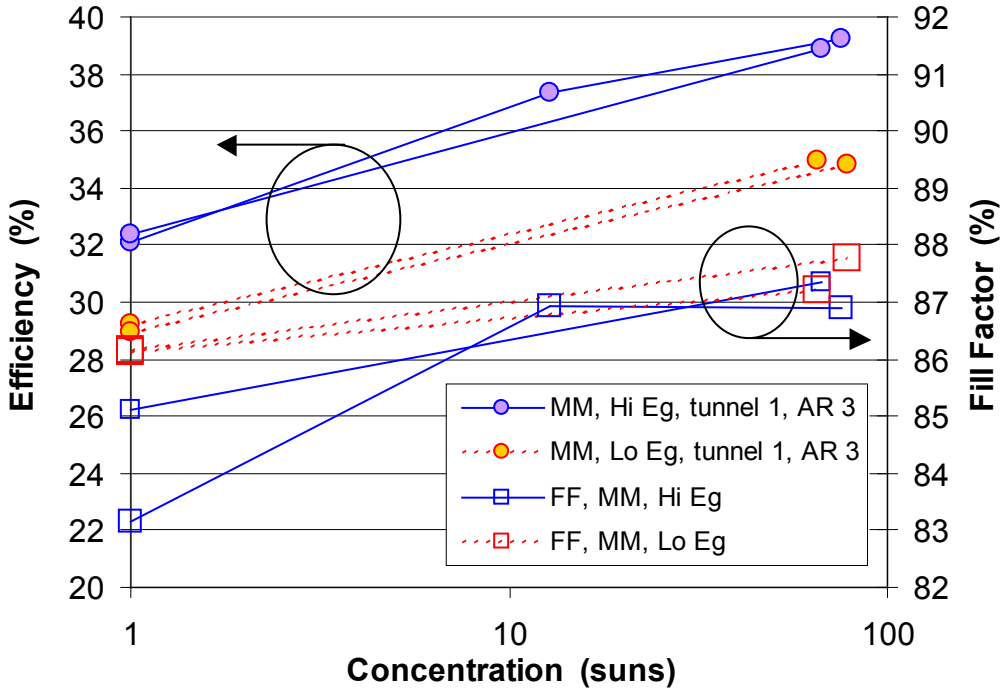

Fig. 2.6.4 Efficiency and fill factor from light I-V cell screening measurements made with a steady-state light source as a function of concentration, for full-process metamorphic 3-junction concentrator solar cells, with high-band-gap (hi-Eg) and low-band-gap (lo-Eg) experimental conditions for the lattice-mismatched GaInP top cell.

In Figs. 2.6.3 and 2.6.4, the experimental cases of a high-band-gap (hi-Eg) and a low-band-gap (lo-Eg) GaInP top cell are shown for these lattice-mismatched 3-junction cells, with the efficiency of the high-band-gap case substantially better for these experimental cells at both one-sun and at ~80 suns. The open-circuit voltage is naturally lower for the low-band-gap case, and both high-Eg and low-Eg cases show about the same rate of increase of ~200 mV per decade in Voc as a function of incident intensity.

The fill factors shown in Fig. 2.6.4 rise gradually with concentration for most cells, however one cell shows the relatively low one-sun FF and rapid rise in FF with increasing intensity that are characteristic of a small shunt or high diode ideality factor in the cell. At intensities approaching 100 suns, the FF has nearly recovered to near that of the other cells.

This type of problem points out the inadequacy of relying on one-sun measurements to evaluate concentrator solar cells. If it is difficult to do all cell evaluation at the typical operating intensity of ~500x, testing at 50-100x is a far better indicator of performance at the design point than extrapolating from one-sun measurements. Screening measurements like those shown here are crucial for analyzing the large amount of cells not only in concentrator cell manufacturing, but also in terrestrial concentrator solar cell experiments. Faster, automated testing is needed, along with the ability to test at higher concentration ratios, and to independently adjust the intensity of light in the response ranges of the GaInP top, GaInAs middle, and Ge bottom subcells.

2.7 Cell Development Progress Report 7

2.7.1 Lattice-Matched and Metamorphic Cell Characterization

Further analysis lattice-matched (LM) and metamorphic (MM) 3-junction concentrator cells from EC-01 build #1, the high-efficiency concentrator cell build which yielded the best results at this point in the program, and in fact demonstrated the highest solar conversion efficiency for a photovoltaic device up to that point in time, with 39.0% efficiency independently confirmed under the terrestrial AM1.5D, low-AOD spectrum at 236 suns [1], for a lattice matched cell. The metamorphic, or lattice-mismatched, 3-junction GaInP/ GaInAs/ Ge cells in the same build also exceeded the previous record efficiency, reaching an independently verified efficiency of 38.8% (241 suns, AM1.5, low-AOD, 25ºC), nearly equaling lattice-matched performance [1]. A large experimental matrix was used in the build, with differing tunnel junction type, amount of lattice mismatch, amount of current mismatch or J-ratio, AR coating type, gridline spacing, cell size, and other semiconductor device design parameters. Figure 2.7.1 shows the dependence of measured efficiency on the J-ratio of the cells, for lattice-matched 3-junction cells based on the 1%-In GaInAs lattice constant (Ge lattice constant), and for metamorphic 3-junction cells based on 8%-In GaInAs. The efficiency was measured under a steady-state solar simulator (Spectrolab X25) at a moderate intensity of 35-95 suns. The J-ratio was determined from quantum efficiency measurements of the GaInP top cell and the GaInAs middle cell, in multijunction cells that are on the same wafer as the cell measured by light I-V or on wafers in a similar position on the growth platter in the same MOVPE run, .

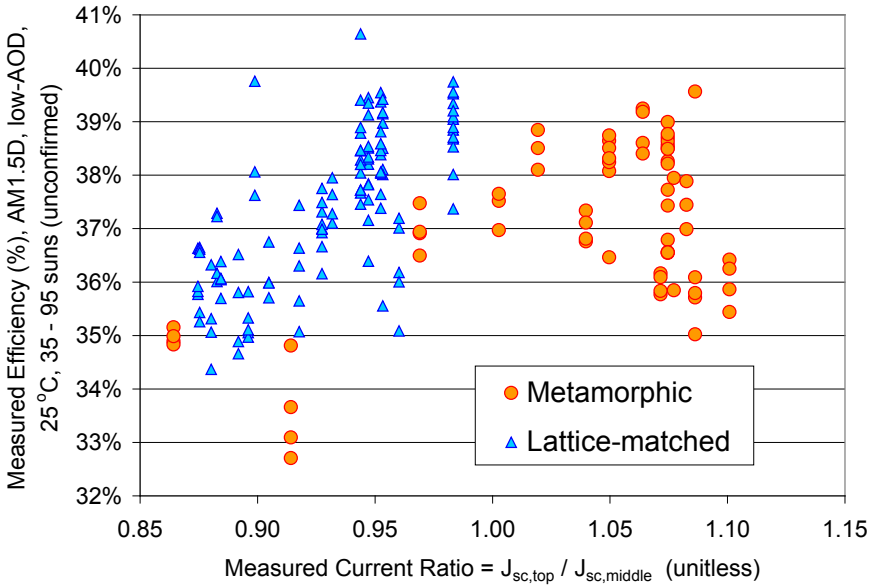

Fig. 2.7.1. Effect of J-ratio on measured lattice-matched and metamorphic cell efficiency.

As can be seen, the desired case for which the J-ratio under the standard AM1.5D, low-AOD terrestrial spectrum is equal to one is easier to achieve in the metamorphic case than in the lattice-matched case. One opportunity for efficiency improvement is to reach still higher top cell current densities, while maintaining the high voltage of the top cell, in order to explore the performance at and beyond unity J-ratio in the lattice-matched case.

These measurements are unconfirmed, as they have not been measured at an independent solar cell testing lab, such as NREL, but the X25 solar simulator was set up using reference cells for the lattice-matched and metamorphic cases that were calibrated at NREL, and so the measurements in Fig. 2.7.1 should be quite accurate. It is worth noting that a substantial number of these cells have above 39.0% efficiency, with some above the next efficiency target of 39.5% in the NREL HiPerf PV program, and one cell measured to be substantially over 40%. The data for this cell measured with over 40% efficiency is being analyzed to determine the accuracy of the measurement.

References – Section 2.7

[4] R. R. King, D. C. Law, C. M. Fetzer, R. A. Sherif, K. M. Edmondson, S. Kurtz, G. S. Kinsey, H. L. Cotal, D. D. Krut, J. H. Ermer, and N. H. Karam, "Pathways to 40%-Efficient Concentrator Photovoltaics," *Proc. 20th European Photovoltaic Solar Energy Conf.*, Barcelona, Spain, June 6-10, 2005, pp. 118-123.

2.8 Cell Development Progress Report 8

2.8.1 Lattice-Matched and Metamorphic Cell Characterization

We measured light I-V curves under concentration for lattice-matched (at the Ge lattice constant), and metamorphic (at the 8%-In GaInAs lattice constant) 3-junction solar cells fabricated using the EC-01 mask set. The cells were characterized under steady state illumination at ~120 suns using the X25 solar simulator coupled with a fresnel lens, and at 100-200 suns using the HIPSS (high-intensity pulsed solar simulator). The cells are measured on the wafer, electrically isolated from each other but still held mechanically by the Ge wafer substrate. Some cells and wafers were selected for calibrated efficiency measurements at NREL. As described earlier, concentrator solar cells built at Spectrolab have reached the highest efficiencies yet achieved for a solar photovoltaic device, at 39.0% [4], independently confirmed by NREL under the AM1.5, low-AOD spectrum. It is hoped that some of the cells in the recent measurement batch sent to NREL will approach or even exceed the 40%-efficiency threshold.

A large part of the wide range of semiconductor band gaps needed to span the solar spectrum and realize higher efficiency cell architectures can be accessed using metamorphic GaInAs and GaInP materials [4]. The ordering state on the group-III sublattice provides an additional lever for band gap adjustment, and is a particularly strong effect in GaInP. The metamorphic cells above at the 8%-In GaInAs lattice constant have a 0.5% lattice mismatch to the Ge substrate in both subcell 1 ($Ga_{0.44}In_{0.56}P$) and subcell 2 ($Ga_{0.92}In_{0.08}As$). The group-III sublattice ordering and disordering effect on band gap has been observed in both metamorphic and lattice-matched GaInP [5]

Epitaxial growth and characterization was also carried out for metamorphic cells based on higher amounts of lattice mismatch. Such subcell compositions, for instance 23%-In and 35%-In GaInAs cells with lattice mismatch values of 1.6% and 2.4% to the Ge substrate, and band gaps of 1.1-eV and 0.95-eV, respectively, enable the use of metamorphic cell architectures that have the potential to reach higher terrestrial concentrator cell efficiencies. These multijunction cell architectures achieve a wavelength division of the solar spectrum that is more efficient for solar energy conversion, by the use of subcell band gaps that can be reached with such highly lattice-mismatched materials. Two examples of high-efficiency cell architectures are shown in Fig. 2.8.1, with a transparent, metamorphic (MM) graded buffer, an inverted MM 1-eV GaInAs subcell 3, and with a lattice-matched (Al)GaInP subcell 1 and Ga(In)As subcell 2, resulting in a high-efficiency inverted metamorphic 3-junction cell structure [4].

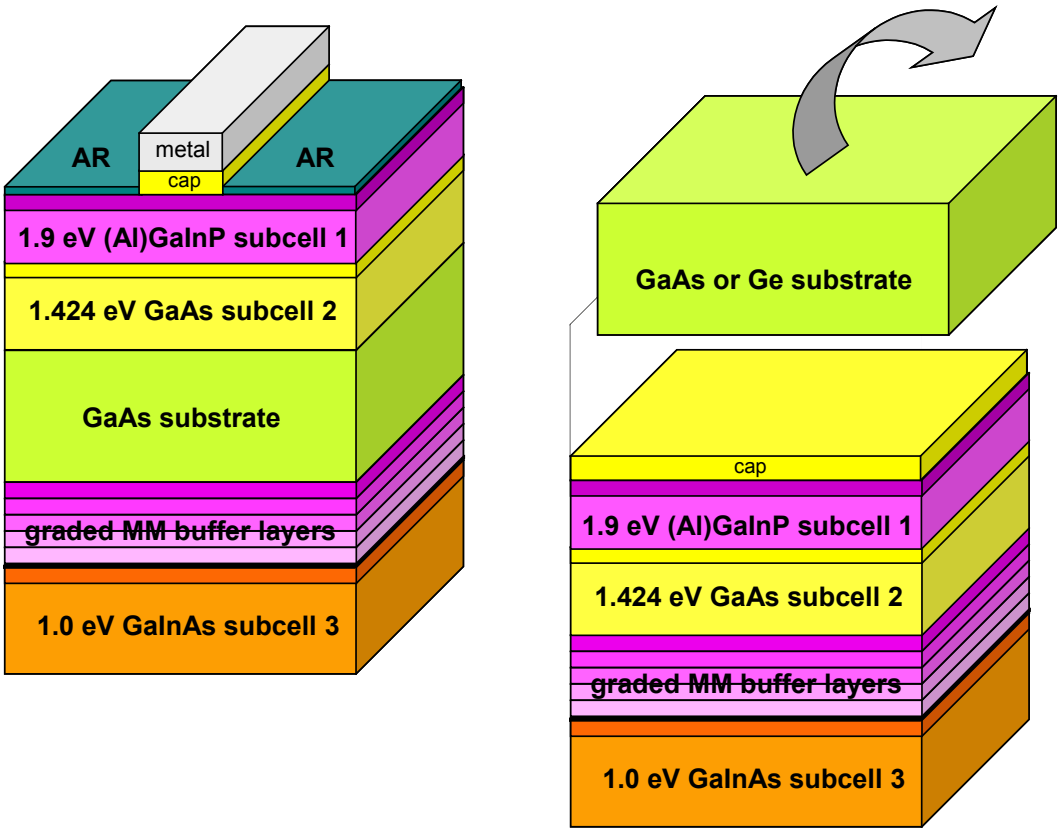

Fig. 2.8.1 Schematic diagram of 3-junction GaInP/ Ga(In)As/ GaInAs cells using transparent metamorphic (MM) graded buffer layer, and an inverted MM GaInAs subcell 3: a) with growth on both sides of a GaAs substrate, and b) with growth on one side of a GaAs or Ge substrate, followed by substrate removal.

Figure 2.8.2 shows measured internal quantum efficiency as a function of photon energy for metamorphic GaInAs solar cells out to a high lattice mismatch of 1.6% to the Ge substrate for 1.1-eV 23%-In GaInAs, and external quantum efficiency for ordered and disordered metamorphic GaInP solar cells. The GaInAs long wavelength response is nearly ideal out to the band edge of 1.12-eV GaInAs with 1.6% lattice mismatch, indicating long minority-carrier diffusion length in this metamorphic material. Disordered metamorphic GaInP with a lattice mismatch of 0.5%, corresponding to the lattice constant of 8%-In GaInAs, has an absorption edge in spectral response that is similar to that of ordered, lattice-matched GaInP, due to their similar band gaps. The ordered GaInP bases were grown thinner in order to achieve the same current density as in the disordered bases, so their softer cut-on near the band edge is due primarily to lower photogeneration in the thin bases, rather than reduced carrier collection. Additionally, the absorption coefficient for ordered GaInP near the band edge is significantly lower than for disordered GaInP, for both lattice-matched and metamorphic GaInP.

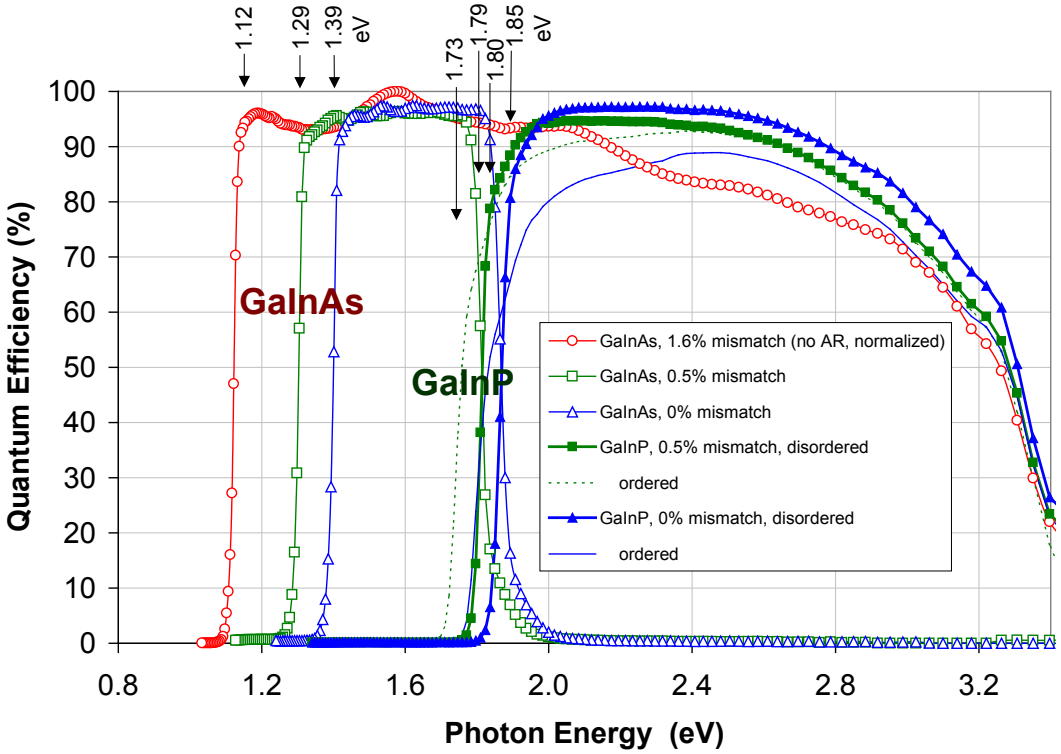

Fig. 2.8.2 Measured quantum efficiency for metamorphic (MM) and lattice-matched (LM) GaInAs and GaInP subcells. Disordered and ordered cases for the group-III sublattice of GaInP are shown, for both MM and LM materials.

2.8.2 4-junction concentrator cells

A serious limitation to terrestrial concentrator cell efficiency is the higher series resistance power loss encountered at high incident intensities. High-efficiency concentrator PV systems using III-V cells still have a significant cost component from the cells themselves, as opposed to the concentrating optical components and the balance of system, driving system design to higher concentration ratios where I^2R series resistance losses become even more severe.

A new type of 4-junction GaInP/ AlGaInAs/ GaInAs/ Ge concentrator cell architecture was grown by metal-organic vapor-phase epitaxy (MOVPE), and quick-process cells were built and tested. In this type of 4-junction, high-voltage, low-current cell [6], the current density is only 2/3 that of 3-junction cells, and the I^2R losses are $(2/3)^2$ as large, or less than half that of the conventional case. Quantum efficiency curves measured for the 4 subcells in these high-voltage concentrator cells are plotted in Fig. 2.8.3. The next steps for this avenue of research will involve optimizing 4-junction terrestrial concentrator cells for current balance among the subcells, and theoretical comparison between the striking benefit of lower series resistance loss in these 4-junction concentrator cells, and the effect of variable solar spectrum on daily and annual energy production.

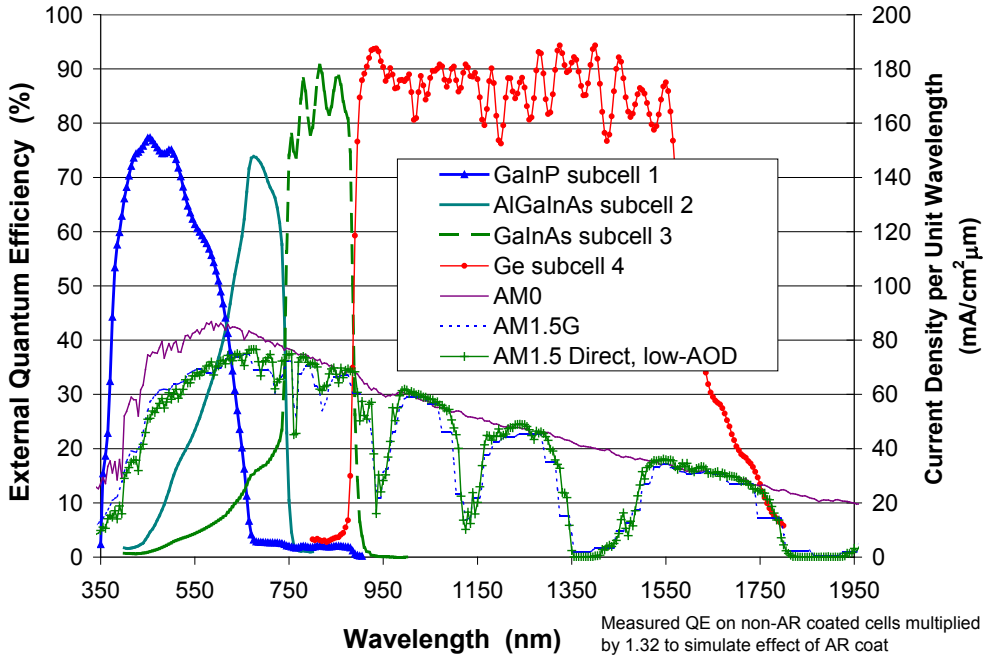

Fig. 2.8.3 Quantum efficiency measurements of the subcells in a four-junction GaInP/ AlGaInAs/ GaInAs/ Ge terrestrial concentrator cell.

2.8.3 Publications

Two abstracts were submitted to the 21st European Photovoltaic Solar Energy Conference, Dresden, Germany, to be held 4-8 Sep. 2006, one entitled "New Horizons in III-V Multijunction Terrestrial Concentrator Cell Research" on the high-efficiency terrestrial concentrator cell approaches described above, and one entitled "Concentrator Triple-Junction Solar Cells & Receivers in Point Focus and Dense Array Modules" on the concentrator triple-junction solar cells and receiver products of Spectrolab.

References – Section 2.8

[4] R. R. King, D. C. Law, C. M. Fetzer, R. A. Sherif, K. M. Edmondson, S. Kurtz, G. S. Kinsey, H. L. Cotal, D. D. Krut, J. H. Ermer, and N. H. Karam, "Pathways to 40%-Efficient Concentrator Photovoltaics," *Proc. 20th European Photovoltaic Solar Energy Conf.*, Barcelona, Spain, June 6-10, 2005, pp. 118-123.

[5] R. R. King, C. M. Fetzer, P. C. Colter, K. M. Edmondson, J. H. Ermer, H. L. Cotal, H. Yoon, A. P. Stavrides, G. Kinsey, D. D. Krut, N. H. Karam, "High-Efficiency Space and Terrestrial Multijunction Solar Cells Through Bandgap Control in Cell Structures," *Proc. 29th IEEE Photovoltaic Specialists Conf.*, New Orleans, Louisiana, May 20-24, 2002 (IEEE, New York, 2002), ISBN 0-7803-7471-1, pp. 776-781.

[6] R. R. King, P. C. Colter, D. E. Joslin, K. M. Edmondson, D. D. Krut, N. H. Karam, and Sarah Kurtz, "High-Voltage, Low-Current GaInP/GaInP/GaAs/GaInNAs/Ge Solar Cells," *Proc. 29th IEEE Photovoltaic Specialists Conf.*, New Orleans, Louisiana, May 20-24, 2002, pp. 852-855.

2.9 Cell Development Progress Report 9

Significant advances were made in the modeling of 3- and 4-junction terrestrial concentrator cells, and in experimental results for terrestrial concentrator 4-junction cells. The text and figures below (with renumbered figures, sections, and references) describing those results are from the paper "New Horizons in III-V Multijunction Terrestrial Concentrator Cell Research," [7], presented at the 21st European Photovoltaic Solar Energy Conference and Exhibition, Dresden, Germany, 4-8 Sep. 2006, and are published in the proceedings for that conference.

2.9.1 Modeling of 3- and 4-junction concentrator cells

A multijunction cell model was developed to calculate efficiency under the terrestrial AM1.5 Direct (ASTM G173-03) solar spectrum, limited only by fundamental loss mechanisms. The dependence of 3-junction and 4-junction cell performance on the bandgaps of subcells 1, 2, and 3, is shown in a series of plots with iso-efficiency contours. One such chart is shown in Fig. 2.9.1, for ideal efficiency of 3-junction cells as a function of the subcell 1 (top subcell) bandgap E_{g1} and the subcell 2 bandgap E_{g2}, with the 3rd subcell bandgap E_{g3} held constant at 0.67 eV, the bandgap of germanium.

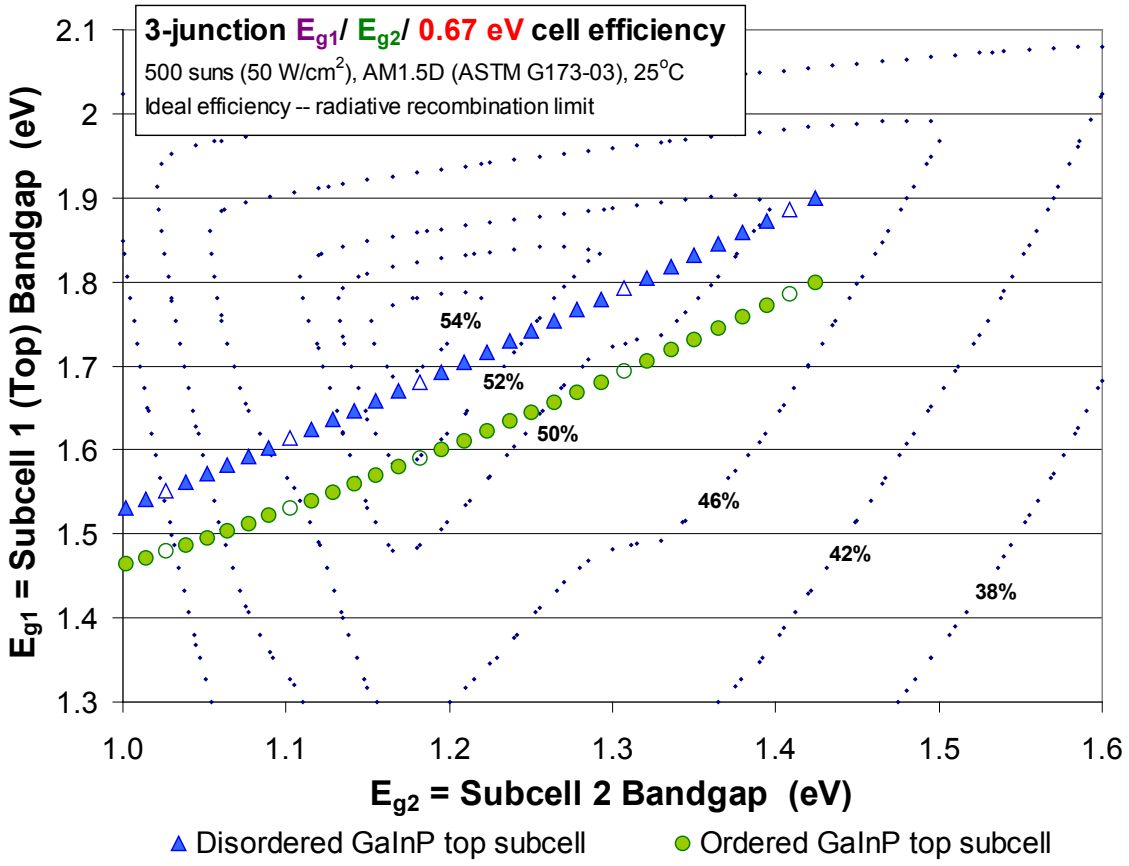

Fig. 2.9.1 Contour plot of ideal efficiencies limited by radiative recombination, for 3-junction solar cells under the concentrated terrestrial solar spectrum at 500 suns.

The basic principles used to calculate ideal efficiency of multijunction solar cells in this model are:

1. Current density is based on the flux of photons available in the terrestrial solar spectrum above the bandgap energy of each subcell;
2. Open-circuit voltage and diode saturation current density are based on the fundamental mechanism of radiative recombination [4];
3. The multijunction cell light I-V curve is based on the diode characteristics of each series-interconnected subcell at the same current density;
4. The MJ cell design allows excess photogenerated current density in one subcell to be used by the cells beneath it to achieve current matching, within a specified subset of subcells.

The number of junctions in the cell is variable, with up to 10-junction solar cells easily accommodated by the model at present.

The recombination current density J_{rec} for radiative recombination is:

$$(1) \qquad J_{rec} = qwBpn = qwBn_i^2 e^{qV/kT} = J_o\left(e^{qV/kT} - 1\right) \approx J_o e^{qV/kT}$$

for the case in which minority-carrier concentration is approximately constant across the solar cell base of thickness w, such that the diode saturation current density J_o of a solar cell limited by radiative recombination can be written:

$$(2) \qquad J_o = qwBn_i^2 = qwBN_C N_V e^{-E_g/kT}$$

where B is the radiative recombination coefficient. To model solar cell efficiency as a function of subcell bandgap, the J_o must be found for the bandgap E_g of each subcell. By far the largest dependence of J_o on E_g arises from the exponential term in Eqn. 2. Different semiconductor materials can have significantly different values of N_C , the conduction band density of states. Materials with low density-of-states electron effective mass, such as InP, InAs, and perhaps ordered GaInP, can be expected to have lower N_C , and therefore lower J_o and higher V_{oc} than they would otherwise. In the model, the values and E_g dependences of B, N_C , and N_V were based on literature expressions and values, *e.g.*, references [8-10], but these dependences are not highly critical for establishing the general trends, because the strong exponential dependence of J_o on E_g dominates.

The subcell bandgaps needed to optimize the efficiency of cells with 3, 4, and more junctions are not always accessible with conventional semiconductors lattice-matched (LM) to common substrates like Ge, GaAs, InP, or Si. Lattice-mismatched, or metamorphic (MM) materials offer much greater flexibility of subcell bandgap selection for optimizing cell

efficiencies, now up to 39.3%, provided that the increased recombination at dislocations in lattice-mismatched materials can be controlled [4,11-13]. The high lifetimes that have been achieved in metamorphic GaInAs and GaInP cells in spite of high lattice mismatch values of 1.6% and 2.4%, corresponding to 1.1-eV and 0.95-eV GaInAs bandgaps respectively [4], enable the use of more radical solar cell architectures such as inverted multijunction cells.

Bandgap combinations for a metamorphic GaInAs subcell 2 at various compositions, and a GaInP subcell 1 at the same lattice constant, are superimposed on the iso-efficiency contours in Fig. 2.9.1. The change in indium mole fraction in these MM materials allow different parts of the subcell bandgap space to be occupied, as does the degree of group-III sublattice disordering in the metamorphic GaInP top subcell. Both the cases of disordered (high E_g) and ordered (low $E_{g)}$ group-III sublattice in metamorphic GaInP are plotted in Fig. 2.9.1.

Iso-efficiency plots for 2-junction cells have been presented in some very valuable articles in the literature, for example in [14] and others. In the time elapsed since those studies, the standard reporting spectrum for terrestrial concentrator cells has changed from the previous, red-rich AM1.5D ASTM E891-92 spectrum, to the AM1.5D low-AOD spectrum, which has now been adopted as the AM1.5D ASTM G173-03 spectrum. In addition to using this up-to-date standard spectrum, the 3- and 4-junction cell efficiency contour plots in this study consider the optimum subcell bandgaps for these higher numbers of junctions. In order to be clear about which trends stem from fundamental physics and which result from real-life effects, separate contour plots are shown for ideal efficiency and for practical cell efficiency grounded in experimental cell measurements.

Figure 2.9.2 plots iso-efficiency contours where series resistance and grid shadowing have been taken into account, as well as other current, voltage, and fill factor losses, so that the calculated efficiency of a lattice-matched 3-junction GaInP/ GaInAs/ Ge cell corresponds to the experimental 39.0% 3J cell efficiency in [4], shown by the triangle in Fig. 2.9.2. This is referred to as the case normalized to measured 3J cell efficiency. Efficiencies of 41% can be seen to be practical in 3J cells with a 1.76/ 1.18/ 0.67 eV bandgap combination.

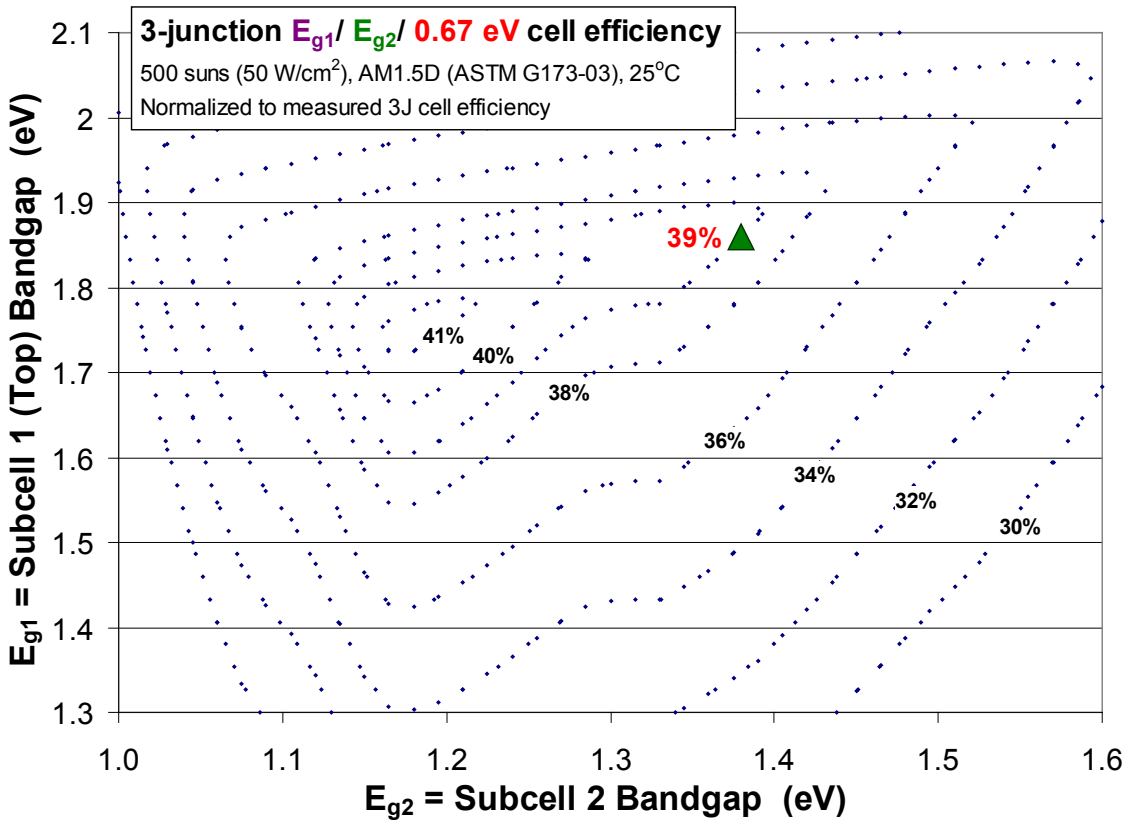

Fig. 2.9.2 Contour plot of 3-junction cell efficiencies, including the effects of grid shadowing and series resistance, and normalized to correspond to the measured 39.0% efficiency for a 3-junction solar cell.

In Fig. 2.9.3, ideal efficiency and practical efficiency contours are plotted for 3-junction solar cells, this time as a function of the subcell 2 and subcell 3 (bottom subcell) bandgaps. The triangle again indicates the bandgap combination corresponding to measured 39% 3J cell efficiency. Ideal efficiencies of 53%, and practical efficiencies of 42%, are possible for 3-junction cells with a bandgap combination of 1.90/ 1.39/ 0.97 eV. These bandgaps can be accessed through the use of GaInP and GaInAs subcells 1 and 2 lattice matched to Ge or GaAs, and a metamorphic 0.97-eV GaInAs subcell grown inverted on a transparent graded buffer layer [4,13].

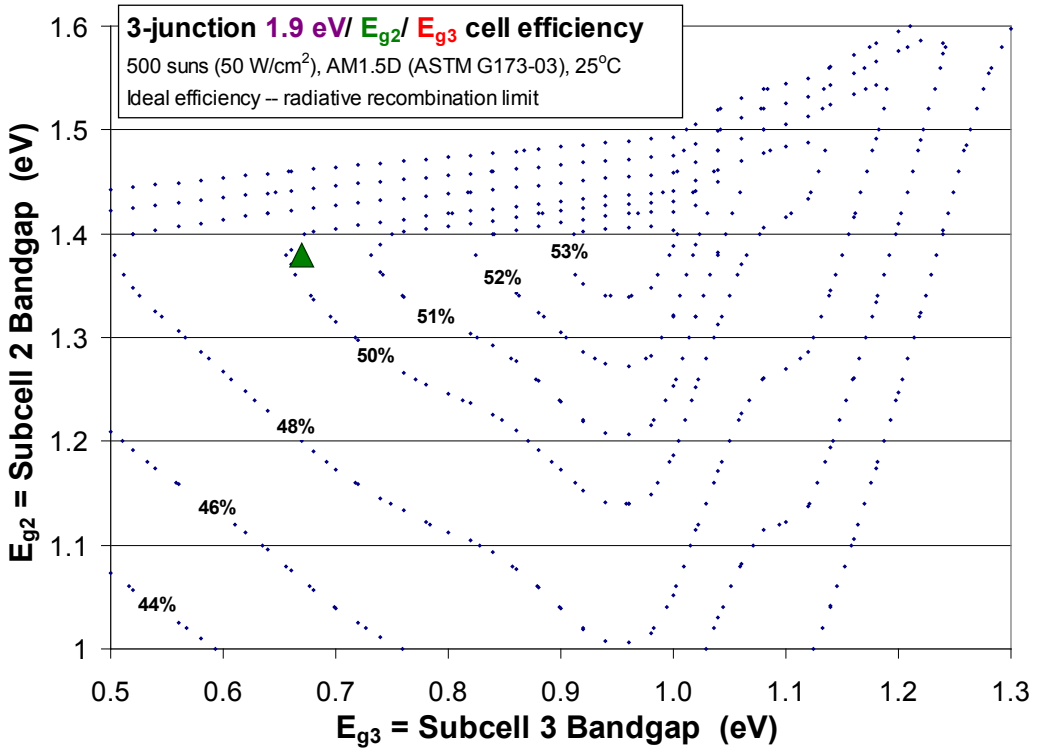

a.

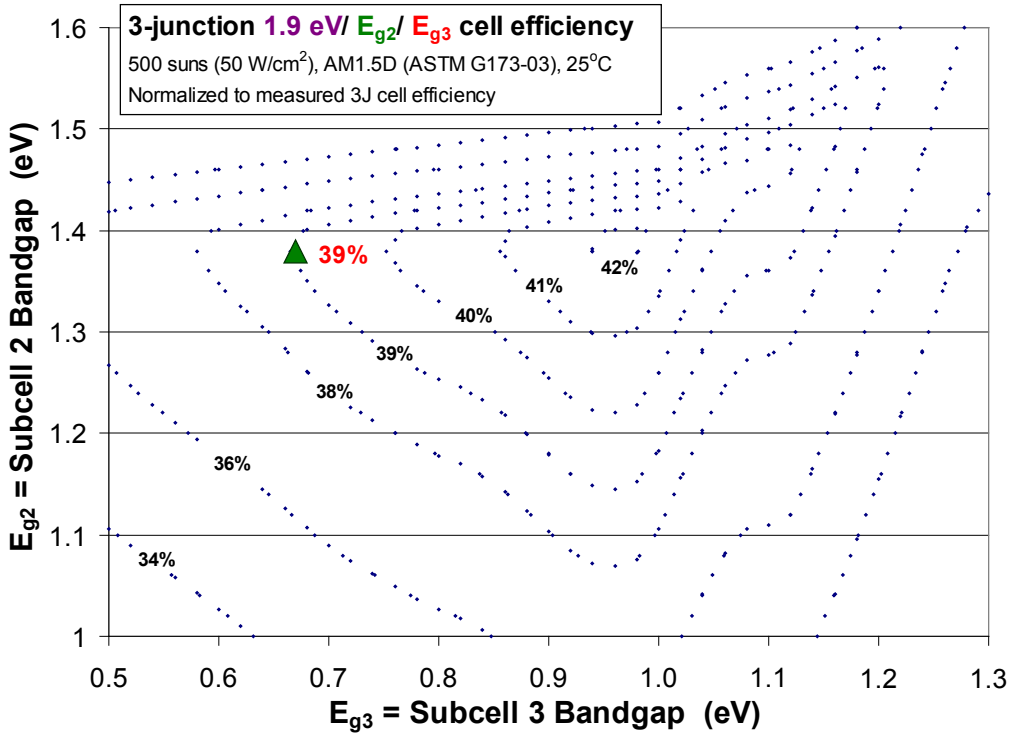

b.

Fig. 2.9.3 Contour plots of a) ideal efficiency and b) efficiency normalized to experiment (39% measurement), for 3-junction cells under the 500X terrestrial spectrum, varying subcell 3 (bottom cell) and subcell 2 bandgaps.

A 4-junction (Al)GaInP/ AlGa(In)As/ Ga(In)As/ Ge terrestrial concentrator solar cell is shown in Fig. 2.9.4, where the parentheses indicate optional elements in the subcell composition. This type of cell divides the photon flux available in the terrestrial solar spectrum above the bandgap of the GaInAs subcell 3 into 3 pieces, rather than 2 pieces in the case of a 3-junction cell. As a result, the current density of a 4-junction cell is roughly 2/3 that of a corresponding 3-junction cell, and the I^2R resistive power loss is approximately $(2/3)^2 = 4/9$, or less than half that of a 3-junction cell.

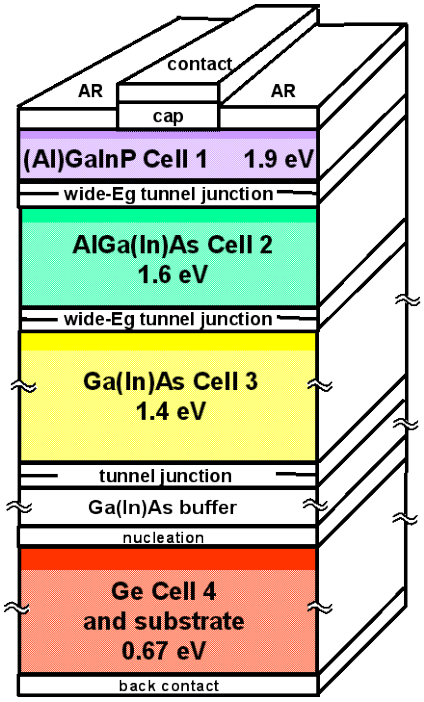

Fig. 2.9.4 4-junction AlGaInP/ AlGaInAs/ GaInAs/ Ge terrestrial concentrator solar cell cross section.

Iso-efficiency contours for 4-junction terrestrial concentrator cells, under the AM1.5D (ASTM G173-03) solar spectrum at 500X, are plotted in Fig. 2.9.5 as a function of the bandgaps of subcells 2 and 3. Ideal 4J cell efficiency is plotted in Fig. 2.9.5a, and practical cell efficiency, consistent with the measured efficiency of 39% for 3J cells, in Fig. 2.9.5b. The bandgap of subcell 1 is held at 1.9 eV, corresponding to GaInP at the Ge lattice constant with a disordered group-III sublattice, and subcell 4 (the bottom subcell) is fixed at the 0.67-eV bandgap of Ge, for this analysis.

The diamond in the plots indicates the 1.62/ 1.38 eV bandgap combination of the AlGaInAs subcell 2 and GaInAs subcell 3 of a 4-junction cell described later (see the quantum efficiency measurement in Fig. 2.9.6). Ideal efficiencies of over 58%, and practical cell efficiencies of 47% are possible for 4-junction terrestrial concentrator cells with a bandgap combination of 1.90/ 1.43/ 1.04/ 0.67 eV. It is worth noting that these practical 4J cell efficiencies are about 5 absolute efficiency points over those for 3-junction cells. 4-junction cells benefit from reduced resistive power losses as described above, and for this bandgap combination, more efficient use of the terrestrial solar spectrum.

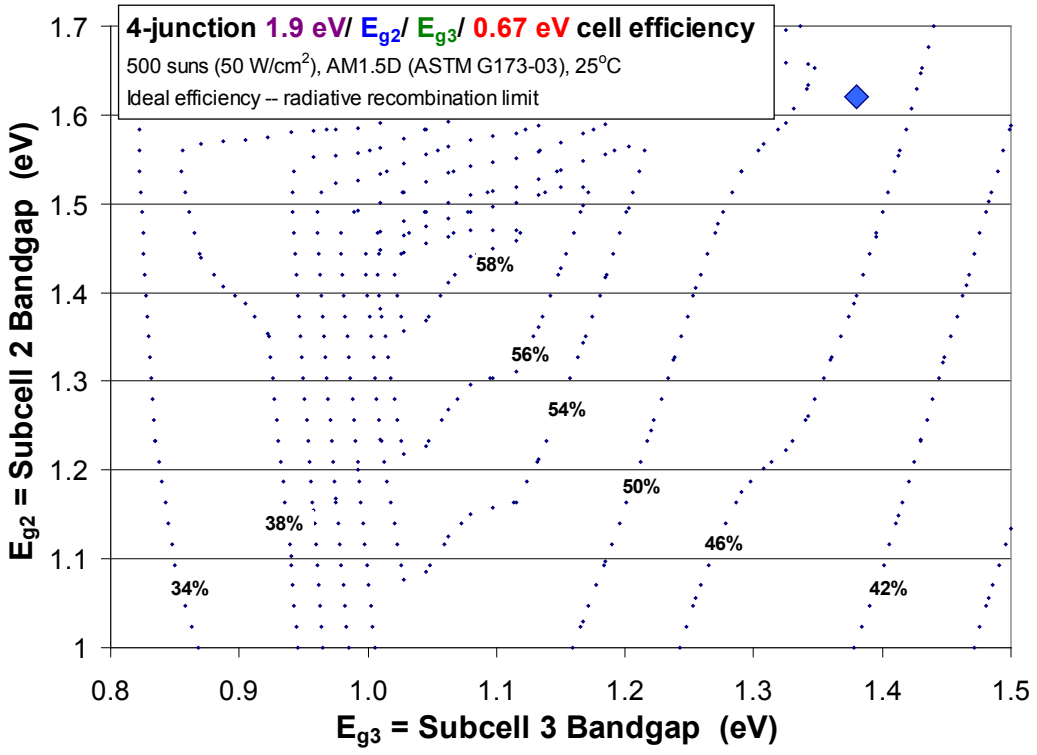

a.

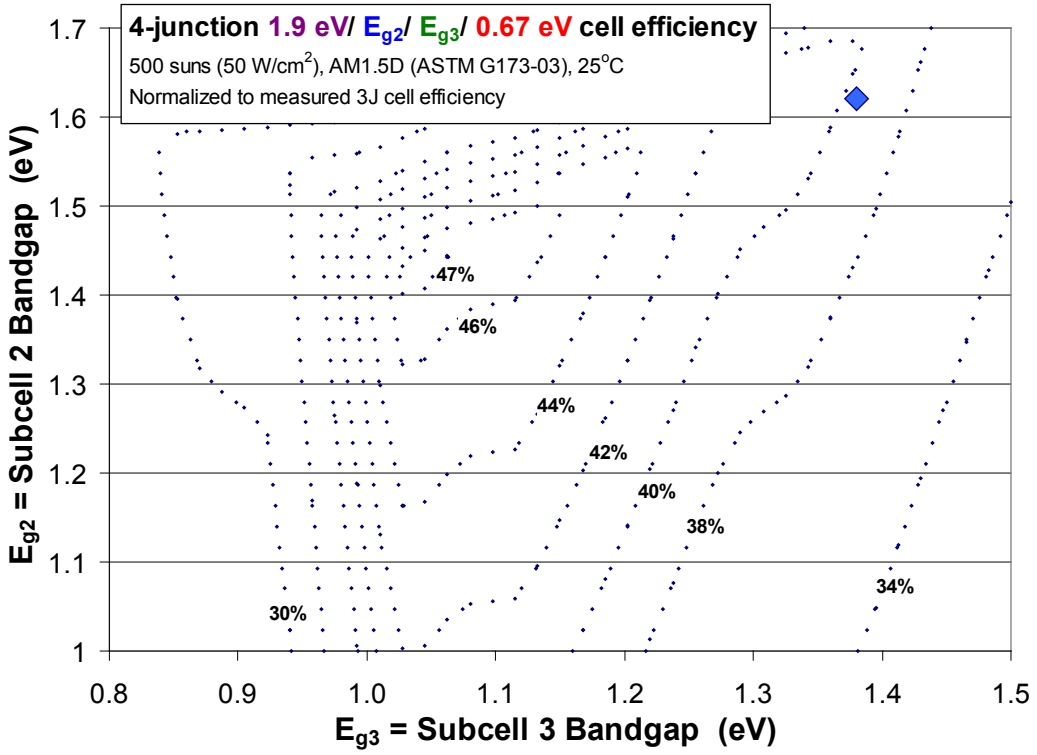

b.

Fig. 2.9.5 Contour plots of a) ideal efficiency and b) efficiency normalized to experiment, for 4-junction solar cells, with variable subcell 3 and subcell 2 bandgaps.

2.9.2 4-Junction Cell Experimental Results

4-junction cells designed for the terrestrial solar spectrum and the high current densities of concentrator operation have been grown by metal-organic vapor-phase epitaxy (MOVPE), processed into devices, and tested. The external quantum efficiency of one such 4J cell is plotted in Fig. 2.9.6 versus photon energy. The bandgaps of each subcell can be determined from the quantum efficiency data, and the extracted values are listed in the legend. By convoluting with the terrestrial AM1.5D (ASTM G173-03) spectrum the current density of each subcell can also be determined. The current densities are 9.24, 9.24, 9.58, and 21.8 mA/cm2 for subcells 1, 2, 3, and 4, respectively, such that the subcells are very close to being current matched for this 4J cell.

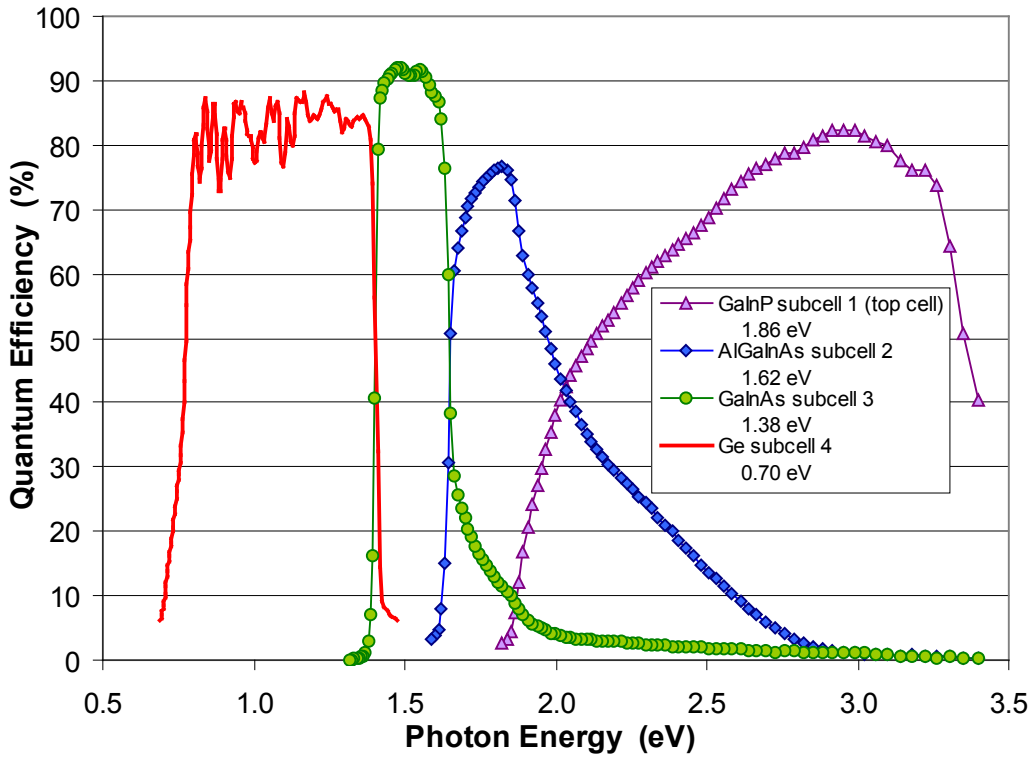

Fig. 2.9.6 External quantum efficiency of a 4-junction GaInP/ AlGaInAs/ GaInAs/ Ge terrestrial concentrator cell.

As noted above, the text and figures in this section (with renumbered figures, sections, and references) are from the paper "New Horizons in III-V Multijunction Terrestrial Concentrator Cell Research," [7], presented at the 21st European Photovoltaic Solar Energy Conference and Exhibition, Dresden, Germany, 4-8 Sep. 2006, and are published in the proceedings for that conference.

References – Section 2.9

[4] R. R. King, D. C. Law, C. M. Fetzer, R. A. Sherif, K. M. Edmondson, S. Kurtz, G. S. Kinsey, H. L. Cotal, D. D. Krut, J. H. Ermer, and N. H. Karam, "Pathways to 40%-Efficient Concentrator Photovoltaics," *Proc. 20th European Photovoltaic Solar Energy Conf.*, Barcelona, Spain, June 6-10, 2005, pp. 118-123.

[7] R. R. King, R. A. Sherif, D. C. Law, J. T. Yen, M. Haddad, C. M. Fetzer, K. M. Edmondson, G. S. Kinsey, H. Yoon, M. Joshi, S. Mesropian, H. L. Cotal, D. D. Krut, J. H. Ermer, and N. H. Karam, "New Horizons in III-V Multijunction Terrestrial Concentrator Cell Research," *Proc. 21st European Photovoltaic Solar Energy Conference and Exhibition*, Dresden, Germany, Sep. 4-8, 2006 (Munich, WIP-Renewable Energies, 2006) (ISBN: 3-936338-20-5), pp. 124-128.

[8] R. K. Ahrenkiel, "Minority-Carrier Lifetime in III-V Semiconductors," Chap. 2, in *Semiconductors and Semimetals*, Vol. 39, Eds. R. K. Willardson, A. C. Beer, E. R. Weber (Academic Press, New York, 1993).

[9] R. N. Hall, *Proc. Inst. Elect. Eng.*, 106B, Suppl. 17, 983 (1960).

[10] S. Adachi, *GaAs and Related Materials*, (World Scientific, River Edge, NJ, 1994).

[11] F. Dimroth, U. Schubert, and A. W. Bett, "25.5% Efficient Ga0.35In0.65P/Ga0.83In0.17As Tandem Solar Cells Grown on GaAs Substrates," *IEEE Electron Device Lett.*, 21, p. 209 (2000).

[12] R. R. King et al., "Metamorphic GaInP/GaInAs/Ge Solar Cells," *Proc. 28th IEEE Photovoltaic Specialists Conf. (PVSC)*, Sep. 15-22, 2000, Anchorage, Alaska, pp. 982-985.

[13] M. W. Wanlass et al., "Lattice-Mismatched Approaches for High-Performance, III-V, Photovoltaic Energy Converters," *Proc. 31st IEEE PVSC*, Lake Buena Vista, Florida, Jan. 3-7, 2005, p. 530.

[14] M. W. Wanlass et al., "Advanced High-Efficiency Concentrator Tandem Solar Cells," *Proc. 22nd IEEE PVSC*, 1991, p. 38.

2.10 Cell Development Progress Report 10

2.10.1 40.7%-Efficient Metamorphic GaInP/ GaInAs/ Ge Triple-Junction Solar Cell

The 40.7%-efficient metamorphic cell result and associated analysis is published in the paper "40% efficient metamorphic GaInP / GaInAs / Ge multijunction solar cells" [1] in *Applied Physics Letters*, and the paper "Metamorphic Concentrator Solar Cells with Over 40% Conversion Efficiency" [15] in *Proc. 4th International Conference on Solar Concentrators (ICSC-4)*. The material below (with renumbered figures and references) is from those papers.

As high as the efficiencies of multijunction III-V concentrator solar cells are, they can be made higher if the combination of subcell bandgaps for the multijunction solar cell can be chosen from semiconductors that are not all lattice-matched to the same growth substrate. Metamorphic multijunction solar cells, in which one or more of the subcells are lattice-mismatched to the growth substrate, offer flexibility in bandgap selection that raises the theoretical efficiency of solar cells. Experiments on step-graded buffers, used to transition from the substrate to the subcell lattice constant, have been used to control the classic problem of dislocations in the active cell regions due to the lattice mismatch. Metamorphic 8%-In GaInAs single-junction cells were built and tested with a bandgap-voltage offset (E_g/q) - V_{oc} of 0.42 V at one sun (where smaller is better), essentially the same as GaAs control cells, reflecting the long minority-carrier lifetimes that can be achieved in metamorphic materials.

A large experimental matrix of 3-junction GaInP/GaInAs/Ge terrestrial concentrator cells was carried out, using metamorphic and lattice-matched configurations, optimization of current ratio, and a variety of high-efficiency semiconductor device structures, cell sizes, grid patterns, and fabrication processes. A metamorphic $Ga_{0.44}In_{0.56}P$/ $Ga_{0.92}In_{0.08}As$/ Ge 3-junction solar cell from these experiments has reached a record 40.7% efficiency at 240 suns [1, 15], independently verified at the National Renewable Energy Laboratory (NREL) under the standard reporting spectrum for terrestrial concentrator cells (AM1.5 direct, low-AOD, 24.0 W/cm^2 25°C). This solar cell had the highest solar conversion efficiency of any type of photovoltaic device from the time it was measured in 2006 until 2008, and is the first solar cell to reach over 40% efficiency.

Figure 2.10.1 shows the light I-V curve of the 40.7%-efficient 3-junction cell. The open-circuit voltage of this metamorphic concentrator cell is 2.911 V, the responsivity is 0.1597 A/W, and the fill factor is 87.5%, all at the peak efficiency concentration of 240 suns. A lattice-matched 3-junction GaInP/ GaInAs/ Ge cell at Spectrolab has also been achieved recently with over 40% efficiency. This lattice-matched concentrator cell, which has been independently confirmed at NREL, has a V_{oc} of 3.054 V, responsivity of 0.1492 A/W, fill factor of 88.13%, and an efficiency of 40.15% at 135 suns (AM1.5 direct, low-AOD, 13.5 W/cm^2 25°C). The illuminated I-V curve of the lattice-matched 40.1% cell, and of the metamorphic 40.7% cell, are shown along with earlier record lattice-matched and metamorphic one-sun cells, in Fig. 2.10.2.

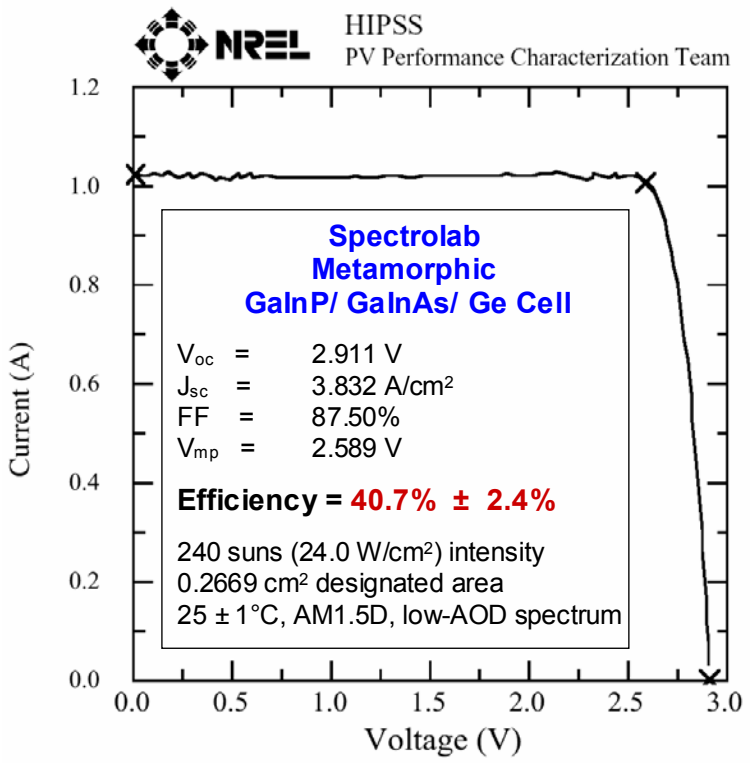

Fig. 2.10.1 Illuminated I-V curve of record 40.7%-efficiency metamorphic 3-junction terrestrial concentrator cell. This solar cell is the first solar cell of any type to reach over 40% efficiency.

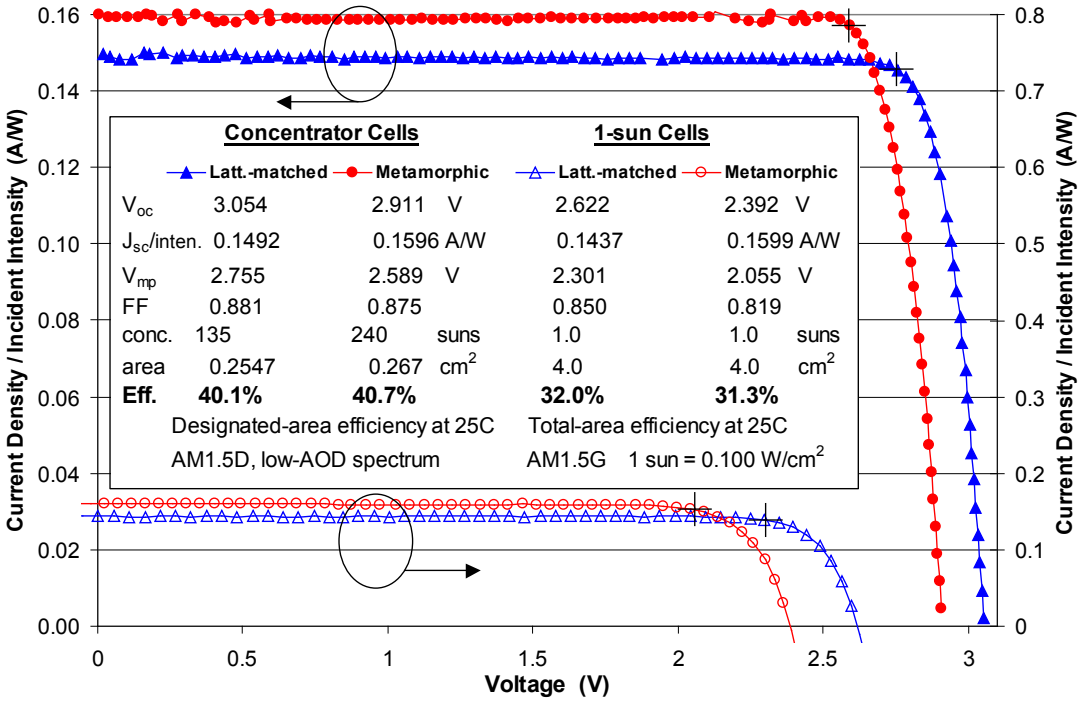

Fig. 2.10.2 Illuminated current-voltage characteristics of record 40.7%-efficient metamorphic and 40.1%-efficient lattice-matched concentrator solar cells, and earlier record-efficiency one-sun cells, with responsivity = (current density / incident intensity) plotted on the vertical axis.

These new record solar cell efficiencies can be plotted against the efficiencies calculated using the model described in the last progress report, and in [7]. Figure 2.10.3 shows the iso-efficiency contours for ideal calculated efficiency of 3-junction solar cells limited only by the fundamental mechanism of radiative recombination, plotted against subcell 1 (top subcell) bandgap E_{g1} and subcell 2 (middle subcell) bandgap E_{g2} . The experimental data points corresponding to the record efficiency metamorphic (MM) 40.7% cell and the lattice-matched (LM) 40.1% cell are plotted, using the values of top and middle cell bandgap for each cell determined from quantum efficiency measurements. Figures 2.10.3 and 2.10.4 also plot the bandgap combinations for GaInP and GaInAs lattice matched to each other for a range of In compositions and lattice mismatch values with respect to the Ge substrate, both for GaInP with a disordered group-III sublattice (high E_g), and with an ordered sublattice (low E_g).

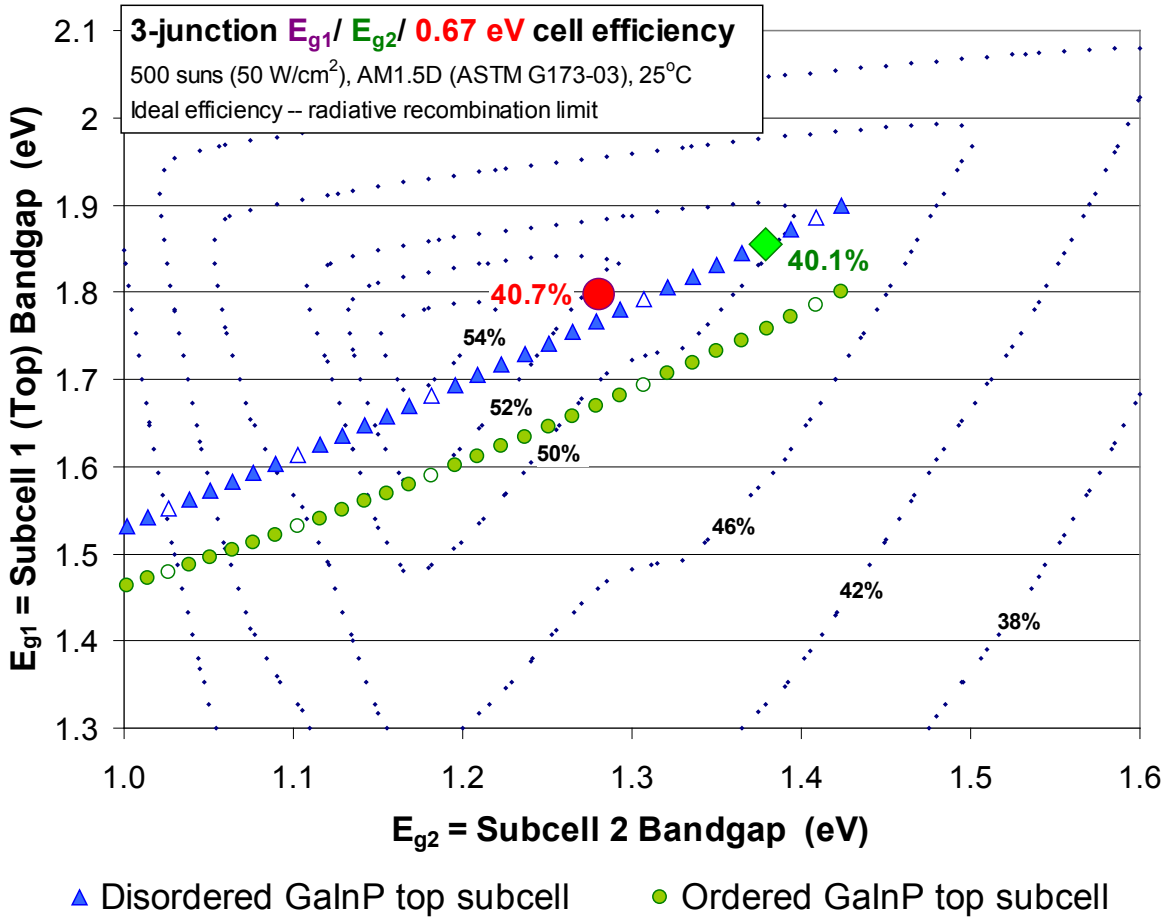

Fig. 2.10.3 Iso-efficiency contours of calculated ideal efficiency of 3-junction cells with a 0.67-eV Ge subcell 3 (bottom subcell), based on the fundamental limit of radiative recombination and on the standard AM1.5D, ASTM G173-03 terrestrial concentrator solar spectrum. The experimental data points corresponding to the record efficiency metamorphic 40.7% cell and the lattice-matched 40.1% cell are plotted for comparison.

The advantage of the metamorphic design is that the bandgap combination of the top two cells is more favorable from a theoretical perspective than that of the lattice-matched cell. In the past, Shockley-Read-Hall recombination due to crystal defects caused by the lattice mismatch has limited the extent to which this theoretical advantage of metamorphic cells could be realized in practice. With the recent experimental results of the record efficiency cells plotted in Fig. 2.10.3, one can see that the more favorable position of the MM cell in (E_{g2} , E_{g1}) space is benefiting the actual performance metamorphic 40.7% cell, compared to the 40.1% lattice-matched cell, by an amount consistent with that predicted by theory.

In Fig. 2.10.4, iso-efficiency contours are plotted based on the radiative recombination limit as before, but now with the shadowing and resistive effects of the concentrator cell metal grid included as well. The experimental points corresponding to the MM 40.7% cell and the LM 40.1% cell are plotted for comparison to the calculated values. By examining the differences between the measured efficiencies achieved to date, and the ideal efficiencies in Fig. 2.10.3 or the efficiencies with series resistance and grid shadowing included as in Fig. 2.10.4, the opportunities for future improvements in cell efficiency were identified, leading up to the recent MM 40.7% and LM 40.1% cell results. This methodology can be applied to identify further technologies to focus on in the cell design to increase efficiency still more in the future, in ways that are consistent with the fundamental limits imposed by semiconductor device physics.

In comparing the actual cell performance of the MM 40.7% cell to the theoretical performance with series resistance included at 240 suns, the modeled fill factor is almost exactly the same as the value measured for this cell (87.8% modeled vs. 87.5% measured). However, we should ultimately be able to reach an efficiency of 47.3% according to this model. This focuses attention on the V_{oc} , which is 78 mV per cell (233 mV total) lower in the actual cell than that allowed by radiative recombination, and current generation, which is 6.8% lower in the actual cell than is possible based on the AM1.5 Direct, ASTM G173-03 terrestrial solar spectrum, due to non-ideal reflectance and minority-carrier recombination effects. Further gains in efficiency can be achieved in the future using bandgap combinations that are closer to the peak efficiency shown in the contour plots in Figs. 2.10.3 and 2.10.4, by using a higher bandgap subcell 3 (bottom subcell in these 3-junction cells), and by the exploration of multijunction solar cells with 4 or more junctions as discussed in the next section.

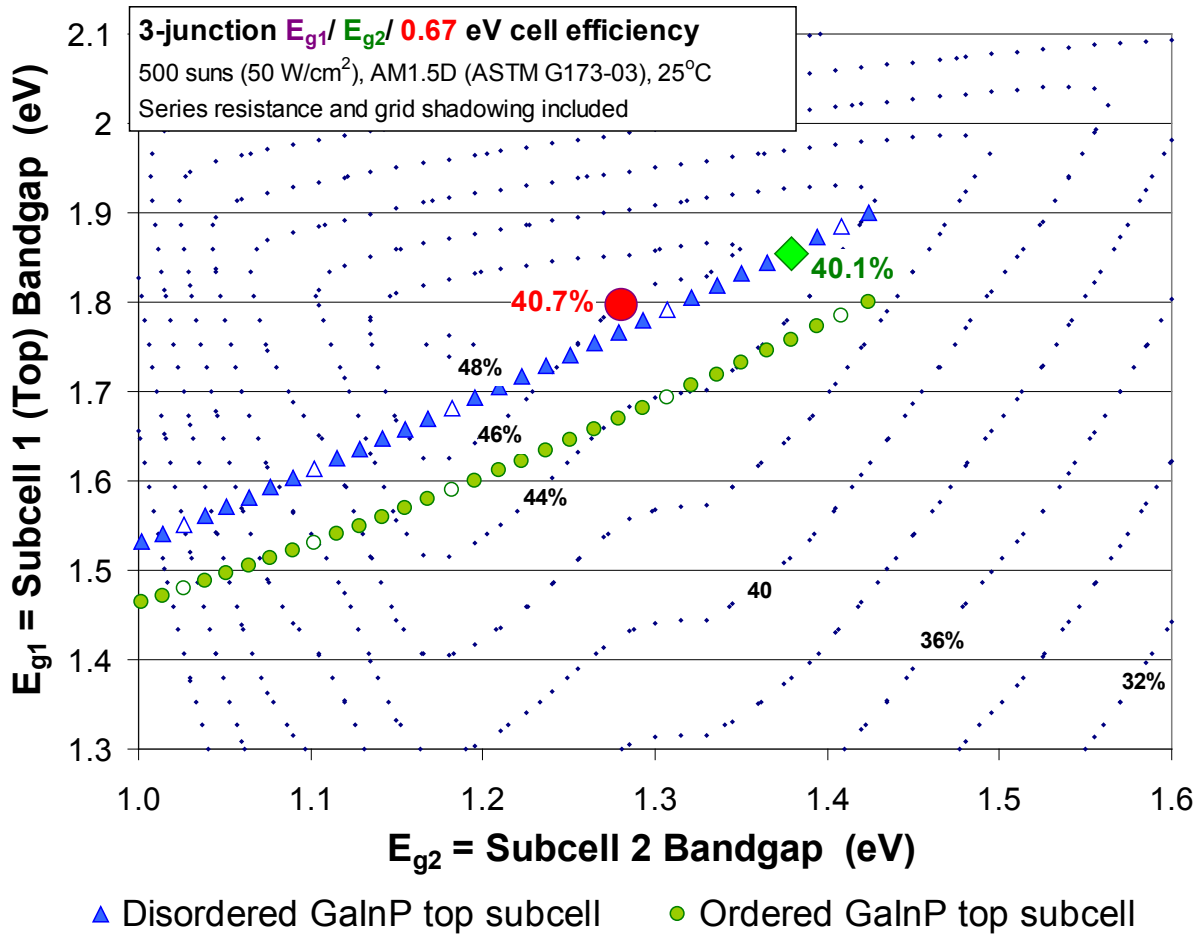

Fig. 2.10.4 Iso-efficiency contours for terrestrial 3-junction concentrator cells based on the radiative recombination limit, and with the additional real-life effects of metal grid shadowing and series resistance included. The experimental data points corresponding to the record efficiency metamorphic 40.7% cell and the lattice-matched 40.1% cell are plotted for comparison, allowing identification of opportunities for future efficiency increases.

As noted above, the 40.7%-efficient metamorphic cell result and associated analysis is published in the paper "40% efficient metamorphic GaInP / GaInAs / Ge multijunction solar cells" [1] in *Applied Physics Letters*, and the paper "Metamorphic Concentrator Solar Cells with Over 40% Conversion Efficiency" [15] in *Proc. 4th International Conference on Solar Concentrators (ICSC-4)*. The material in this section (with renumbered figures and references) is from those papers.

2.10.2 Experimental Results for 4-Junction Terrestrial Concentrator Cells

Significant advances in experimental results for terrestrial concentrator 4-junction cells, and in the modeling of the energy production of 3-, 4-, 5-, and 6-junction cells under the ever-changing terrestrial solar spectrum. The text and figures in sections 2.10.2 and 2.10.3 below (with renumbered figures and references) describing those results are from the paper "New Horizons in III-V Multijunction Terrestrial Concentrator Cell Research," [7], presented at the 21st European Photovoltaic Solar Energy Conference and Exhibition, Dresden, Germany, 4-8 Sep. 2006, and are published in the proceedings for that conference.

Four-junction terrestrial concentrator cells offer the potential for higher efficiency not only due to a finer division of the solar spectrum, but also because their high-voltage, low-current design cuts series resistance power losses significantly under concentration. Illuminated light I-V curves are shown in Fig. 2.10.5 for a 4-junction GaInP/ AlGaInAs/ GaInAs/ Ge solar cell measured at 256 suns, and for a similar solar cell with only the upper 3 junctions active (inactive Ge). The open-circuit voltage of the 4-junction cell is 4.364 V, compared to 3.960 V for the cell with an inactive subcell 4, indicating the Ge bottom cell accounts for about 400 mV of the V_{oc} at this concentration. I-V curves for earlier record efficiency cells, a 39.0% lattice-matched cell, and the previous record 39.3%-efficient metamorphic 3-junction cell, are also shown in the figure. Preliminary measured efficiency for the still non-optimized 4J cell is 35.7% at 256 suns.

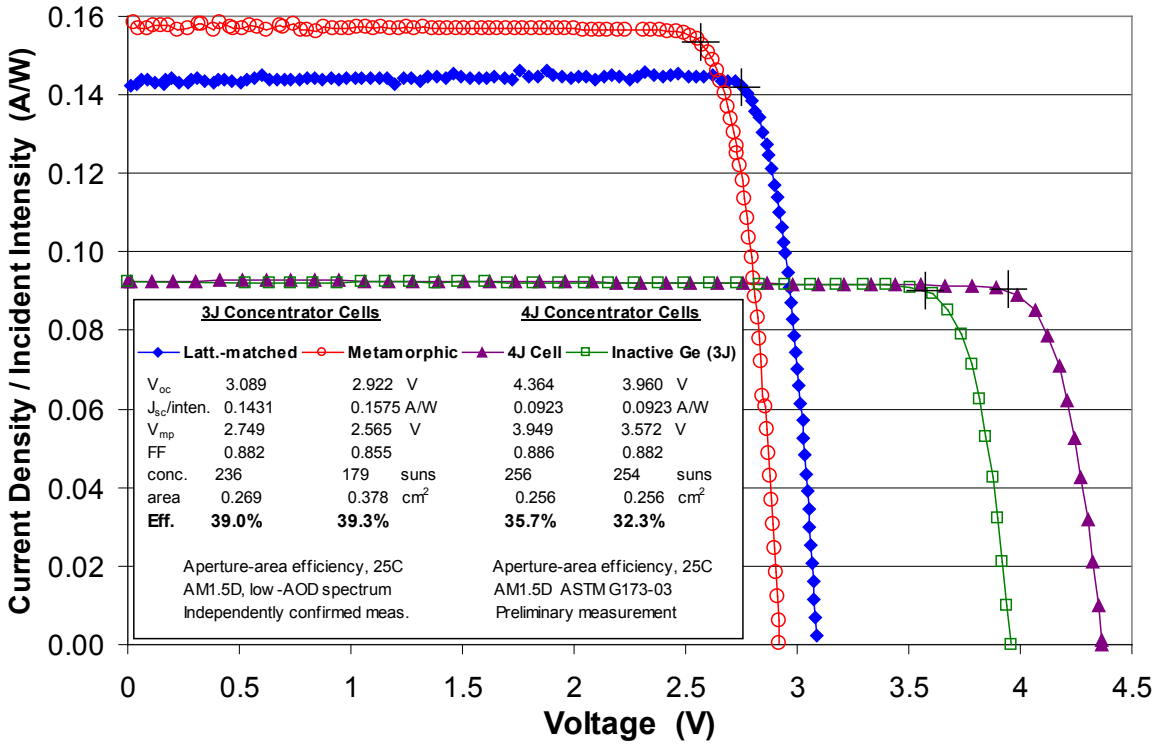

Fig. 2.10.5 Illuminated I-V characteristics of an unoptimized 4-junction terrestrial concentrator cell with 35.7% efficiency, and V_{oc} over 4.3 volts. I-V curves for the previous record 39.0%-efficient lattice-matched cell and 39.3%-efficient metamorphic 3-junction cells are also shown.

2.10.3 Modeling of Energy Production Over Typical Day for 3- to 6-Junction Cells

The variable angle of the sun causes a change in the air mass that sunlight must traverse before hitting the earth's surface, which tends to diminish the blue wavelengths of the solar spectrum more than longer wavelengths, as shown in Fig. 2.10.6. This results in a shift in current balance among the subcells between solar noon and the hours of the early morning or late afternoon.

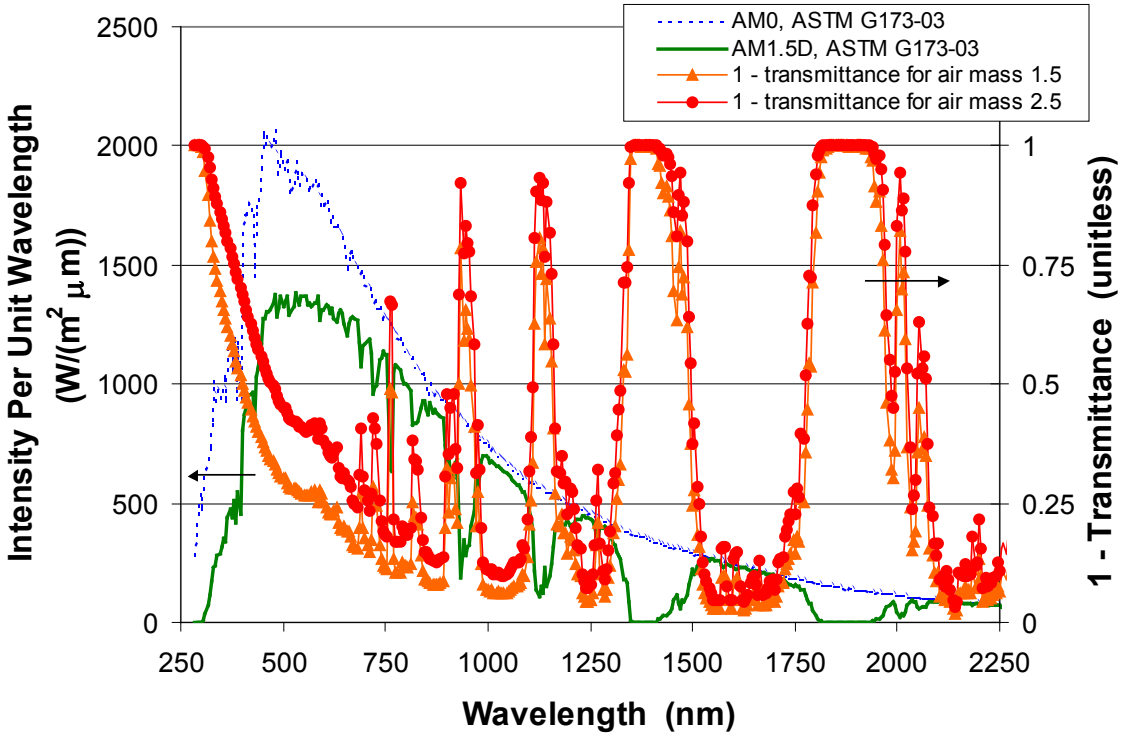

Fig. 2.10.6 Attenuation of light intensity due to the atmosphere, for air mass 1.5 and 2.5.

When considering cells with 3, 4, 5, 6, or even more junctions under the shifting terrestrial solar spectrum, the question arises as to "which number of junctions is best for energy production over the day and year?" Energy production over the course of the day is calculated using ideal and practical efficiencies from the model described in the last quarterly report in order to answer this question. The calculations are for the autumnal equinox, to provide data for a typical day of the year, halfway between summer and winter.

The sun angle and air mass are calculated as a function of time on the autumnal equinox, and the terrestrial solar spectrum is calculated at 15 minute intervals based on the difference between the AM0 and the AM1.5D solar spectra in the ASTM G173-03 standard. Energy production is calculated for 3-, 4-, 5-, and 6-junction cells lattice-matched to Ge. Each type of MJ cell is first current balanced at a particular time of day, say at 12 noon or 3 PM (15:00 hours), by adjusting the bandgap of the subcells above the 1.4-eV GaInAs subcell. The cells can also be current balanced for a particular air mass by adjusting subcell thicknesses. The energy production is then calculated for that fixed cell design under each spectrum as a function of time of day.

Figure 2.10.7 shows the energy production over the course of the day for 3-, 4-, 5-, and 6-junction cells, using practical cell efficiencies normalized to measured 3J cell efficiency. Each cell design was current balanced for the 1.75 air mass at 3 PM, near the optimum time of day for current balancing. The total intensity available in the solar spectrum as a function of time of day is also plotted for comparison, on a different axis. At extremely high air masses, the MJ cells with 4 and more junctions do have lower efficiency than 3-junction cells, but this has a negligible effect on total energy production for the day. For the vast majority of daylight hours, the energy production increases for each junction added to the MJ cell, for the MJ cell configurations in this study. This is due largely to the lower resistive power loss for cells with more junctions, and also to more efficient use of the solar spectrum. The increase in 4J cell energy production is substantially larger than for 3J cells, while the increase for 5J cells is smaller. The large difference between 5J cells and 6J cells is due to the inclusion of a 1-eV subcell 5 in the 6-junction case.

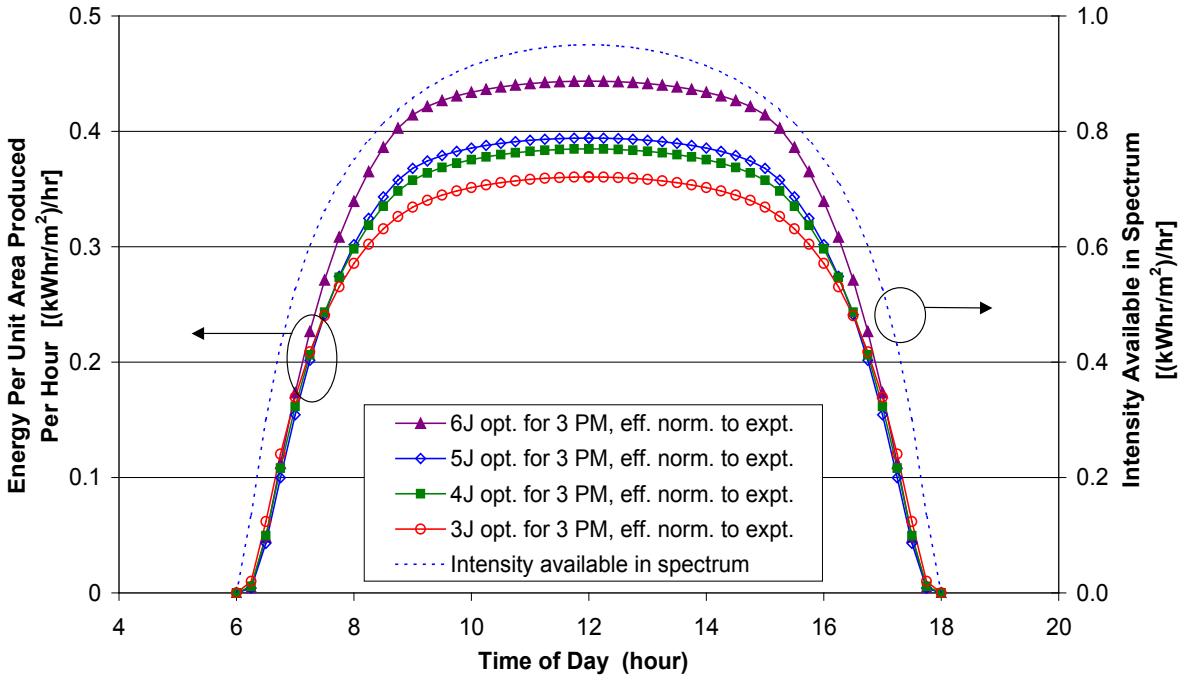

Fig. 2.10.7 Energy production of multijunction cells with 3 to 6 junctions, with cell efficiency normalized to correspond to experimental values. Due largely to reduced series resistance losses, the energy production increases with each additional junction.

Figure 2.10.8 plots the energy produced per day for cells with 3 to 6 junctions, as a function of the time of day at which the MJ cell is current balanced. Current balance at 12 noon can be seen to be a local minimum for energy production, and the energy production is maximized if the cell is instead current balanced for the spectrum at 2:30-3:00 PM (or equivalently, 9:00-9:30 in the morning). The difference between current balancing at 12 noon and at the more optimal time later in the day becomes more pronounced with an increasing number of junctions. As before, the total energy generation per day is seen to increase with each added junction, in spite of concerns about current matching under variable air mass.

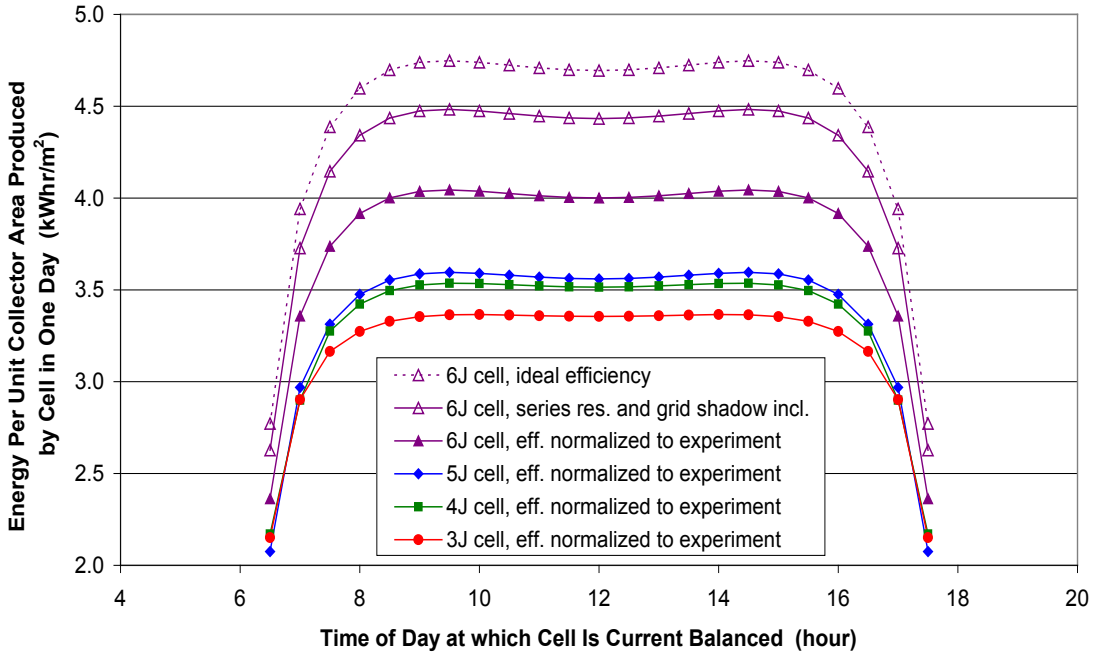

Fig. 2.10.8 Energy production per day of terrestrial concentrator cells with 3 to 6 junctions, as a function of the time of day at which subcells are current balanced.

As noted above, the text and figures in sections 2.10.2 and 2.10.3 (with renumbered figures and references) are from the paper "New Horizons in III-V Multijunction Terrestrial Concentrator Cell Research," [7], presented at the 21st European Photovoltaic Solar Energy Conference and Exhibition, Dresden, Germany, 4-8 Sep. 2006, and are published in the proceedings for that conference.

References – Section 2.10

[1] R. R. King, D. C. Law, K. M. Edmondson, C. M. Fetzer, G. S. Kinsey, H. Yoon, R. A. Sherif, and N. H. Karam, "40% efficient metamorphic GaInP / GaInAs / Ge multijunction solar cells," *Appl. Phys. Lett.*, Vol. 90, No. 18, 183516, 4 May 2007.

[7] R. R. King, R. A. Sherif, D. C. Law, J. T. Yen, M. Haddad, C. M. Fetzer, K. M. Edmondson, G. S. Kinsey, H. Yoon, M. Joshi, S. Mesropian, H. L. Cotal, D. D. Krut, J. H. Ermer, and N. H. Karam, "New Horizons in III-V Multijunction Terrestrial Concentrator Cell Research," *Proc. 21st European Photovoltaic Solar Energy Conference and Exhibition*, Dresden, Germany, Sep. 4-8, 2006 (Munich, WIP-Renewable Energies, 2006) (ISBN: 3-936338-20-5), pp. 124-128.

[15] R. R. King, D. C. Law, K. M. Edmondson, C. M. Fetzer, G. S. Kinsey, D. D. Krut, J. H. Ermer, R. A. Sherif, and N. H. Karam, "Metamorphic Concentrator Solar Cells with Over 40% Conversion Efficiency," *Proc. 4th International Conference on Solar Concentrators (ICSC-4)*, El Escorial, Spain, March 12-16, 2007 (ISBN: 978-84-690-6463-4), pp. 5-8.

2.11 Cell Development Progress Report 11

The latest technical results were presented in the Jan. 23 High Performance PV program review, on:

- achievement of a record 40.7%-efficiency metamorphic 3-junction cell, the first solar cell to reach over 40% efficiency, and the highest solar conversion efficiency achieved to date for any type of photovoltaic device;

- achievement of a lattice-matched 40.1%-efficiency 3-junction cell, also over the 40% milestone;

- modeling developed for 3- and 4-junction terrestrial concentrator solar cell efficiency, capable of handling up to 10-junction solar cells;

- modeling of energy generation of 3-, 4-, 5-, and 6-junction solar cells as a function of sun angle, integrated over the course of the day and the year;

- experimental results on prototype terrestrial concentrator 4-junction solar cells, with preliminary measured efficiency up to 35.7%.

Details of this work are found in the slides for the Jan. 23 program review, and in the sections above in this report.

2.12 Cell Development Progress Report 12

A concentrator cell build (EC-01 Build #3) was started using epitaxial wafers with a wide variety of high-efficiency lattice-matched and metamorphic cell architectures, which are candidates for the next generation of concentrator multijunction cells. A number of experimental matrices in the device structure were carried out to determine the effect on cell voltage and cumulative current density, as well as current balance among subcells. A schematic of the EC-01 mask used in the build, as well as in the build that yielded the recent record efficiency 40.7% metamorphic and 40.1% lattice-matched cells, is shown in Fig. 2.12.1 below, along with a photo of a 100-mm Ge wafer processed with that mask in Fig. 2.12.2.

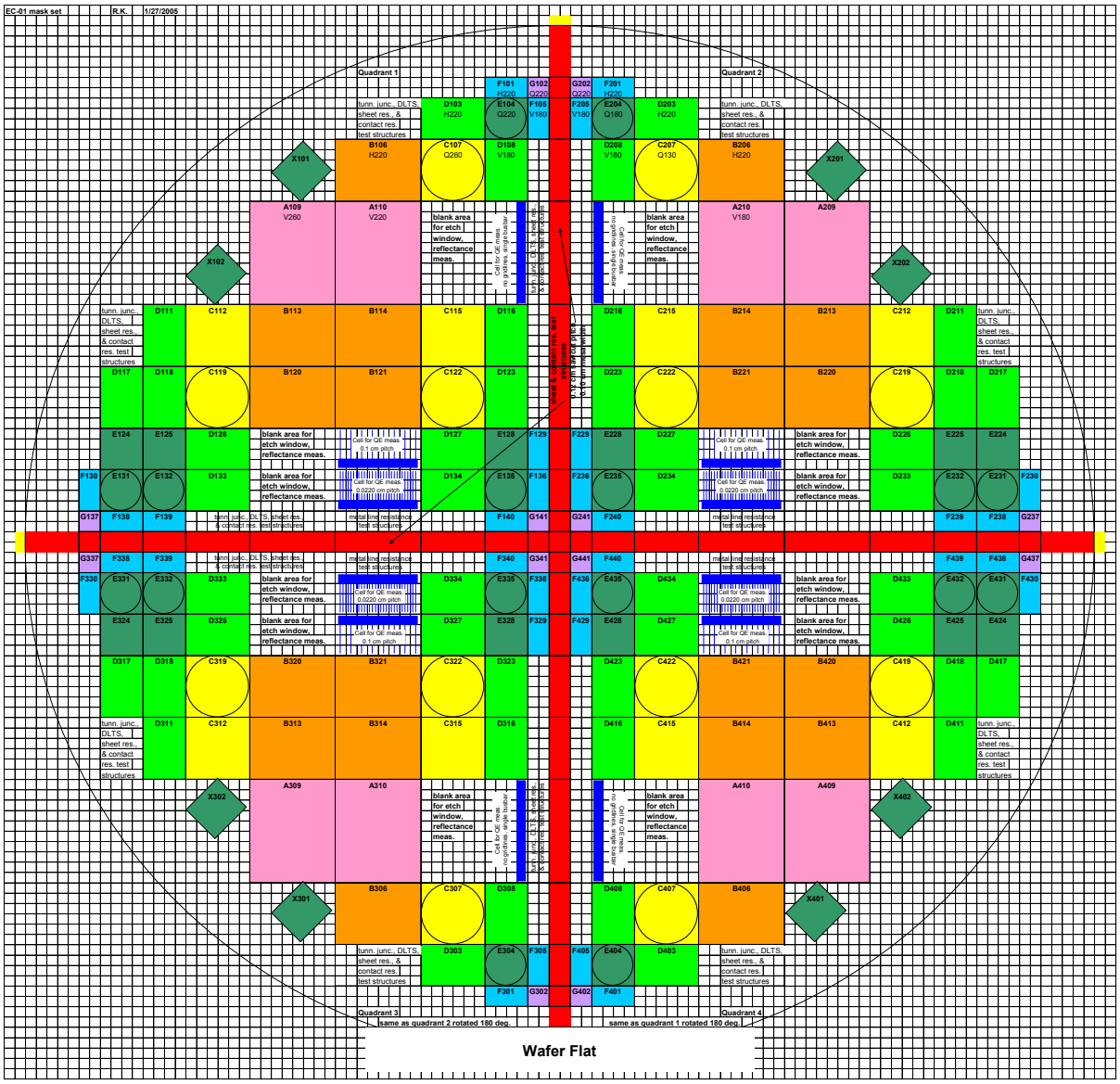

Fig. 2.12.1 Schematic of experimental concentrator cell mask 1 (EC-01) used in EC-01 cell builds #1, #2, and #3.

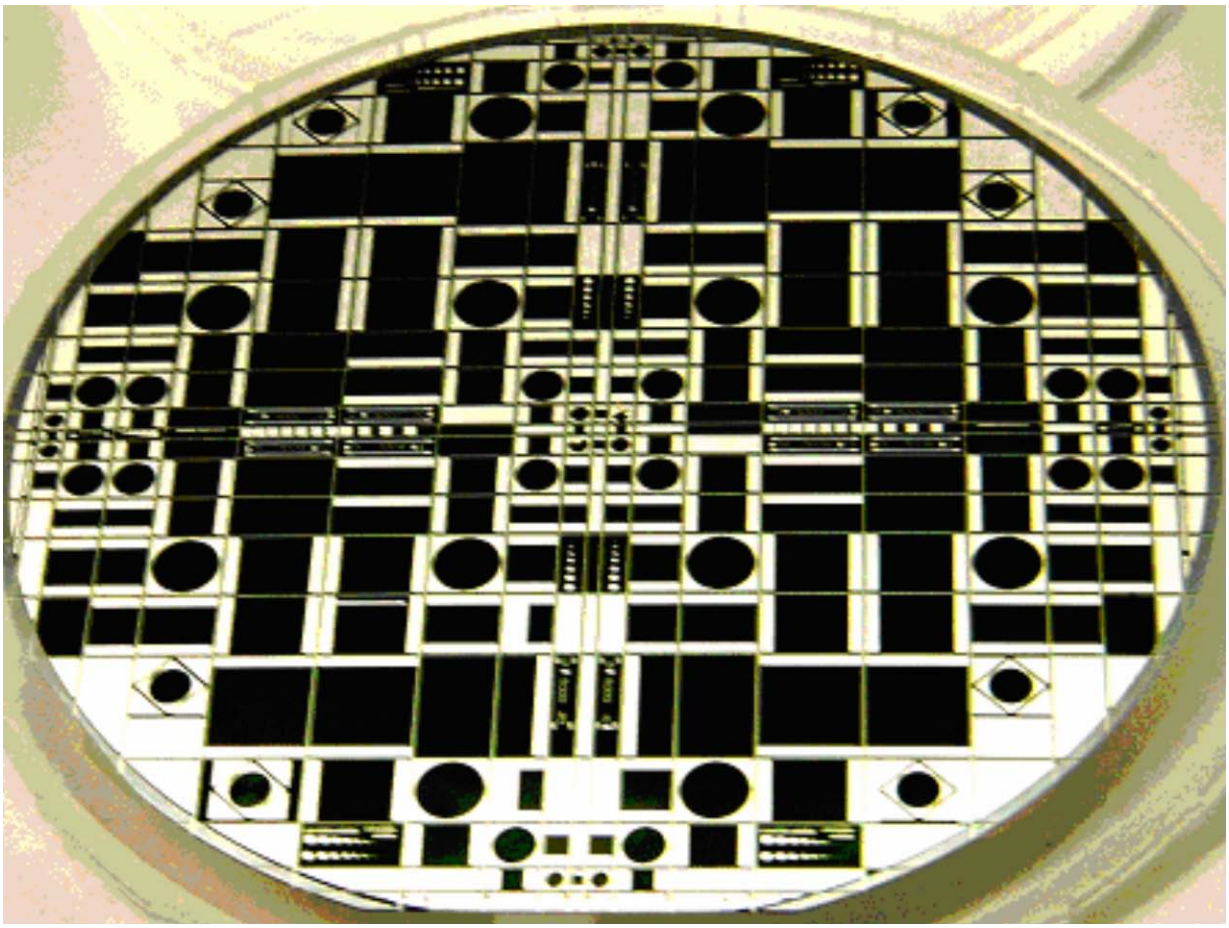

Fig. 2.12.2 Photograph of the metallization pattern on a 100-mm diameter concentrator cell wafer from EC-01 build #1.

In this time frame, a paper was published in Applied Physics Letters describing the recent record 40.7%-efficient metamorphic cell and 40.1%-efficient lattice-matched cell results, and discussing the physics of high-efficiency metamorphic terrestrial concentrator solar cells [1]. Figures 2.12.3 and 2.12.4 below are from that paper. Figure 2.12.3 shows the fundamental loss mechanisms in metamorphic (MM) and lattice-matched (LM) 3-junction GaInP/ GaInAs/ Ge solar cells from the paper, while in Fig. 2.12.4 the bandgap-voltage offset $(E_g/q) - V_{oc} \equiv W_{oc}$ at one sun is plotted for a wide range of bandgaps in LM and MM (Al)GaInP and (Al)GaInAs subcells.

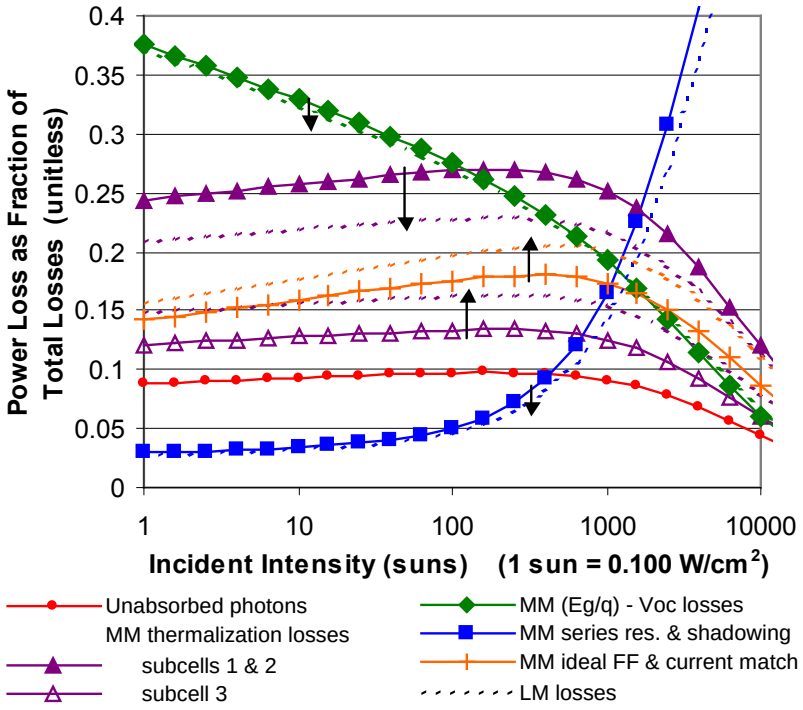

Fig. 2.12.3 Loss mechanisms in metamorphic $Ga_{0.44}In_{0.56}P$/ $Ga_{0.92}In_{0.08}As$/ Ge and lattice-matched $Ga_{0.50}In_{0.50}P$/ $Ga_{0.99}In_{0.01}As$/ Ge 3-junction terrestrial solar cells as a function of incident intensity of sunlight.

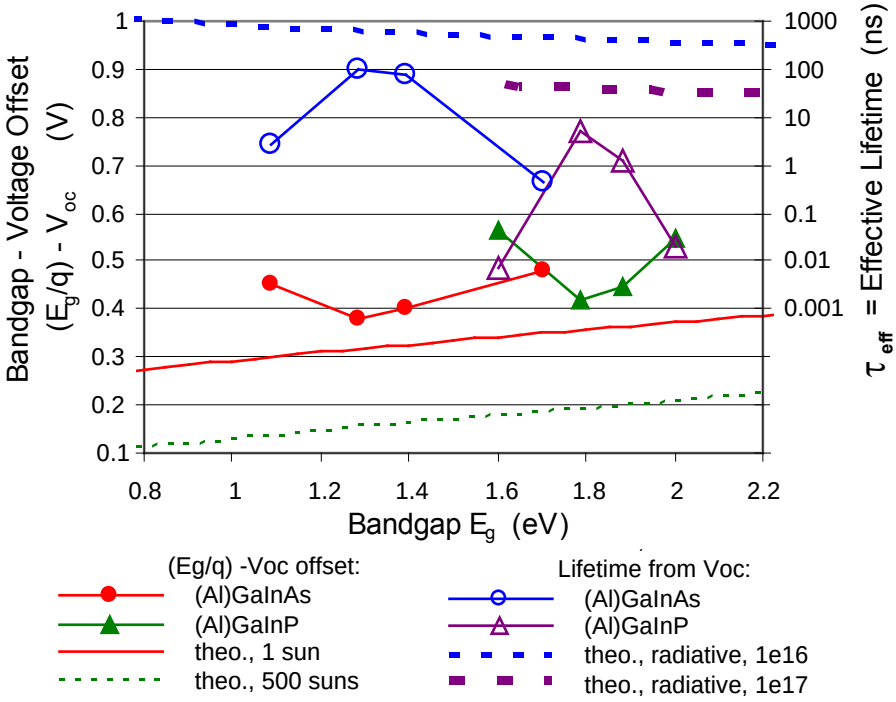

Fig. 2.12.4 Measured bandgap-voltage offset for a range of LM and MM subcell materials and bandgaps at one sun. Comparison to theory gives a measure of the SRH recombination present. The effective lifetime, an upper limit on the bulk lifetime, is derived from the cell measurements.

A series of experiments was started on stand-alone GaInP top subcells, in order to better understand recombination mechanisms in the GaInP subcell, as well as the tradeoff between current and voltage in these cells, and to increase voltage and current collection in GaInP top subcells. In these experiments, structures are used in which the GaInAs subcell 2 and Ge subcell 3 are made isotype and inactive, so that only the GaInP top subcell is active, in order to allow more complete characterization of the GaInP subcell without being influenced by variations in the other subcell parameters. These experiments are still ongoing, but have already yielded promising results.

References – Section 2.12

[1] R. R. King, D. C. Law, K. M. Edmondson, C. M. Fetzer, G. S. Kinsey, H. Yoon, R. A. Sherif, and N. H. Karam, "40% efficient metamorphic GaInP / GaInAs / Ge multijunction solar cells," *Appl. Phys. Lett.*, Vol. 90, No. 18, 183516, 4 May 2007.

2.13 Cell Development Progress Report 13

Some of the figures describing the high-performance lattice-matched (LM) and metamorphic (MM) concentrator cells developed by Spectrolab in the NREL HiPerf PV program are discussed below and in [15,16]. In Fig. 2.13.1, the measured efficiency, V_{oc}, and fill factor are plotted as a function of incident intensity, or concentration ratio, for the record 40.7% MM and 40.1% LM cells, as well as for an additional MM cell with good performance at high intensities. Fill factors for both types of cell are quite high at about 88% in the 100-200 sun range. As described in [15,16], the open-circuit voltage V_{oc} increases at rates of approximately 210 mV/decade and 190 mV/decade for the MM and LM record cells respectively, in the 100-200 suns range. Subtracting off the 59 mV/decade increase for the Ge subcell, with diode ideality factor γ very close to unity, gives an average γ for the upper two subcells of 1.26 in the MM case and 1.10 in the LM case in the same concentration range, though γ decreases as the incident intensity increases.

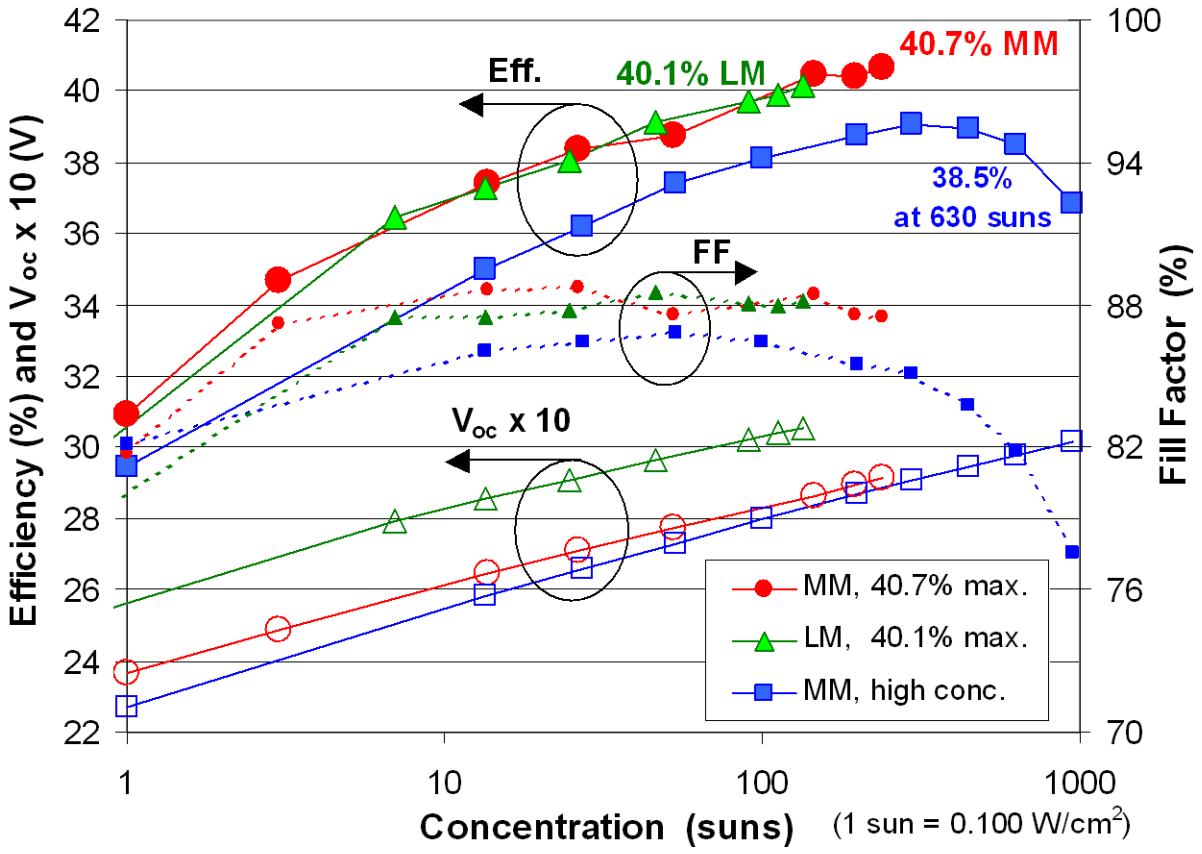

Fig. 2.13.1 Efficiency, open-circuit voltage, and fill factor of the record performance 40.7% metamorphic and 40.1% lattice-matched 3-junction cells as a function of incident intensity. An additional cell is shown which maintains an efficiency of 38.5% over 600 suns, and 36.9% over 950 suns.

In Fig. 2.13.2, measured external quantum efficiencies are shown for the GaInP, GaInAs, and Ge subcells in MM and LM 3-junction cells, superimposed on the air mass zero and terrestrial solar spectra. The downward shift in band gap in the upper two MM subcells is evident, allowing the higher voltage upper subcells to use a larger part of the solar spectrum. The long wavelength response of the MM $Ga_{0.44}In_{0.56}P$ and $Ga_{0.92}In_{0.08}As$ subcells can be seen to be high near the band edge, reflecting the long lifetimes and diffusion lengths in these metamorphic materials.

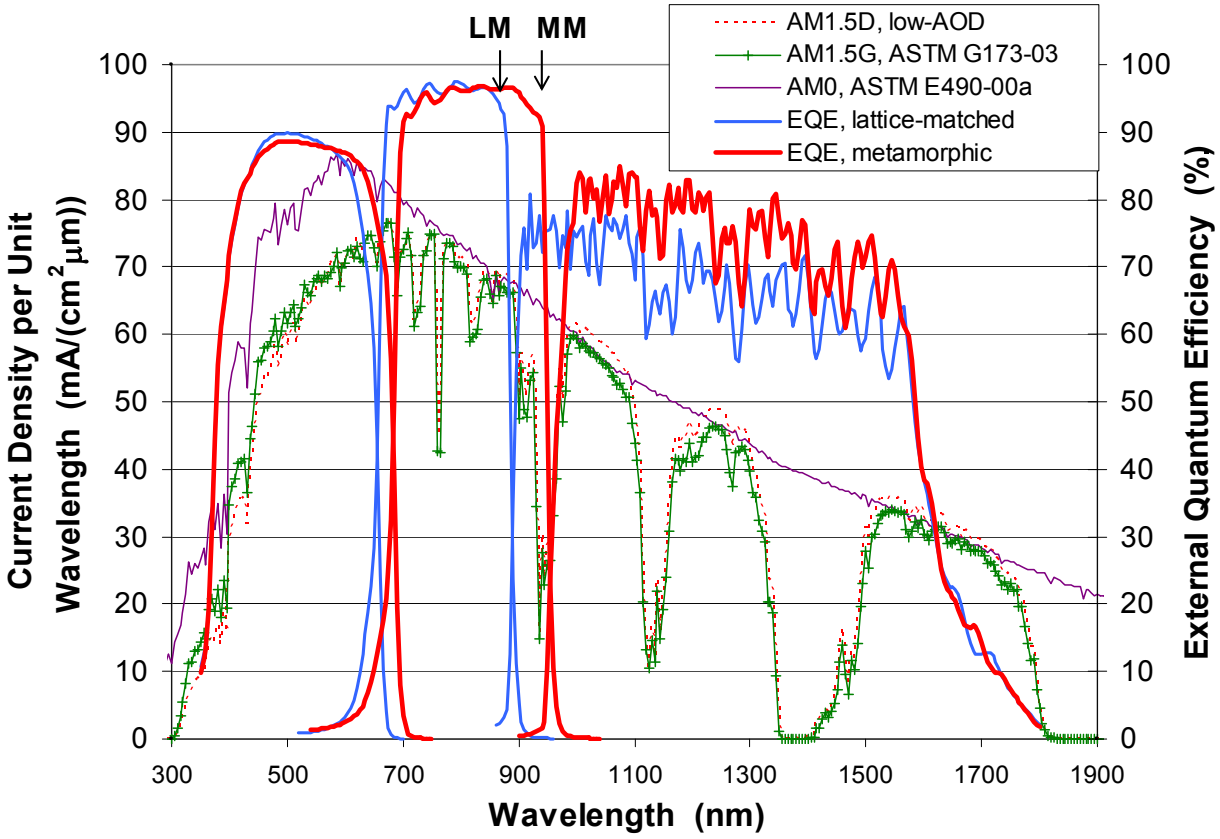

Fig. 2.13.2 External quantum efficiency for GaInP, GaInAs, and Ge subcells in MM and LM 3-junction cells, and the space and terrestrial solar spectra.

Full-process cell fabrication was completed for HiPerf PV cell build #3, including experimental device structures in lattice-matched and metamorphic 3-junction GaInP/ GaInAs/ Ge cells, and in 4-junction GaInP/ AlGaInAs/ GaInAs/ Ge solar cells. Quantum efficiency and concentrated light I-V testing and analysis is in progress.

References – Section 2.13

[1] R. R. King, D. C. Law, K. M. Edmondson, C. M. Fetzer, G. S. Kinsey, H. Yoon, R. A. Sherif, and N. H. Karam, "40% efficient metamorphic GaInP / GaInAs / Ge multijunction solar cells," *Appl. Phys. Lett.*, Vol. 90, No. 18, 183516, 4 May 2007.

[15] R. R. King, D. C. Law, K. M. Edmondson, C. M. Fetzer, G. S. Kinsey, D. D. Krut, J. H. Ermer, R. A. Sherif, and N. H. Karam, "Metamorphic Concentrator Solar Cells with Over 40% Conversion Efficiency," *Proc. 4th International Conference on Solar Concentrators (ICSC-4)*, El Escorial, Spain, March 12-16, 2007 (ISBN: 978-84-690-6463-4), pp. 5-8.

[16] Richard R. King, Daniel C. Law, Kenneth M. Edmondson, Christopher M. Fetzer, Geoffrey S. Kinsey, Hojun Yoon, Dimitri D. Krut, James H. Ermer, Raed A. Sherif, and Nasser H. Karam, "Advances in High-Efficiency III-V Multijunction Solar Cells," *Advances in OptoElectronics*, Vol. 2007, Article ID 29523, 8 pages, doi:10.1155/2007/29523.

2.14 Cell Development Progress Report 14

2.14.1 HiPerf PV Build #3

The experimental matrix of prototype full-process multijunction solar cells known as HiPerf PV Build #3 was completed and tested. This build incorporated a wide range of new high-efficiency terrestrial concentrator cell architectures, including both lattice-matched (LM) and metamorphic (MM) 3-junction designs, and 4-junction (4J) terrestrial concentrator cells, with a variety of new semiconductor device features designed to increase cell current, voltage, and fill factor. These high-efficiency, high-current solar cell device structures (referred to as HECS for high-efficiency cell structures) for lattice-matched and metamorphic terrestrial concentrator multijunction cells were first demonstrated in the Spectrolab/NREL HiPerf PV program, over the past several years of experiments.

Table 2.14.1 shows a general outline of the advanced cell structure groups investigated in HiPerf PV Build #3. Within each general cell group, there are additional experimental conditions to examine the effect of variations in cell structure design (thicknesses, compositions), HECS design, doping profiles, J-ratio among subcells, MOVPE growth conditions, etc.

Table 2.14.1. Outline of the advanced cell structure groups investigated in HiPerf PV Build #3.

Run ID	Run description
3-junction cells, lattice-matched (3J-L)	
6x-15677	3J-L, lo Eg TC, control, run 1
6x-15686	3J-L, lo Eg TC, MC doping, run 2
6x-15678	3J-L, lo Eg TC, TC doping, run 3
6x-15882	3J-L, hi Eg TC, TC doping, run 4
6x-15875	3J-L, hi Eg TC, TC doping, run 5
3-junction cells, lattice-matched, with HECS (3J-LW)	
6x-15692	3J-LW, lo Eg TC, HECS #1, run 6
6x-15700	3J-LW, lo Eg TC, HECS #1, run 7
6x-15704	3J-LW, lo Eg TC, HECS #1, run 8
6x-15957	3J-LW, hi Eg TC, HECS #2, run 9
6x-15977	3J-LW, hi Eg TC, HECS #3, run 10
6x-15964	3J-LW, hi Eg TC, HECS #3, run 11
6x-15721	3J-LW, hi Eg TC, HECS #1, run 12
6x-15726	3J-LW, hi Eg TC, HECS #1, run 13
3-junction cells, metamorphic (3J-M)	
6e-17270	3J-M, hi Eg TC, control, run 14
6e-17889	3J-M, hi Eg TC, control, run 15
6e-17992	3J-M, hi Eg TC, control, run 16
6e-17278	3J-M, hi Eg TC, TC doping, run 17
6e-17277	3J-M, hi Eg TC, thick TC, run 18
3-junction cells, metamorphic, with HECS (3J-MW)	
6x-16746	3J-MW, hi Eg TC, HECS #4, run 19
6x-16769	3J-MW, hi Eg TC, HECS #4, run 20
6x-16738	3J-MW, hi Eg TC, HECS #5, run 21
6x-16739	3J-MW, hi Eg TC, HECS #6, run 22
4-junction cells, lattice-matched, standard (4J-L) and with HECS (4J-LV)	
6x-15728	4J-L, hi Eg TC, run 23
6x-15749	4J-LV, Hi Eg TC, HECS #7, run 24

HECS = High-efficiency cell structure

Figure 2.14.1 plots illuminated I-V characteristics for the various types of experimental cells in HiPerf PV Build #3, measured at concentration, near 23 W/cm^2 (230 suns) incident intensity, using the high-intensity pulsed solar simulator (HIPSS) at Spectrolab. The simulator was calibrated using standard terrestrial concentrator GaInP and GaInAs reference component cells. These are some of the better cells measured from each group of experimental cells in the build. These measured values are preliminary, primarily because of uncertainties in current density calibration for these new cell designs with widely varying subcell spectral response.

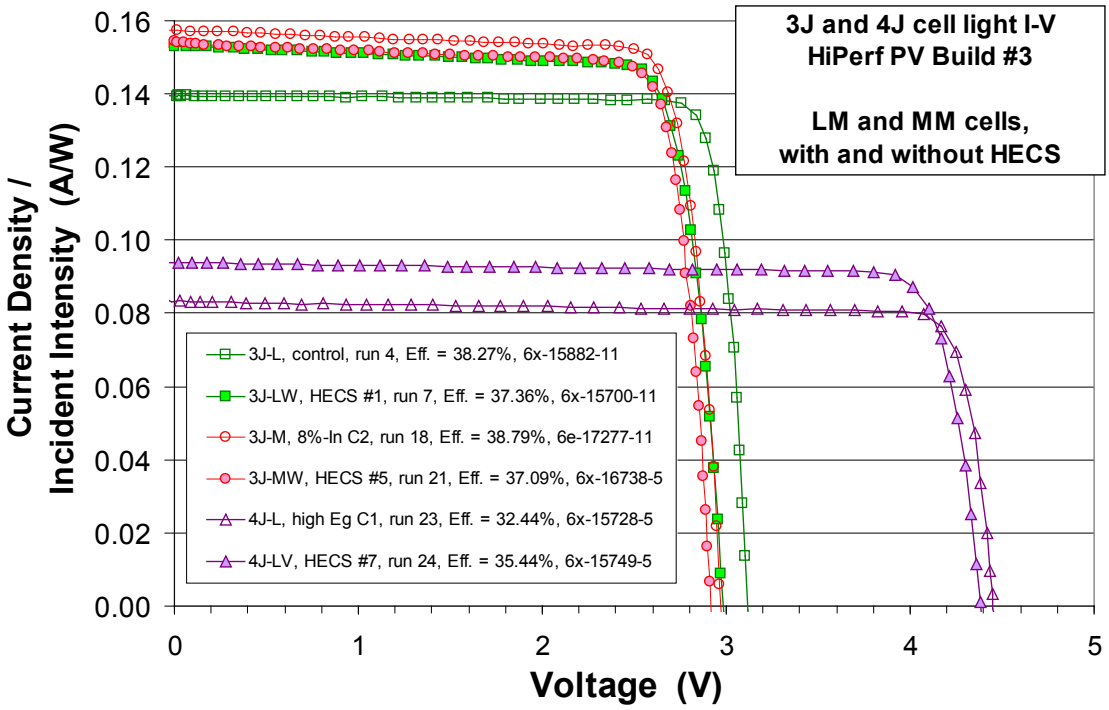

Figure 2.14.1 Illuminated I-V curves measured at ~23 W/cm^2 (~230 suns) for the main types of experimental cells in HiPerf PV Build #3.

The light I-V characteristic for the 3J-L (3-junction, lattice-matched) cell can serve as a comparison point for the other I-V curves. This particular cell has a high-band-gap, disordered GaInP top cell, resulting in a relatively high open-circuit voltage V_{oc} . The 3J-LW (3-junction, lattice-matched, HECS) cell has a much higher short-circuit current density J_{sc} due to the inclusion of the HECS. The V_{oc} is lower, in part due to the low-band-gap, ordered GaInP top cell in this 3J-LW cell. The 3J-M (3-junction, metamorphic) cell has still higher current than the 3J-LW cell, and similar open-circuit voltage, giving a preliminary efficiency measurement of 38.79%. The 3J-MW (3-junction, metamorphic, HECS) cell shown here is somewhat lower in both J_{sc} and V_{oc} than the 3J-M cell example, probably due to less experience with this experimental device structure.

The remaining I-V curves in Fig. 2.14.1 are examples of 4-junction GaInP/ AlGaInAs/ GaInAs/ Ge terrestrial concentrator cells. In some experiments, aluminum is added to the top subcell to form a higher band gap AlGaInP subcell 1. As described in earlier reports, a strong

advantage of the 4-junction cell design for concentrator cells is that their high-voltage, low-current design dramatically reduces the I^2R power losses due to series resistance at high concentrations. Open-circuit voltage of the 4J-L (4-junction, lattice-matched) cell shown here is over 4.4 V at this relatively low incident intensity. In comparison, both the short-circuit current and the efficiency are strongly augmented for the 4J-LV (4-junction, lattice-matched, HECS) cell shown here, with preliminary efficiency measured at 35.44% for this cell.

The quantum efficiencies (QEs) of these various cell configurations in Build #3, and the way these QEs convolute with the available current density and power per unit area available in the solar spectrum as a function of wavelength, are key considerations for optimizing efficiency of these terrestrial concentrator cells. The current density per unit wavelength and intensity per unit wavelength (irradiance) available in the standard AM1.5D, ASTM G173-03 solar spectrum, normalized to an intensity of 0.100 W/cm^2 (1.00 suns), are plotted in Fig. 2.14.2. Note the current density per unit wavelength reflects the greater abundance of photons at longer wavelengths, increasing the ability to current balance the subcells with lower band gaps in the multijunction stack, and in fact to give these subcells excess photogenerated current density to counteract the low fill factors associated with low band gap cells. In comparison, the higher intensity per unit wavelength at short wavelength values reflects that most of the power available for conversion in the solar spectrum is in the wavelength range converted by the high-band-gap, upper subcells in the stack, emphasizing the need for these high-band-gap cells to be as high quality as possible.

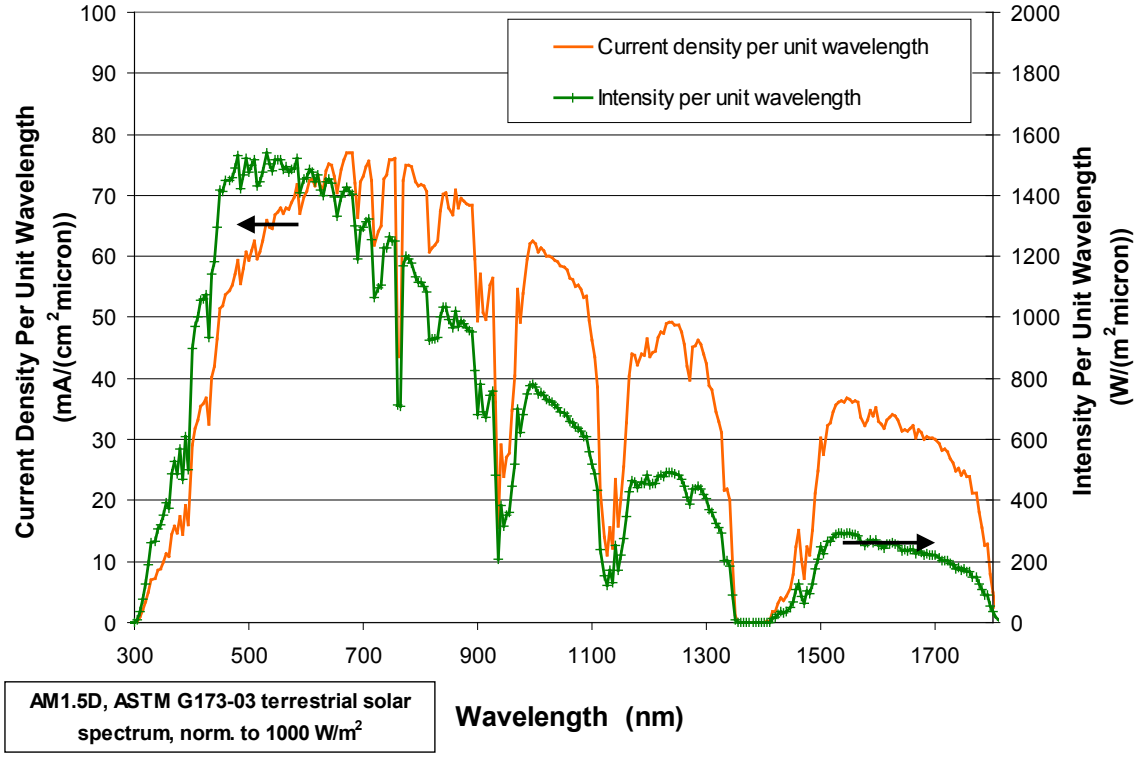

Fig. 2.14.2 Current density per unit wavelength and intensity per unit wavelength (irradiance) available in the standard AM1.5D, ASTM G173-03 solar spectrum, normalized to 0.100 W/cm^2 (1.00 suns)

Figure 2.14.3 plots the external quantum efficiency of the top and middle cells of 3-junction lattice-matched and metamorphic cells in Build #3, showing the extended long wavelength response of both the metamorphic GaInP top cell and the metamorphic 8%-In GaInAs middle cell. The cumulative QE (top cell QE + middle cell QE) shows a reduced dip in between subcells for the metamorphic cell, in the wavelength range where tunnel junction absorption is most significant. In addition to the extended wavelength response of the metamorphic cells, it is interesting to note that for the cells selected for the following charts, the external quantum efficiency of the metamorphic cells was measured to be higher across the entire top and middle cell wavelength response range. The additional current density available due to the extended long wavelength response of the metamorphic middle subcell can be gauged by the area under the convolution of the current density per unit wavelength in the solar spectrum with the cumulative QE of the 3J-M cell (plotted in red), compared to that for the 3J-L cell (blue curve) between ~880 and 980 nm. Figure 2.14.4 is a similar type of plot, but one showing the convolution of cell QEs with intensity per unit wavelength in the solar spectrum, showing the impact of additional power harvested by the long wavelength response of the metamorphic GaInAs middle cell.

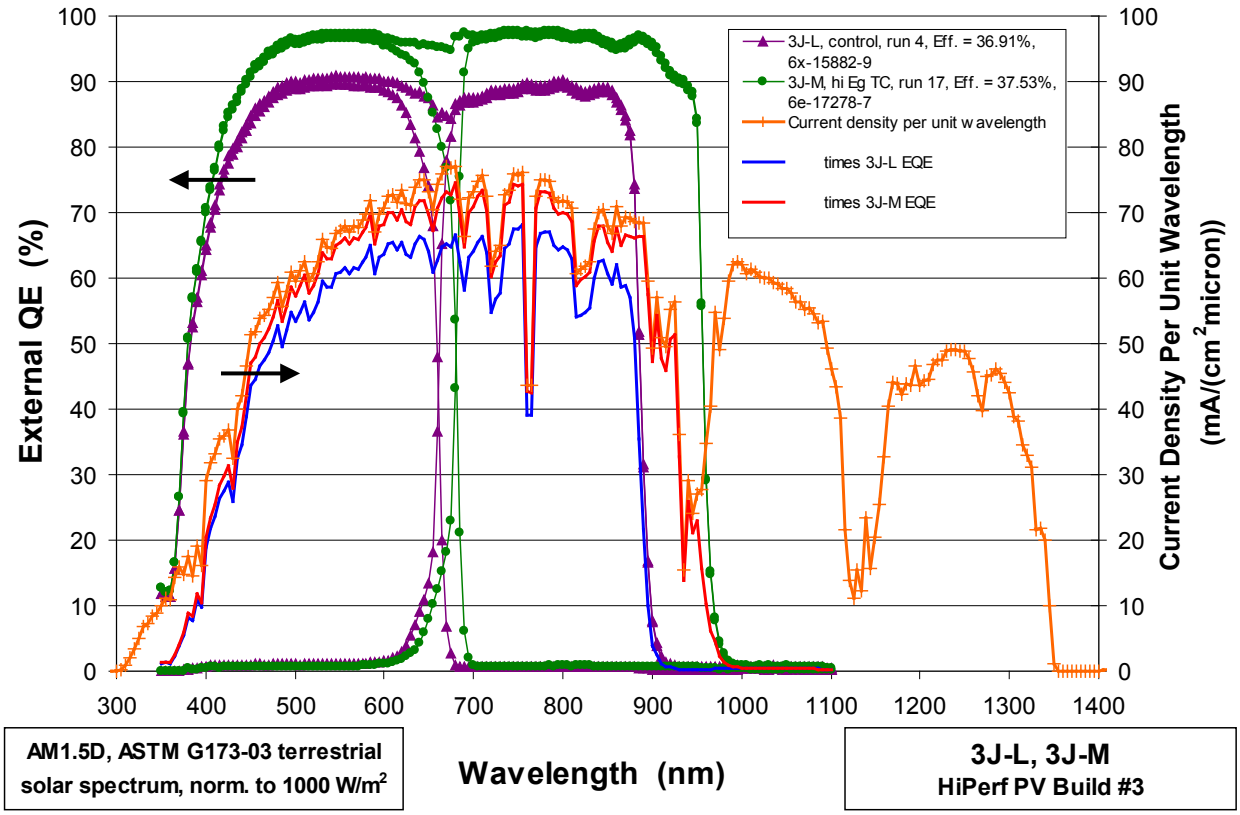

Fig. 2.14.3 Top subcell, middle subcell, and cumulative external quantum efficiency of 3-junction lattice-matched (3J-L) and metamorphic (3J-M) cells in Build #3, and convolution with the available current density per unit wavelength in the solar spectrum.

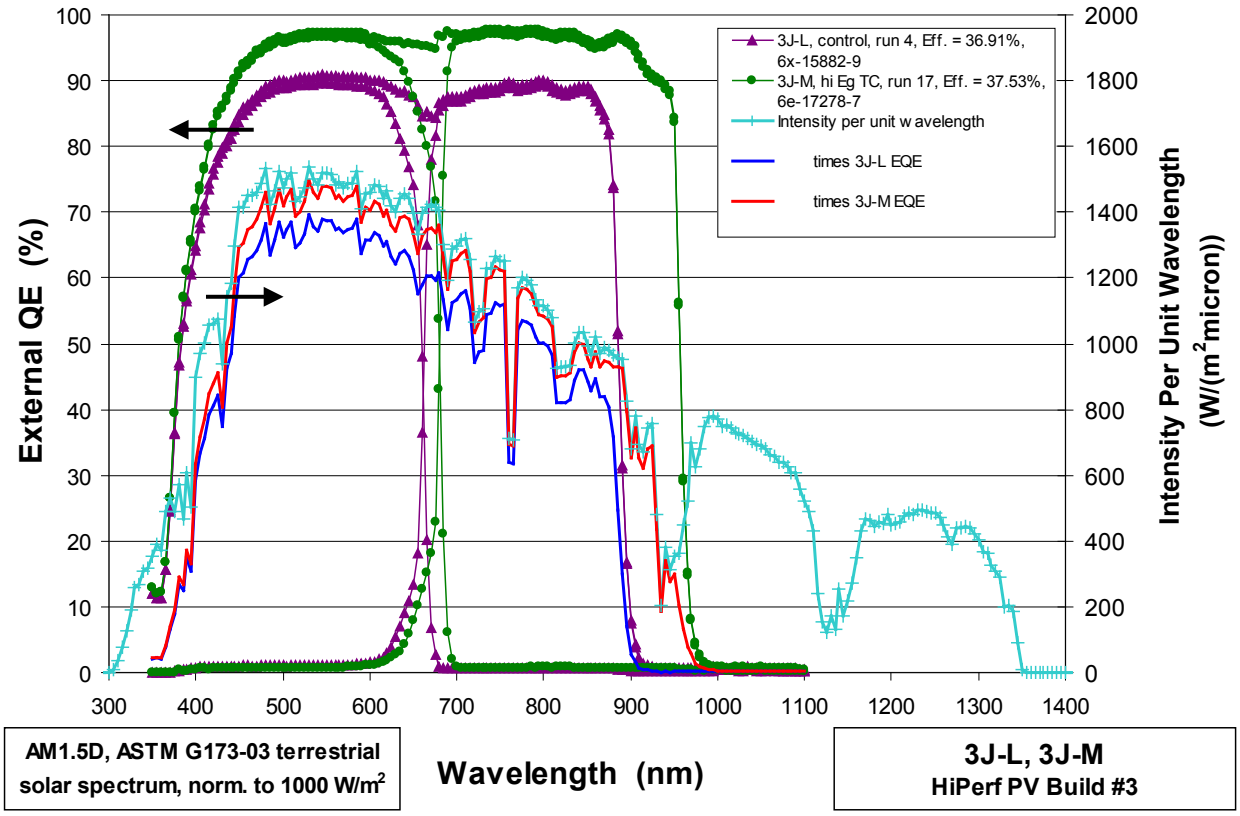

Fig. 2.14.4 Top subcell, middle subcell, and cumulative external quantum efficiency of 3-junction lattice-matched (3J-L) and metamorphic (3J-M) cells in Build #3, and convolution with the available intensity per unit wavelength in the solar spectrum.

In Fig. 2.14.5, the efficiencies measured by high-intensity pulsed solar simulator (HIPSS) at an incident intensity of ~23 W/cm^2 (~230 suns) are plotted, for a range of the different cell configurations representative of the run splits in HiPerf PV Build #3. Measurements for 3-junction cell designs with lattice-matched and metamorphic structures, and with and without HECS, as well as lattice-matched 4-junction cells with and without HECS are shown. Metamorphic 3-junction (3J-M) cells had the highest efficiency among the sample of cells in this chart, at 38.8% in these preliminary HIPSS measurements, followed closely by 3-junction lattice-matched (3J-L) cells. Several lattice-matched 3-junction cells with HECS (3J-LW) also performed quite well, with preliminary efficiency measurements over 37%. A metamorphic 3-junction cell with HECS (3J-MW) cell also had a preliminary efficiency of 37.1%. These results for lattice-matched and metamorphic cells with HECS, though not yet higher than their counterparts without HECS, are impressive given the early stage of development of these terrestrial concentrator cells with HECS. Terrestrial concentrator 4-junction cells performed much better when the HECS was included in subcell 3 of the 4-junction cell, reaching a preliminary efficiency of 35.4%, again a significant result for this relatively new technology.

The efficiency calculated using the integrated current density from EQE of the current limiting subcell as the one-sun J_{sc} of the cell is also plotted in Fig. 2.14.5. This gives a

comparison between the current calibration on the HIPSS using standard reference cells, and the current calibration using integrated J_{sc} from quantum efficiency measurements. As before, the HIPSS light I-V measurements should be considered preliminary, because of the wide range of spectral responses of the experimental prototype cells in HiPerf PV Build #3. The current calibrated from EQE should not be subject to this same limitation. The efficiencies using the EQE current calibration generally follow the same trends in efficiency as the HIPSS measurements, with the efficiencies using EQE current calibration tending to be somewhat higher.

To better gauge the potential performance of each design, by accounting for current mismatch in the particular implementation of the cell designs in the experiment, the efficiency was also calculated using the average of top and middle subcell current densities from EQE and plotted in Fig. 2.14.5. This efficiency is a projection, rather than a measurement, but is representative of what the efficiency could be if the top and middle subcell were current-balanced in future runs. In most cases it is relatively straightforward to current balance these cell designs by changing top subcell base thickness. Efficiencies of the cells in this build are projected in this way to be capable of up to 40.9%, if top and middle subcells were current balanced in later runs.

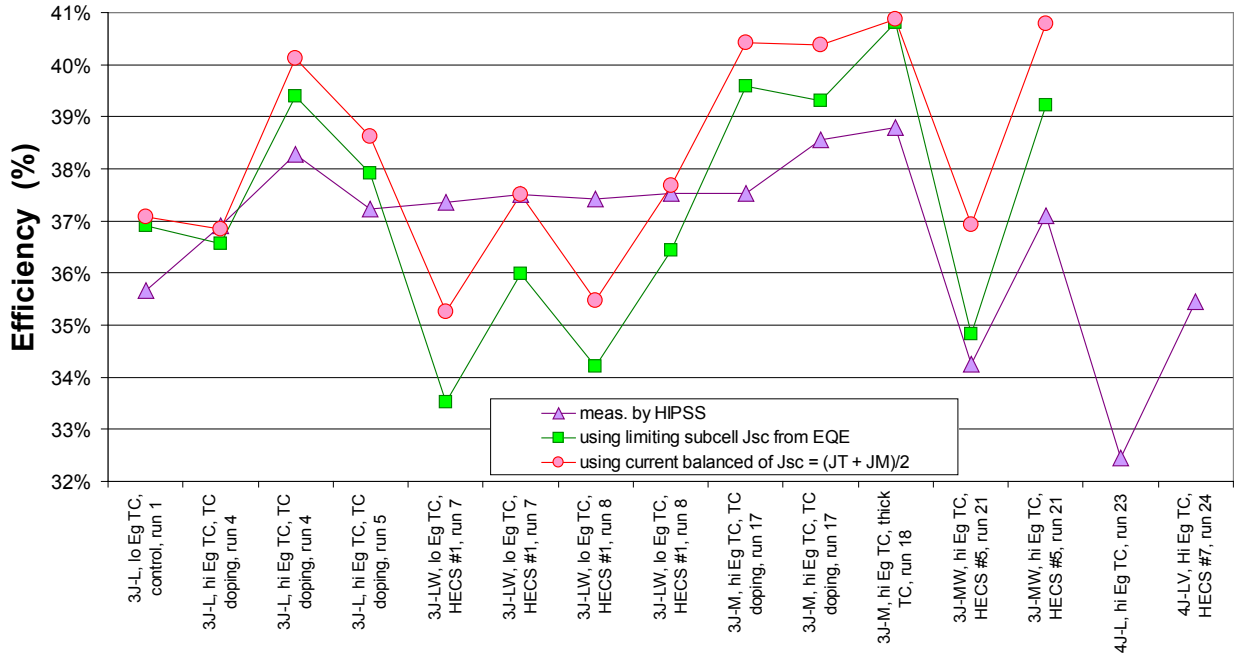

Fig. 2.14.5 Efficiency measured by HIPSS at ~23 W/cm^2 (~230 suns) for a range of different 3-junction cell configurations, with lattice-matched and metamorphic cell structures, with and without HECS, as well as lattice-matched 4-junction cells with and without HECS. The efficiency calculated using the integrated current density from EQE of the current limiting subcell as the one-sun J_{sc} of the cell is also plotted. In addition, the projected efficiency calculated using the average of top and middle subcell current densities from EQE is shown, representative of what the efficiency would be if the top and middle subcell were current-balanced in future runs.

In Fig. 2.14.6, the responsivity of the same HiPerf PV Build #3 run splits are shown: 1) from HIPSS measurements; 2) using the limiting subcell J_{sc} from EQE; and 3) projecting the responsivity based a current-balanced J_{sc} equal to the average of top and middle cell current densities from EQE. Similar trends are seen, with the higher current densities of the 3J-LW design with HECS and of the 3J-M design evident in both the HIPSS measurements and in the average of top and middle cell EQE currents. The open-circuit voltage of the cell at ~23 W/cm^2 (~230 suns) is also plotted, and generally shows an inverse relationship to the responsivity, as one expects from the opposite dependences of voltage and responsivity on band gap.

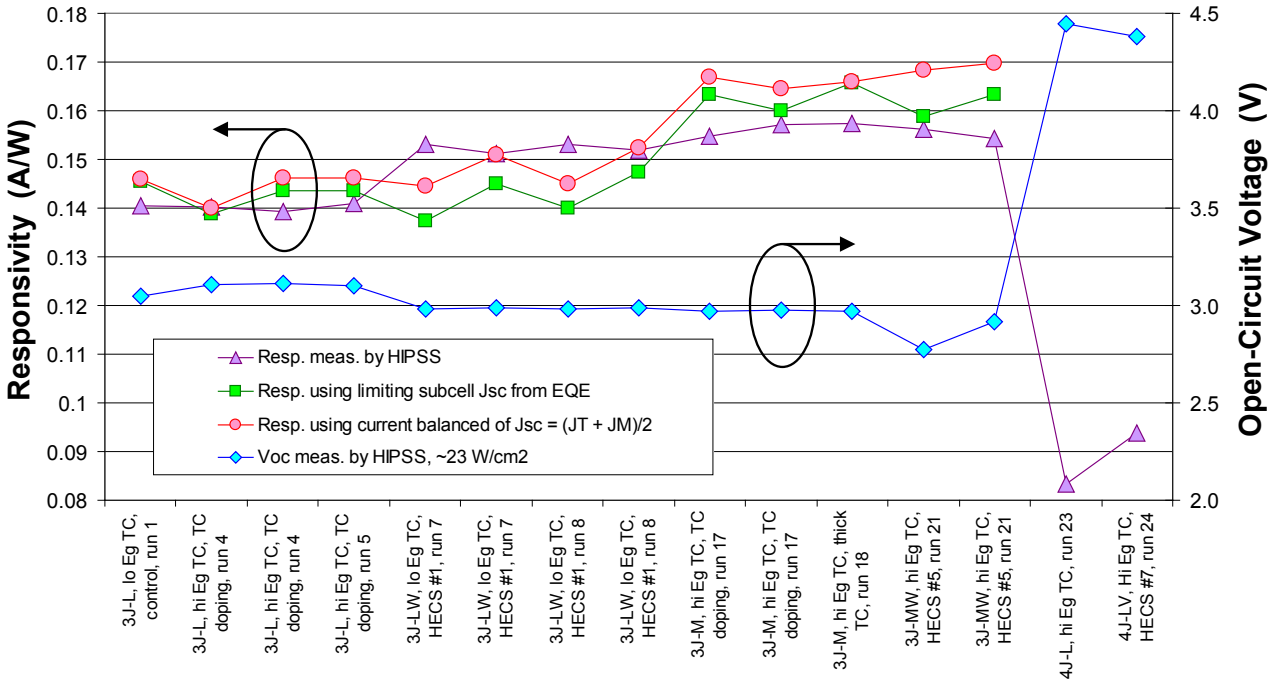

Fig. 2.14.6 Responsivity measured by HIPSS for a range of different 3-junction cell configurations with lattice-matched and metamorphic cell structures, and with and without HECS, as well as lattice-matched 4-junction cells with and without HECS. The open-circuit voltage of the cell at ~23 W/cm^2 (~230 suns) is also plotted, and generally shows an inverse relationship to the responsivity.

To probe this inverse relationship between responsivity and open-circuit voltage further, the cumulative current density, equal to the sum of top and middle subcell current densities from integrated EQE measurements, is plotted versus the V_{oc} at ~23 W/cm^2 (~230 suns) in Fig. 2.14.7. The inverse trend between current and voltage is seen in both the comparison of cells with and without HECS, and in the comparison of metamorphic and lattice-matched cells. However, the effect of the metamorphic architecture is significantly stronger than that of the HECS.

Figure 2.14.7 gives a measure of the V_{oc} of a cell technology for a given current generating capability. It is desirable to be on the upper right side of the trend line, since this indicates higher current and/or higher voltage than points on the lower left side of the line. For

the cells from HiPerf PV Build #3 in this chart, both the lattice-matched and metamorphic cells without HECS have higher open-circuit voltage for a given current generating capability than their counterparts with HECS. Further optimization of HECS may be able to reverse this trend, but it is an interesting observation in the time frame of HiPerf PV Build #3. Plotting the cumulative current density from EQE versus V_{oc} is a quick way to gauge the potential of these cell experiments.

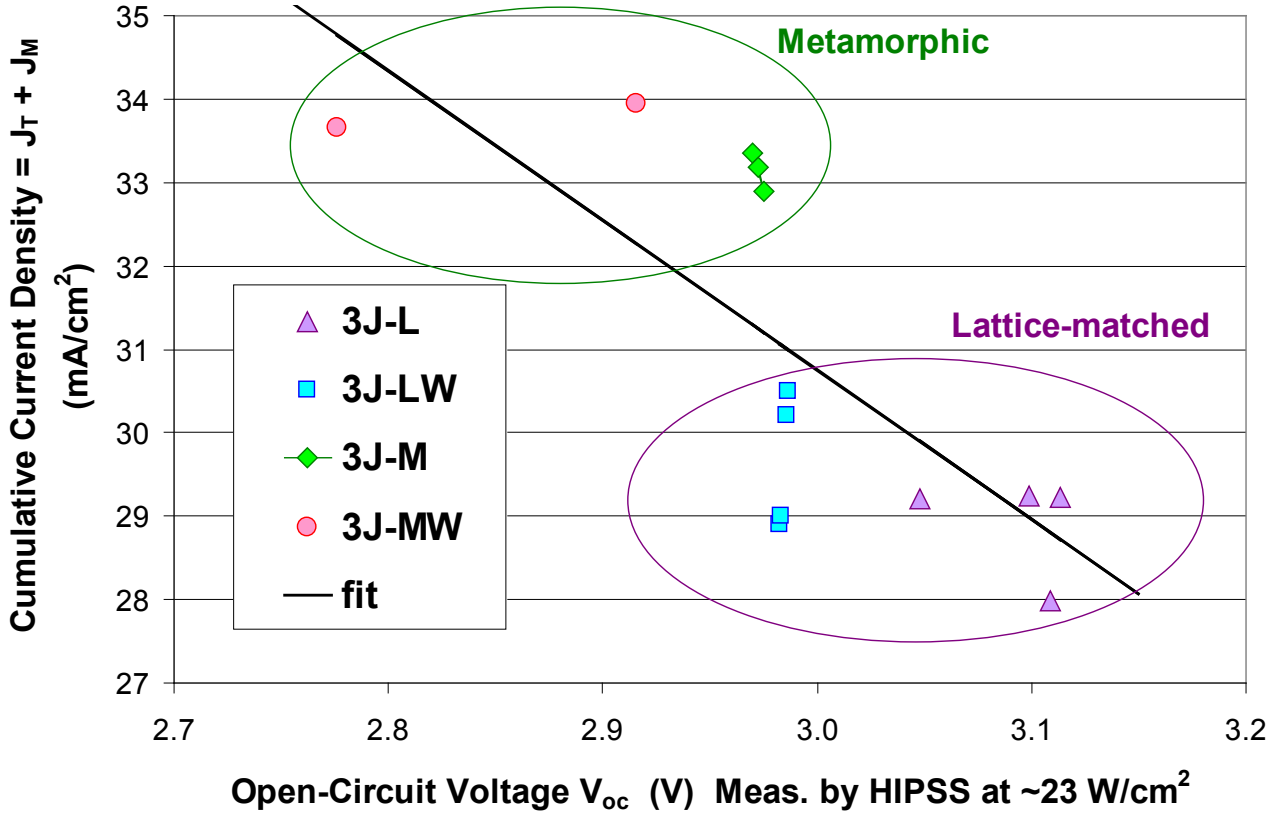

Fig. 2.14.7 Plot of the cumulative current density, equal to the sum of top and middle subcell current densities from integrated EQE measurements, versus the V_{oc} at ~23 W/cm^2 (~230 suns). The inverse trend between current and voltage is seen in both the comparison of cells with and without HECS, and in the comparison of metamorphic and lattice-matched cells. However, the effect of the metamorphic architecture is significantly stronger than that of the HECS.

2.14.2 Single-Junction Component Cells for Characterization of Field Test Conditions

Single-junction component subcells (also called "isotype" cells) were grown for characterization of spectral balance in real-world, field conditions under a fresnel lens. These component cells have been delivered June 19, 2008 to Amonix for testing in their fresnel lens system, satisfying the deliverable associated with Task 30 of the revised statement of work for Spectrolab's HiPerf PV program.

Multiple MOVPE runs were grown spanning a range of J-ratios, *i.e.*, the top cell to middle cell short-circuit current ratio. The range of J-ratios were grown using top-cell-active-only and middle-cell-active-only structures, also called top component cells and middle component cells, respectively, that would be a Jt/Jm matched pair if they were combined in an active multijunction cell. It should be noted that component cells are designed to have the same optical absorption as a full stack, that is, a middle-cell-active-only cell structure will have an inactive GaInP top cell layer on it with the same thickness as an the active GaInP subcell in a normal 3-junction cell, to filter the light that the middle cell collects. Multiple MOVPE runs were grown targeting the Jt/Jm targets. Fresnel lens transmission data provided by Amonix was included in the analysis to decide on the range of J-ratio covered. Selected wafers from each MOVPE run were fabricated into fully processed cells using the Amonix cell size that can be used in their concentrating system.

Preliminary high-intensity pulsed solar simulator (HIPSS) measurements were performed on a sampling of cells from each cell type. From the HIPSS data, some of the designs showed unacceptable performance and were not used. Some of the low performance was not observed at the quick process (QP) level and only appeared at HIPSS testing. Some of the middle-cell-active-only structures showed lower fill factor than expected at high concentration (~555X) in these particular growth runs, however the FF was improved at lower concentration (~250X). Amonix was informed about the middle cell FF and it was agreed that the cells will be suitable for current monitoring (Isc) only. Current monitoring of Isc is sufficient for determining actual Jt/Jm in operation. No issue was observed with the top-cell-active-only structures. It is possible that one or more of the inactive layers is not doped sufficiently in these particular component cell runs, as regions of resistance are seen in the LIV curves.

Additional HIPSS and external quantum efficiency (EQE) measurements were performed and a set of Jt/Jm-matched top and middle cells were chosen for the experiment that spanned the desired range of Jt/Jm. Four Jt/Jm designs were chosen for this experiment. Selected cells were interconnected and received final HIPSS and EQE characterization before shipment to Amonix. Two cells of each type of subcell, for a total of sixteen cells, were delivered to Amonix for preliminary on-sun characterization in their system. More cells are available to Amonix should the need arise. The following sections review the final characterization data of the component cells.

HIPSS Characterization

The following charts show the final HIPSS LIV characterization of all the deliverable component cells. Cells were characterized at two intensities. The first measurement is at an intensity of 555X and is calibrated with setup standard reference cells. The second measurement is at approximately half that intensity by placing wire mesh screens in the beam path as filters. The second measurement at ~230X is not calibrated but gives the approximate expected performance of the cells in the Amonix system which is designed for 250X. Only the lower intensity LIV curves at ~230X are shown. There are two cells per type shown in each chart. The J-ratios range from less than 1 to greater than 1 and are numbered from J1 to J4 by increasing Jt/Jm.

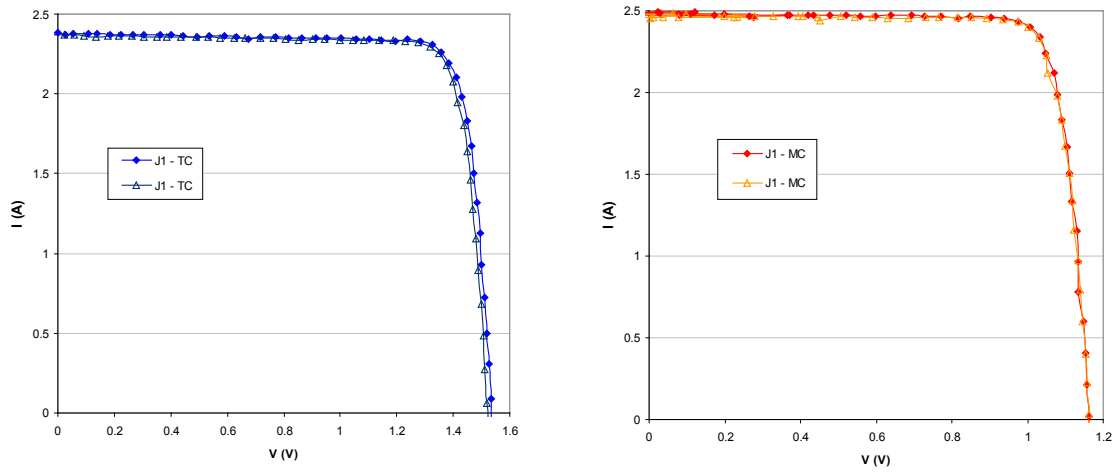

Fig. 2.14.8 Final HIPSS LIV curves for top and middle cell Jt/Jm matched pair J1 @ ~230X.

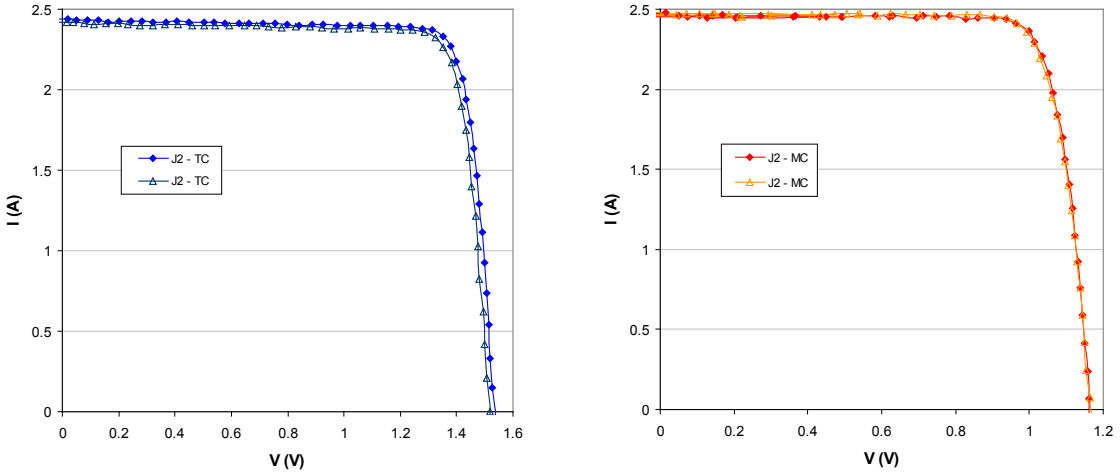

Fig. 2.14.9 Final HIPSS LIV curves for top and middle cell Jt/Jm matched pair J2 @ ~230X.

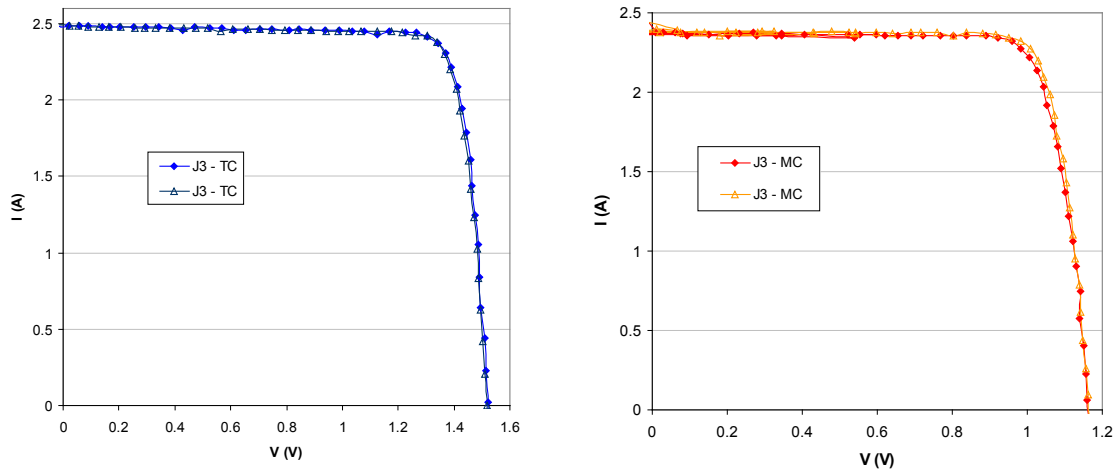

Fig. 2.14.10 Final HIPSS LIV curves for top and middle cell Jt/Jm matched pair J3 @ ~230X.

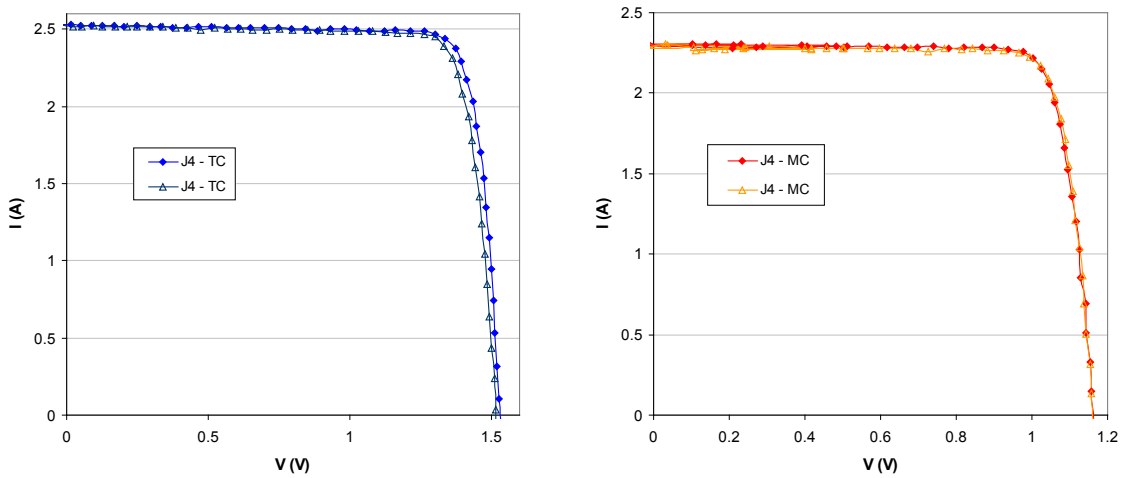

Fig. 2.14.11 Final HIPSS LIV curves for top and middle cell Jt/Jm matched pair J4 @ ~230X.

Note that all the cells exhibit good shunt resistance at the short-circuit point. That is essential for accurate Isc monitoring. All the other PV parameters are nominal. At the higher concentration (555X), some of the fill factors of the middle component cells show some resistive behavior. This resistive behavior is generally not observed in full triple-junction structures.

EQE Characterization

External quantum efficiency (EQE) measurements were performed on all the component cells prior to shipment. EQE measurements can be used in conjunction with data for the incident spectrum to give an accurate determination of Jsc for each cell. As noted above, these component cells are current-matched "pairs". The Jsc of each subcell was designed so that they represent the Jt/Jm of a full multijunction cell, in that way each subcell of a certain design can be

examined individually under LIV test and field conditions. Individual subcell currents under illumination are not generally able to be determined from a full multijunction cell stack.

For completeness, the EQE is shown for each set of Jt/Jm matched subcells. Each chart is a composite EQE curve consisting of separate component cells (also called "isotype" cells) paired for each other.

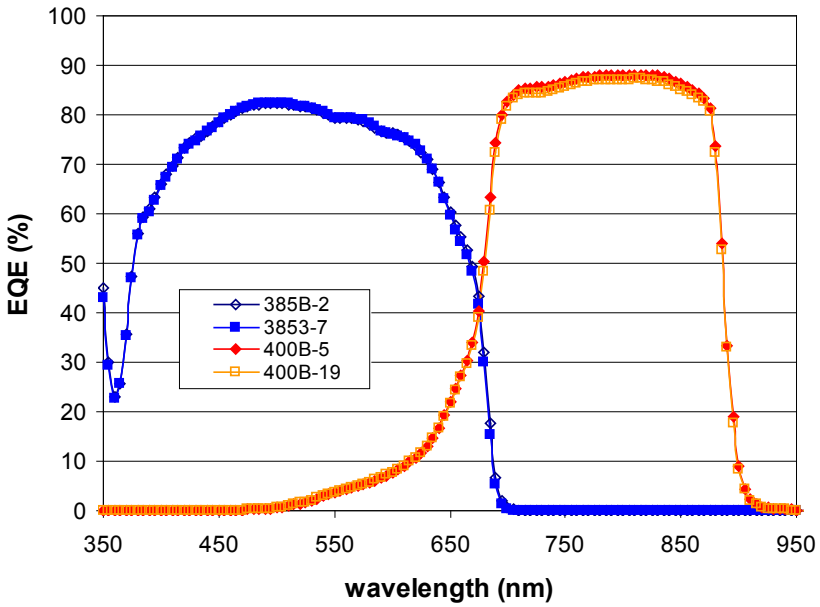

Fig. 2.14.12 Final EQE of separate top and middle component cells for Jt/Jm-matched pair J1.

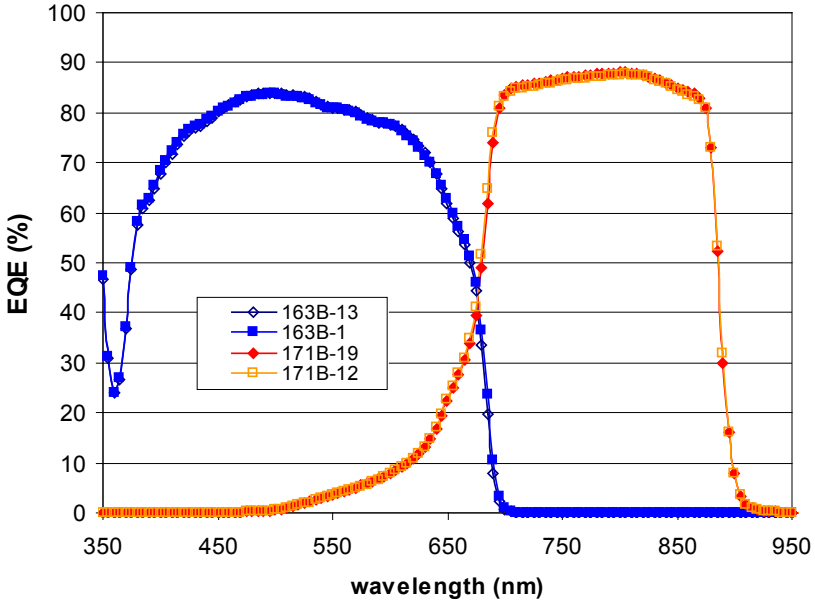

Fig. 2.14.13 Final EQE of separate top and middle component cells for Jt/Jm-matched pair J2.

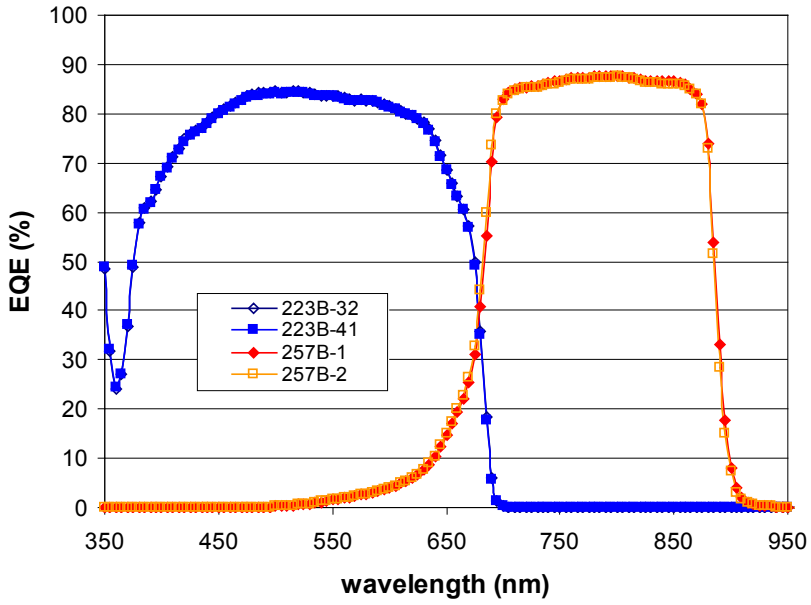

Fig. 2.14.14 Final EQE of separate top and middle component cells for Jt/Jm-matched pair J3.

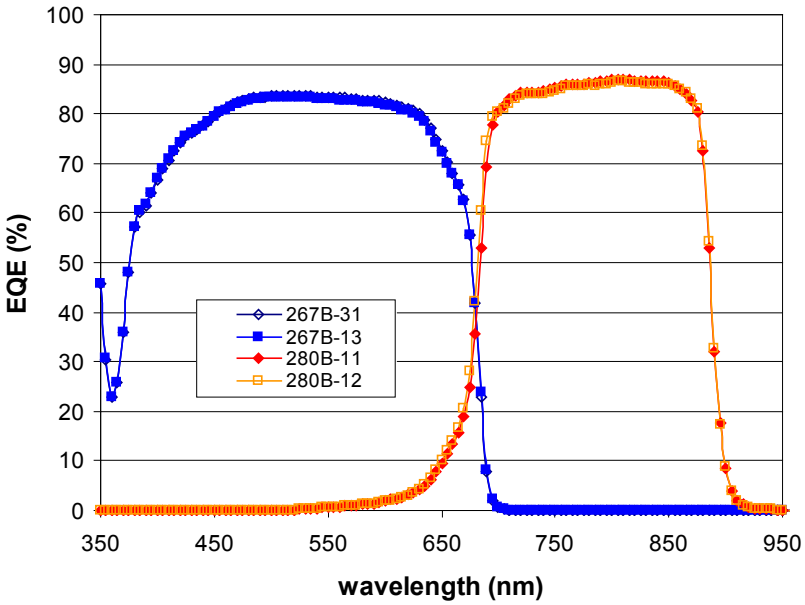

Fig. 2.14.15 Final EQE of separate top and middle component cells for Jt/Jm-matched pair J4.

A representative top cell and middle cell from each Jt/Jm pair is shown in Figs. 2.14.16 and 2.14.17 below. One can see the increasing top cell response with thicker top cell base thickness in Fig. 2.14.16. The corresponding reduction in middle cell response due to thicker top cells is evident in Fig. 2.14.17. The response for the top J2 cell is a little lower than expected. A slightly thicker top cell would have been preferable.

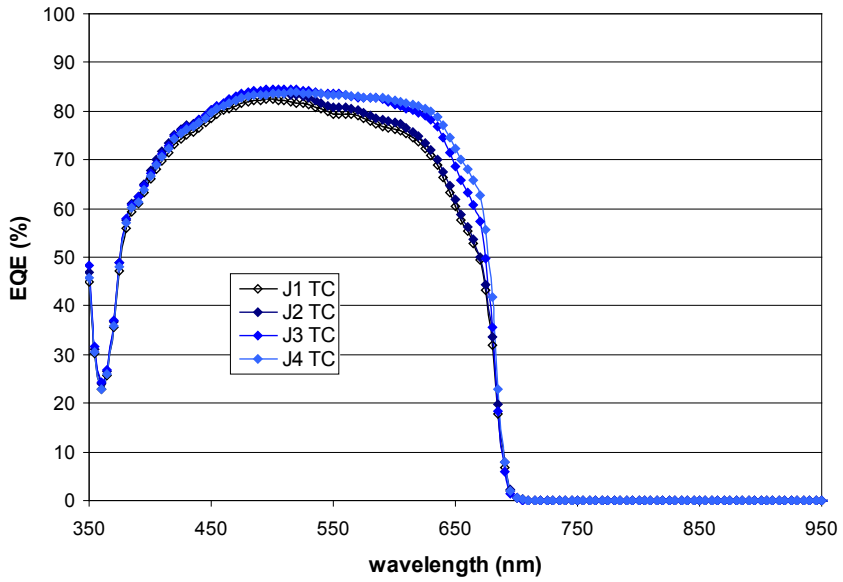

Fig. 2.14.16 Representative top component cell EQE, showing increased top cell response with increasing top cell base thickness.

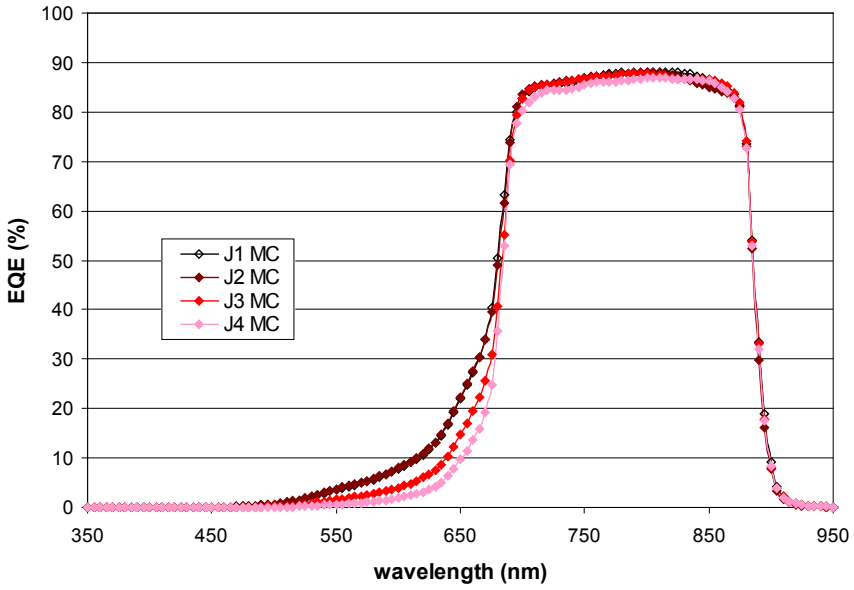

Fig. 2.14.17 Representative middle cell EQE, showing corresponding decrease in middle cell response with increasing top cell base thickness.

Figure 2.14.18 below shows a representative EQE measurement for each Jt/Jm pair, superimposed on the same graph. On-sun field measurements performed by Amonix will be performed to help determine how the J-ratio Jt/Jm affects multijunction cell energy production for varying sun angles and meteorological conditions, in actual operating conditions under fresnel concentrator lenses.

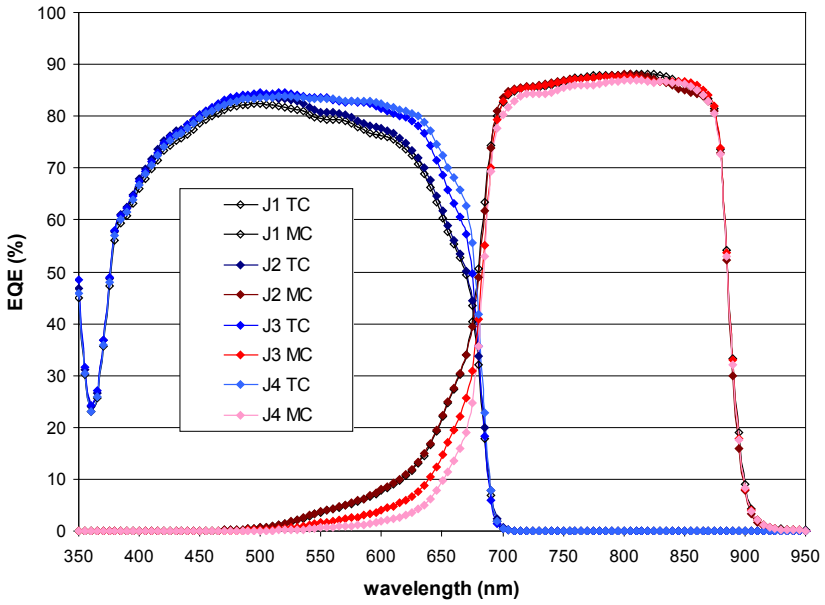

Fig. 2.14.18 Representative EQE measurements for each subcell type. Note increasing top cell response and corresponding middle cell reduction in response.

The Amonix field data will help understand how cells with different J-ratios will perform in their system as a function of time of day, temperature, and incident intensity. This data will help determine what is the best J-ratio and cell design that will give the highest integrated power over the course of a day, month, and year, etc. The first characterization will be to measure these cells under concentration near solar noon and compare this data with laboratory characterization data.

Component Jt/Jm Summary

The table below summarizes the range of Jt/Jm values achieved for this component cell experiment and deliverables to Amonix. The first column is the Jt/Jm calculated from EQE measurements in conjunction with the AM1.5D, low-AOD (0.1000 W/cm^2) spectrum. The second column, labeled 'filtered', shows the expected Jt/Jm from spectrum transmitted through a fresnel lens, as used by Amonix. This is the expected Jt/Jm for these cells in the Amonix system. Note the slight drop in Jt/Jm indicating a reduction of top cell current.

The third column shows the calculated Jt/Jm from HIPSS LIV measurements, which are fairly close to the values after transmission through the fresnel lens. The next step is to obtain actual on-sun measurement of these cells in the Amonix system.

Table 2.14.2 Summary of the range of Jt/Jm achieved for this component cell experiment, using several different methods.

			filtered	
		AM1.5D, low-AOD	AM1.5D, low-AOD	HIPSS
		(AOD = 0.085)	(AOD = 0.085)	~230X
		EQE Jt/Jm	EQE Jt/Jm	Jt/Jm
J1	Avg (TC/MC)	0.97	0.95	0.96
J2	Avg (TC/MC)	0.99	0.97	0.99
J3	Avg (TC/MC)	1.07	1.05	1.05
J4	Avg (TC/MC)	1.12	1.10	1.10

The actual Jsc of each subcell and the resulting Jt/Jm will depend on many factors including the cell temperature, time of day, time of year, and atmospheric conditions. As the actual solar spectrum is constantly changing with time, this experiment will provide valuable data on how the individual subcells of a multijunction cell perform under actual operating conditions and help determine optimal multijunction cell designs for CPV systems. It would be ideal if the cells could be kept on sun for as long as possible (>1 year), however any field data will be very valuable for analysis and further cell optimizations.

Deliverables

Two top and two middle component subcells of each J-ratio were delivered to Amonix June 19, 2008, for a total of 16 component subcells. The cells will be incorporated into the Amonix concentrator system and preliminary characterization and performance data is pending. The photo below shows one of the Amonix CDO-080 cells with dual interconnects (IC's) on each ohmic pad delivered to Amonix. Additional subcells are available for Amonix if needed.

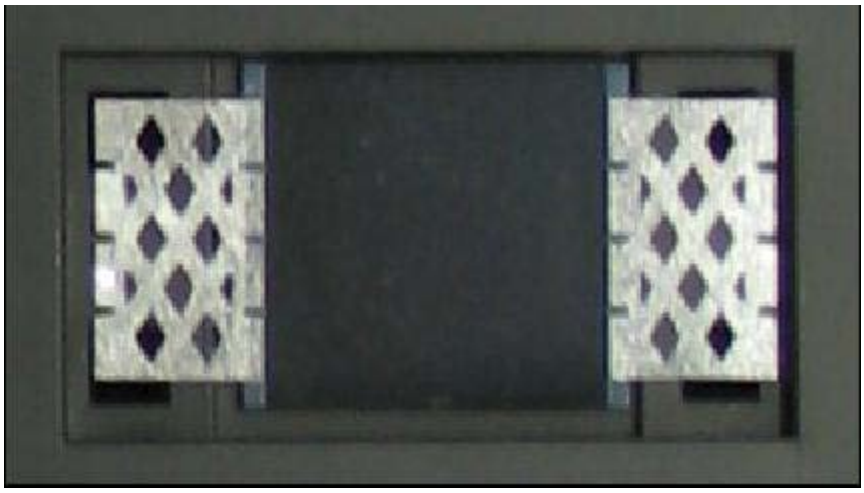

Fig. 2.14.19 Photo of one of the Amonix CDO-080 cells, with dual interconnects (IC's) on each ohmic pad, delivered to Amonix.

2.15 Cell Development Progress Report 15

2.15.1 High-Efficiency 3-Junction Cell Deliverable for Demonstration Module and Field Testing at Amonix

High-efficiency 3-junction terrestrial concentrator cells were built and tested at Spectrolab, with a non-standard current ratio between top and middle subcells and improved front metal grid, targeting improved efficiency and energy production under real-world operating conditions in fresnel lens concentrator PV systems. The current ratio (J-ratio) was adjusted upward to improve performance under the spectrum transmitted through fresnel lenses, and also to achieve an anticipated improvement in the energy production of these 3-junction concentrator cells under the varying solar spectrum over the course of the day and year. The improvements in cell metallization reduce shadowing and series resistance associated with the front metal grid.

The cell size produced for this deliverable was the CDO-080 (0.8 cm^2) configuration, to be consistent with Amonix' requirements for incorporating the cells into their demonstration module. Multiple runs were grown, fabricated, and characterized. The cells were characterized via light I-V (LIV) at a concentration of 555X (50.0 W/cm^2, or 500 suns), and selected cells were chosen for welding with interconnect (IC) tabs. The cells with ICs were then retested and delivered to Amonix.

Table 2.15.1 below summarizes the LIV parameters for the 50 cells tested. Spectrolab's specification for CITJ maximum power point efficiency is 36.7% minimum average for CDO-100 sized cells. These experimental cells are grown with a thicker top cell base, allowing for more optimal current balancing under LIV test.

Table 2.15.1 Summary of LIV parameters (555X, 50.0 W/cm^2, AM1.5D, ASTM G173-03) for 50 high-efficiency Spectrolab 3-junction terrestrial concentrator solar cells, delivered for field testing at Amonix in fresnel lens concentrator PV systems.

	Voc	Isc	Jsc	Vmp	Imp	Jmp	Pmp	FF	Eff @ 555X
	(V)	(A)	(A/cm^2)	(V)	(A)	(A/cm^2)	(W)		AM1.5D
average	3.13	5.86	7.19	2.79	5.75	7.05	16.03	0.87	39.3
stdev	0.01	0.03	0.04	0.01	0.03	0.04	0.05	0.00	0.1

The LIV curves for the highest and lowest efficiency cells from this set of 50 cells are shown in Fig. 2.15.1 below. Note the uniformity and desirable high shunt resistance of these cells.

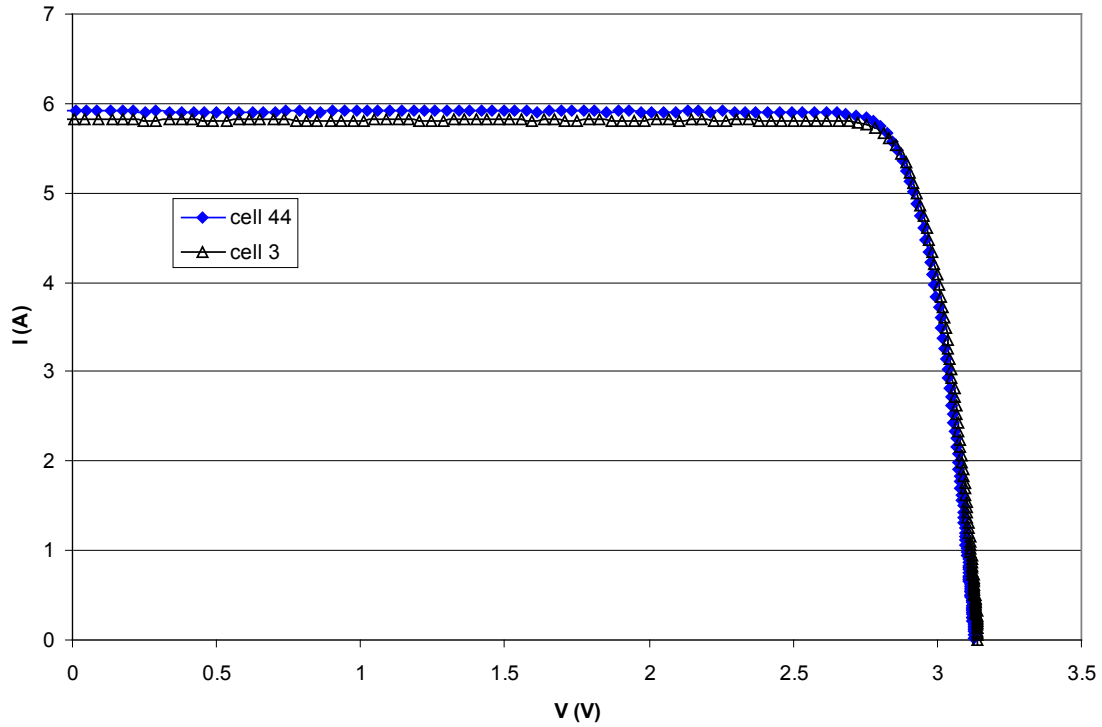

Fig. 2.15.1 Illuminated I-V curves for the cells with the highest and lowest efficiency in the batch of 50 delivered cells.

Figure 2.15.2 below plots Isc and Voc vs. Pmp, all at 555X (50 W/cm^2) concentration. The inverse relationship between Isc and Voc is probably due to slight variations in the top cell band gap (Eg), however, the Eg extraction would have to be done from EQE measurements on cells that lie along the trend line to verify this assumption. The FF is fairly uniform for this group of cells, with an average of 0.87.

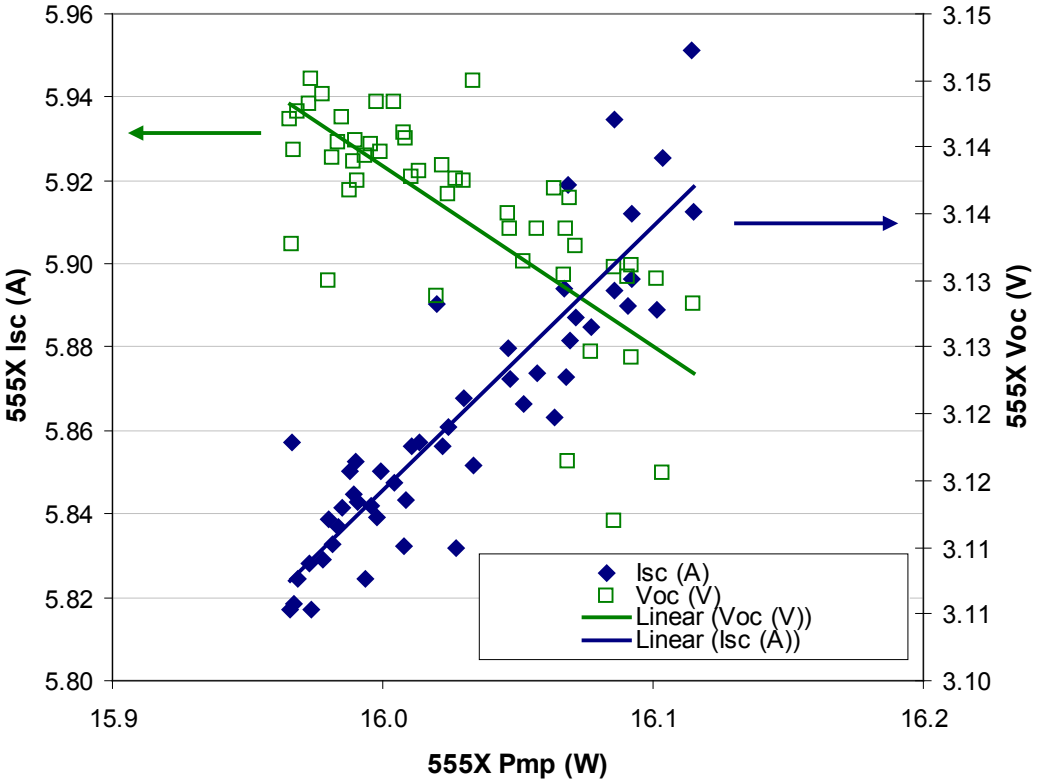

Fig. 2.15.2 Plot of short-circuit current Isc and open-circuit voltage Voc versus power at the maximum power point Pmp, for the batch of 50 delivered high-efficiency 3-junction concentrator cells.

External quantum efficiency (EQE) was performed on a subset of the cells and the LIV and EQE data were provided to Amonix. Some representative EQE curves of the 50 cell deliverables are shown in Fig. 2.15.3 below. Note the high degree of uniformity in the spectral response of these cells. The 50 multijunction cells have been delivered to Amonix for incorporation into their concentrator module.

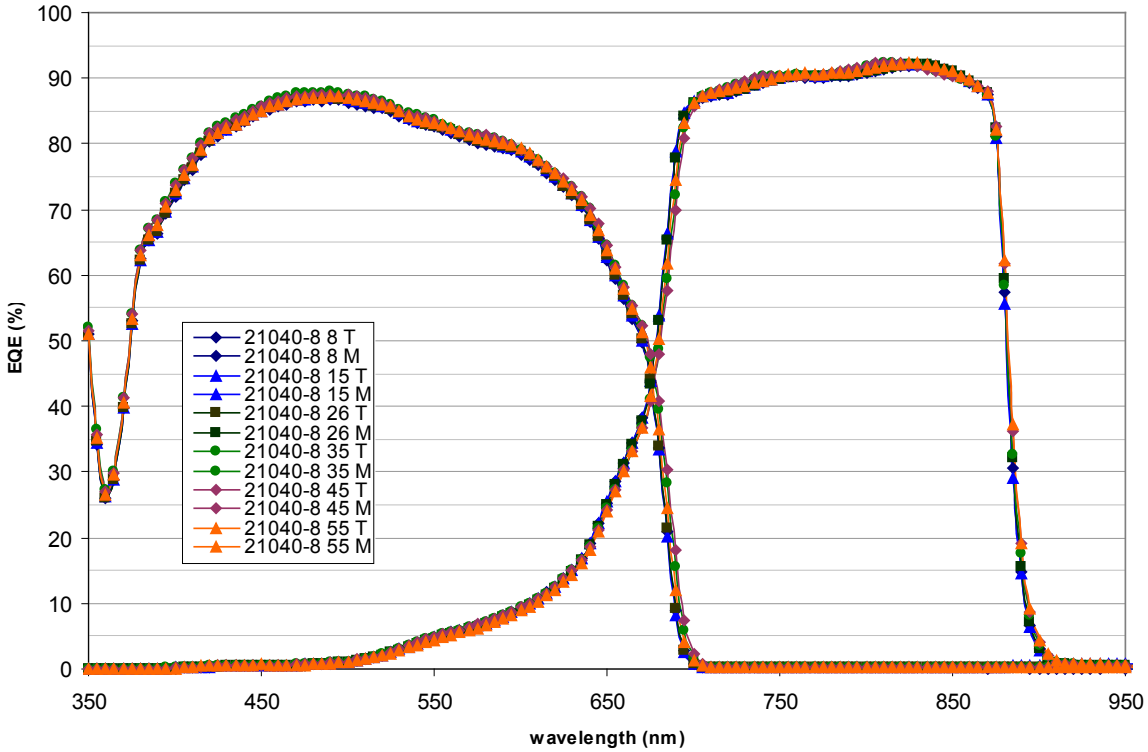

Fig. 2.15.3 Representative external quantum efficiency (EQE) measurements for the batch of the 50 high-efficiency 3-junction concentrator cell deliverables.

2.15.2 J-Ratio (Jt/Jm) Mapping Field Experiment

Experiment Description

In addition to the 50-cell delivery described in the last section, Spectrolab has planned an additional experiment to be performed in collaboration with Amonix, to further probe the relationship between J-ratio and energy production. Spectrolab grew and fabricated a number of CDO-080 cells that span a range of the top to middle subcell current density ratio Jt/Jm. These cells are designed to be used in the Amonix concentrator experiment and the photovoltaic measurements produced under field conditions will be useful for further optimization of subcell current balancing.

Current balancing of multijunction solar cells is crucial in order to produce the most power possible from a given solar cell bandgap combination. Among the key open questions for terrestrial CPV are:

- What is the effect of daily and seasonal spectral variation on multijunction cell output under operation?

and

- What is the optimal Jt/Jm to maximize the power produced during operation?

In order to address these questions experimentally, a series of CITJ-based cells were grown that span a range of J-ratios (Jt/Jm). It is assumed that the Ge subcell current will not limit the cell in operation.

The additional wafers from the Jt/Jm experiment were grown, processed and fabricated into CDO-080 solar cells designed for the Amonix system. Cells were screened on the LIV auto tester at 555X (50.0 W/cm^2) and a subset of those cells were further processed by attaching metal interconnects to them.

External quantum efficiency (EQE) measurements were performed on a small number of the cells to confirm the variation in Jt/Jm. Table 2.15.1 below shows the range of Jt/Jm as determined by EQE measurements (performed at room temperature) and integrating with the AM1.5D, low-AOD terrestrial spectrum.

Table 2.15.1 Range of Jt/Jm in the experiment as determined by EQE measurements, and integration with the AM1.5D, low-AOD terrestrial spectrum.

	avg. Jt/Jm
J1	0.95
J2	0.97
J3	1.03
J4	1.06
J5	1.09
J6	1.12

Figure 2.15.4 below shows a representative EQE curve for each of the six Jt/Jm multijunction cells for this experiment. Note that as the top cell response increases there is a corresponding decrease in the high energy side of the middle cell response, as less light is transmitted to the middle cell. The average sum of Jt + Jm gives 28 mA/cm^2 for this terrestrial spectrum based on these measurements.

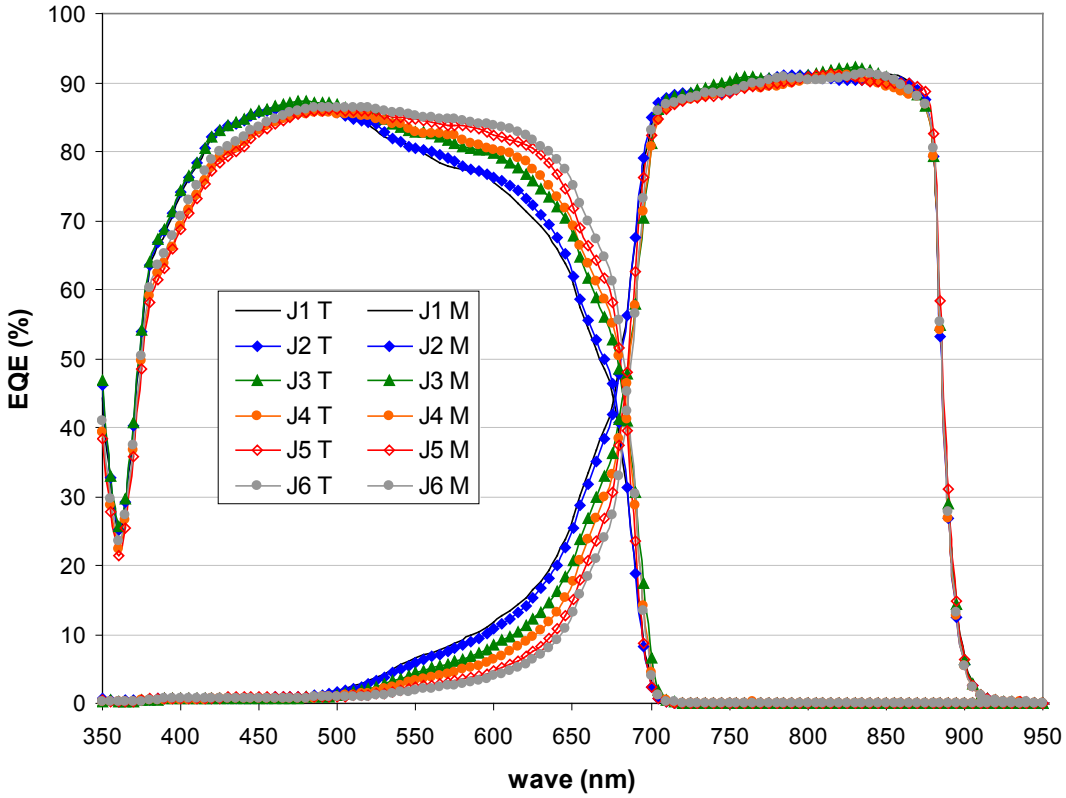

Fig. 2.15.4 Representative EQE curves for each of the six Jt/Jm conditions for the multijunction cells in this experiment.

For clarity, the top cell and middle cell responses are shown separately in Figs. 2.15.2a and 2.15.2b below. An interesting observation based on this small sampling of the measurements is that the cells with the lowest Jt/Jm (denoted as J1, J2, and J3), show a slightly better blue response in the range ~380-490 nm in the top cell than the three cells with the highest Jt/Jm (J4, J5, and J6). More measurements and analysis need to be performed to verify this observation and determine if it is material-related (*i.e.*, thicker GaInP degrades the top cell emitter response) or due to device variation related to MOVPE growth variation.

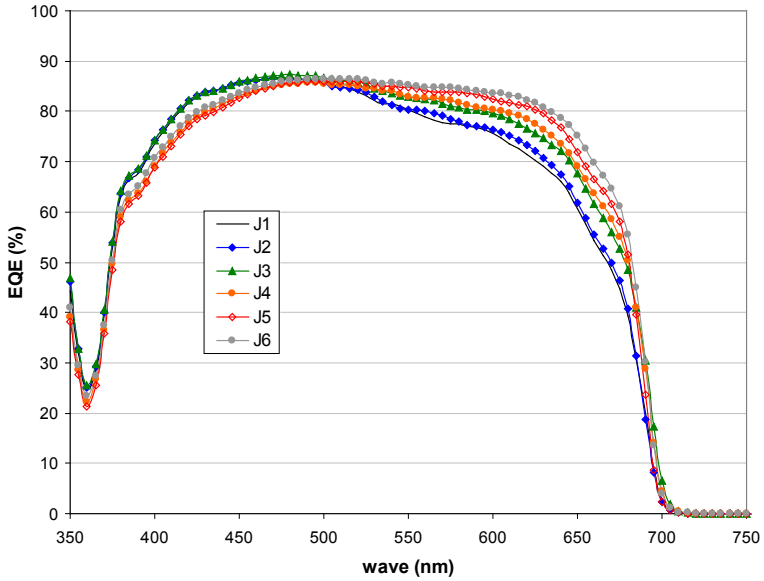

(a)

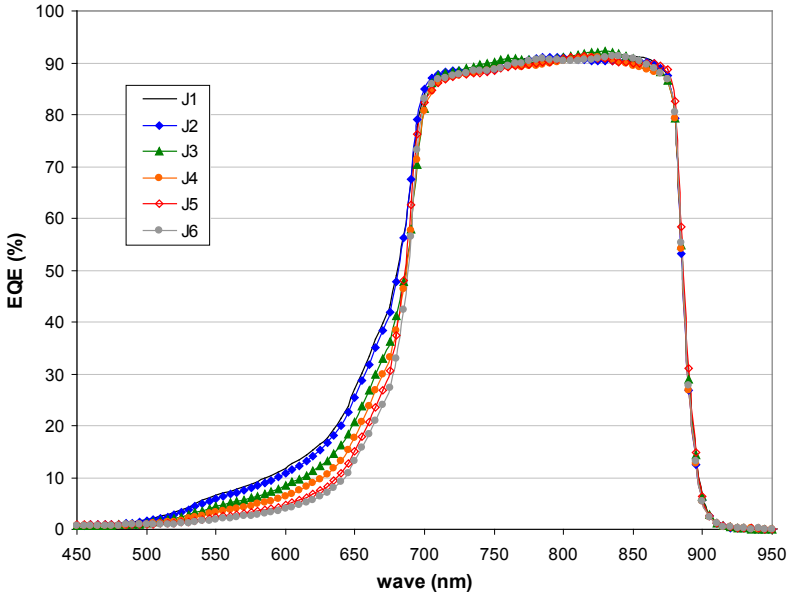

(b)

Fig. 2.15.2 External quantum efficiency measurements for (a) the GaInP top cell and (b) the GaInAs middle cell for the six Jt/Jm conditions in this experiment.

The four charts below in Fig. 2.15.3 show averages of the 16 cells used for each Jt/Jm (labeled J1-J6). In this case the Voc is relatively uniform. The Isc does appear to increase with increasing Jt/Jm, as expected for a top-subcell limited design. It should be noted that the LIV-based Isc measurement is relatively uncertain, due to using the same calibration standards for all the Jt/Jm experimental cells as opposed to different setup standards for each Jt/Jm. Another observation is that there appears to be a slight decrease in FF with increasing Jt/Jm, presumably due to better current matching at higher J-ratios.

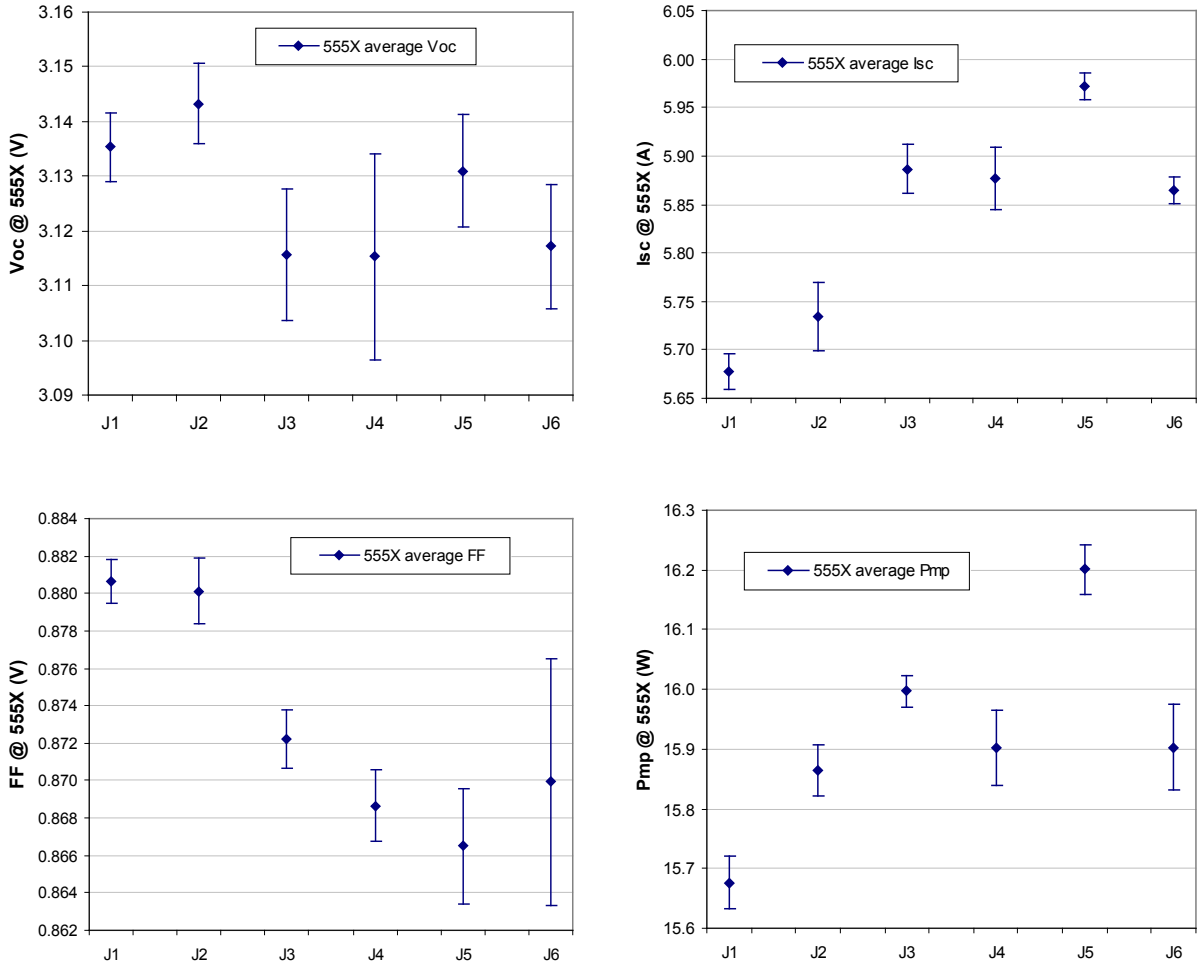

Fig. 2.15.3 Plots of Voc, Isc, FF, and Pmp, measured on the HIPSS at 555X (50.0 W/cm^2), for the various Jt/Jm values represented by experimental conditions J1 through J6.

The chart in Fig. 2.15.4 below plots FF vs. Isc for each of the six Jt/Jm groups of cells in the experiment. The FF appears to decrease fairly consistently with higher Isc.

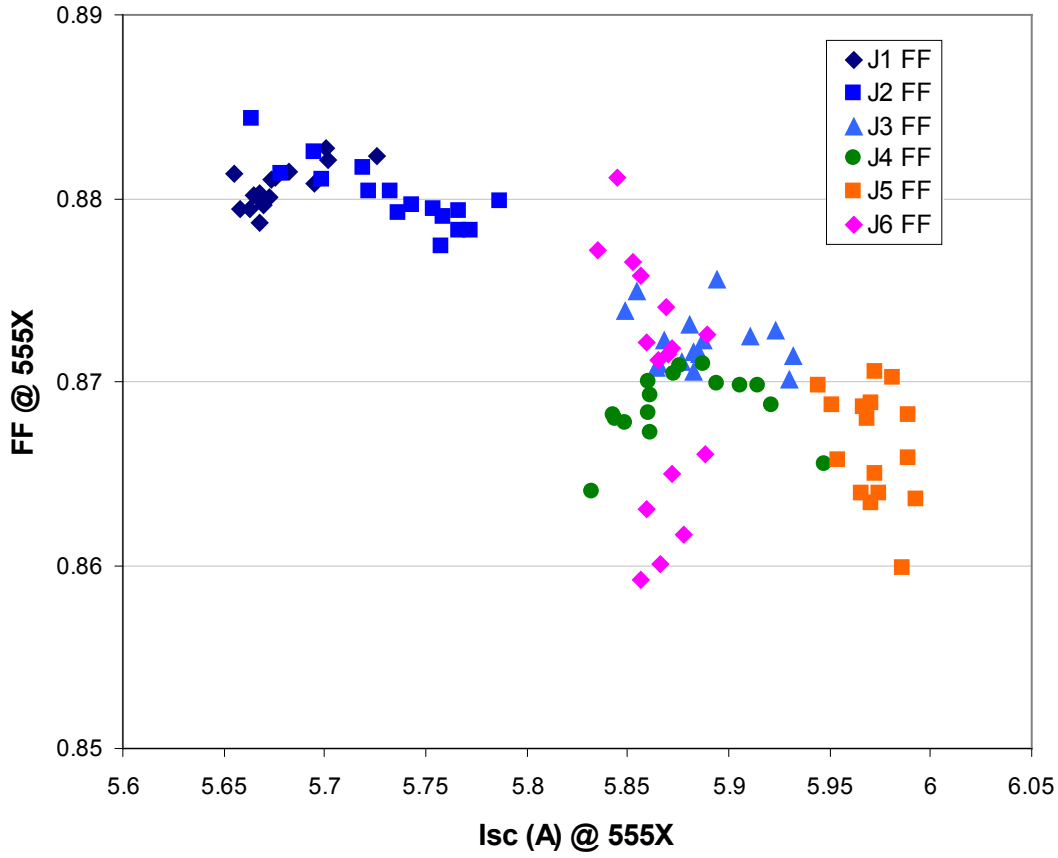

Fig. 2.15.4 Plot of FF vs. Isc measured using the high-intensity pulsed solar simulator (HIPSS), for each of the six Jt/Jm groups of cells in the experiment.

Figure 2.15.5 is a plot of six LIV curves at 555X (50.0 W/cm^2) concentration, representing each of the six Jt/Jm sets. Note the high performance of each representative cell, with high shunt resistance and FF evident from the LIV curves. It should be noted that all of these runs are single MOVPE runs and would require optimization to improve the uniformity of each Jt/Jm design.

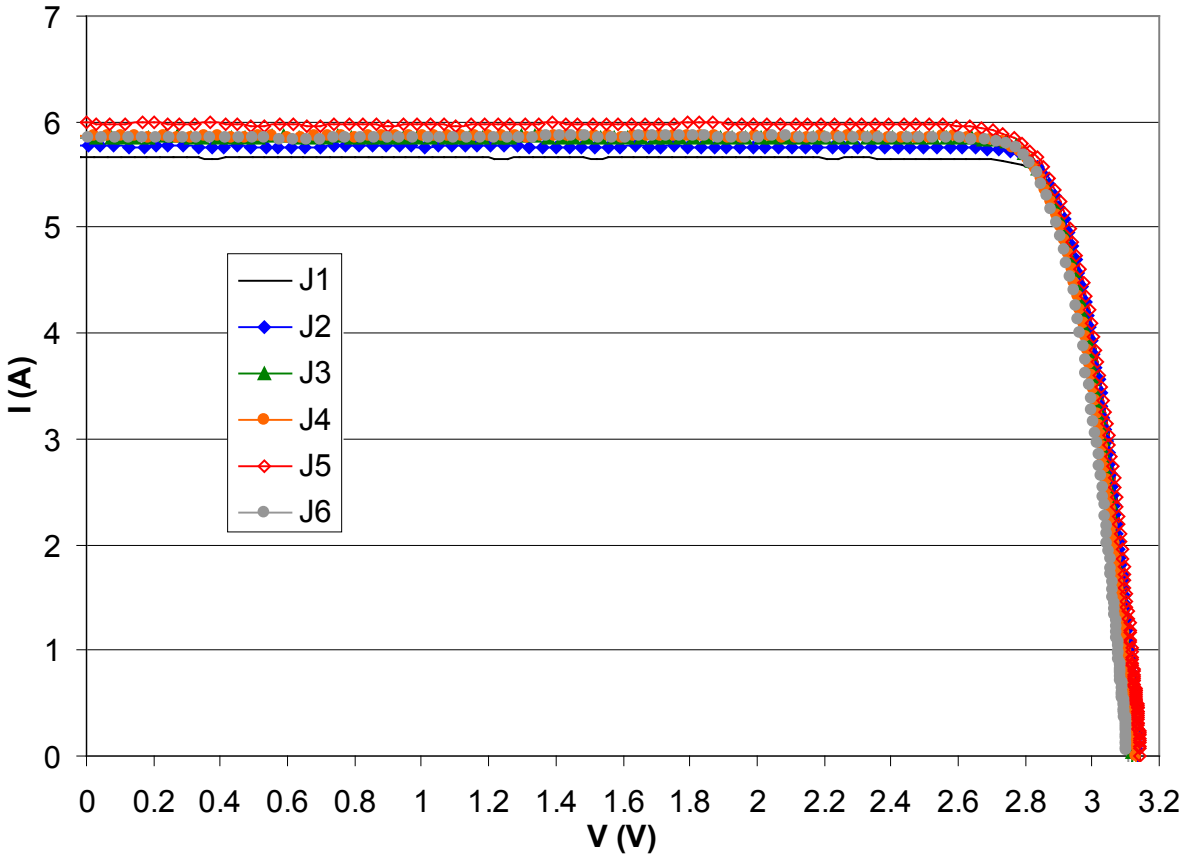

Fig. 2.15.5 Plot of LIV curves measured using the HIPSS at 555X (50.0 W/cm^2), for representative cells from each of the Jt/Jm groups in the experiment.

The variable Jt/Jm of the experimental groups of high-efficiency Spectrolab cells in this study, in conjunction with measured efficiency and energy production in the field from the Amonix system, should provide very useful information for further cell optimization for real-world concentrator photovoltaic systems.

2.15.3 Studies of Inverted Metamorphic 0.8-1.1 eV GaInAs Subcells

Experiments were carried out to characterize the nature of dislocation defects and their minority-carrier recombination properties in inverted metamorphic (IMM) 0.8-1.1 eV GaInAs subcells, as well as inverted lattice-matched (ILM) 1.4-eV GaInAs subcells, for use in high-efficiency multijunction terrestrial concentrator cells with an inverted metamorphic design. The results were summarized in a paper [17], and an excerpt from that paper describing the IMM GaInAs subcell study, with revised figure numbers, is given below.

Description of Inverted Metamorphic GaInAs Subcell Study from [17]

Semiconductor compositions with the desired band gaps for solar photovoltaic energy conversion can be grown easily enough, but many of those compositions are not lattice-matched to any readily available epitaxial growth substrate. As a result, the crystal lattice of these lattice-mismatched materials can become riddled with dislocations, which mediate Shockley-Read-Hall (SRH) recombination in the cell and lower cell voltage. The formation of dislocations tends to become more severe the greater the amount of lattice mismatch to the substrate, and constitutes the main barrier to using lattice-mismatched compositions freely to reach the optimal band gaps for maximum terrestrial solar cell efficiency.

The formation of dislocations can be mitigated by the use of a metamorphic buffer layer, in which the lattice-constant is transitioned to a different value than that of the growth substrate. In the metamorphic buffer, a layer or series of layers with graded composition is grown, allowing the strain in those graded layers to relax by dislocation formation in the metamorphic buffer, so that relaxed semiconductor layers can be grown with a much reduced density of dislocations on the virtual substrate with a new lattice constant formed by the metamorphic buffer. These low-defect-density layers with relaxed crystal structure grown on top of the metamorphic buffer are also termed metamorphic, such as the metamorphic active subcell regions in a multijunction solar cell, since they benefit from the metamorphic buffer. In many multijunction cell architectures, such as inverted metamorphic multijunction solar cells, sunlight must pass through the metamorphic buffer to subcells beneath, so it is advantageous to use high-band-gap semiconductors such as AlGaInAs or GaInP to form a transparent metamorphic buffer region.

It is important to quantify the degree to which the metamorphic buffer can suppress dislocation density in metamorphic cells to better understand how metamorphic materials can be used in multijunction solar cells. Since there are a wide variety of multijunction cell designs in which metamorphic cells can be used, such as 4-, 5-, and 6-junction cells, wafer-bonded solar cells, and others, and the optimal band gaps vary widely for these different designs, it is valuable to know how the dislocation density varies as a function of composition and lattice mismatch to the substrate. Furthermore, since it is the electron-hole recombination mediated by the dislocations that influences solar cell performance, it is important to measure the recombination activity of dislocations in metamorphic materials. The recombination activity of a single dislocation is found to vary widely depending on degree of lattice mismatch, semiconductor composition, *e.g.*, In content in GaInAs, as well as in GaInP contrasted to GaInAs, and dislocation type, *e.g.*, dislocation clusters vs. dislocation dipoles. This variation in the

recombination activity of dislocations has a profound effect on the efficiency of metamorphic solar cells, separate from the effects of dislocation density alone.

To investigate the properties of dislocations in a relevant metamorphic device structure, single-junction inverted metamorphic GaInAs solar cells were grown on a transparent AlGaInAs metamorphic buffer by metal-organic vapor-phase epitaxy (MOVPE), on 100-mm Ge substrates. A range of GaInAs inverted solar cell base compositions were grown, from ~2 to 44% indium, corresponding to band gaps from 1.39 to 0.84 eV, and lattice mismatch from ~0 to 3.1%. Solar cell parameters such as open-circuit voltage Voc and external quantum efficiency (EQE) were measured by illuminating the inverted cells through a grid on the back surface, to characterize the cells in a state close to their as grown condition, without the complicating factors introduced by the usual process for bonding inverted epitaxial solar cells to a handle substrate, removing the growth substrate to expose the sunward surface, and completing device fabrication on the now right-side-up cell. Dislocation density was measured on the same solar cells for which I-V characteristics were measured, by cathodoluminescence (CL) and electron-beam-induced current (EBIC) at the National Renewable Energy Laboratory (NREL). In addition, the recombination activity of the dislocations was measured by CL, by comparing the lowest photon intensity corresponding to the dislocation to the background intensity in parts of the base away from dislocations. A schematic of the inverted solar cell test structure is shown in Fig. 2.15.6.

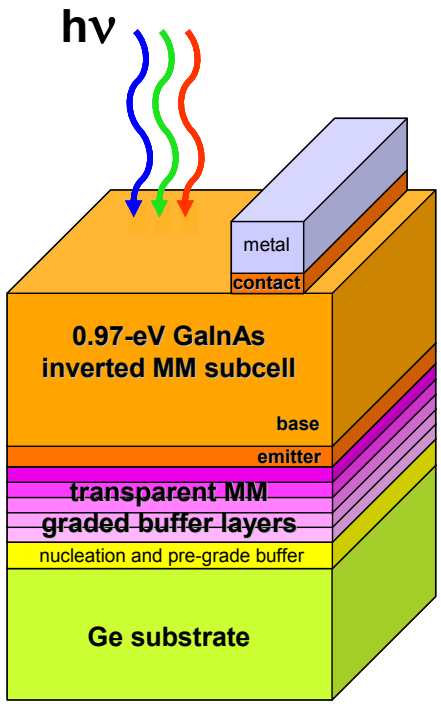

Fig. 2.15.6 Schematic of the single-junction inverted metamorphic solar cell test structure used in the experiment, with illumination from the back surface of the inverted cell, for the case with a 0.97-eV GaInAs base.

Images formed by EBIC are shown in Fig. 2.15.7, for inverted solar cells with band gaps of 1.39, 1.10, 0.97, and 0.84 eV as measured by EQE, corresponding to indium compositions in the GaInAs base of approximately 2% (nearly lattice matched), 23%, 33%, and 44%, respectively. The expected increase in dislocation density with increasing lattice mismatch can be seen, as well as a change in the type of dislocation as the In content is increased. At the lowest indium concentration at 1.39 eV, dislocations are seen in pairs, or dipoles, presumably propagating from a single defect deeper in the epitaxial material. For the 1.1-eV sample, two different types of dislocations are seen, a darker type on the EBIC scan and a lighter type with less severe recombination activity. In the 0.97 and 0.84 eV samples with highest indium content, alignment of the dislocations in streaks, aligned to the crystal lattice can be seen, perhaps due to interactions with the cross-hatch patterns seen in the surface topography of these highly lattice-mismatched samples.

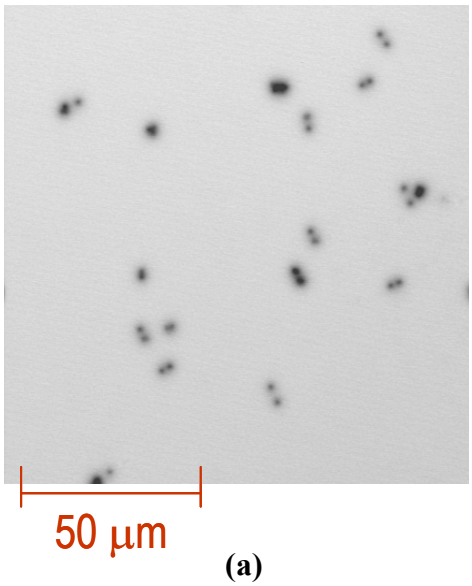

(a)

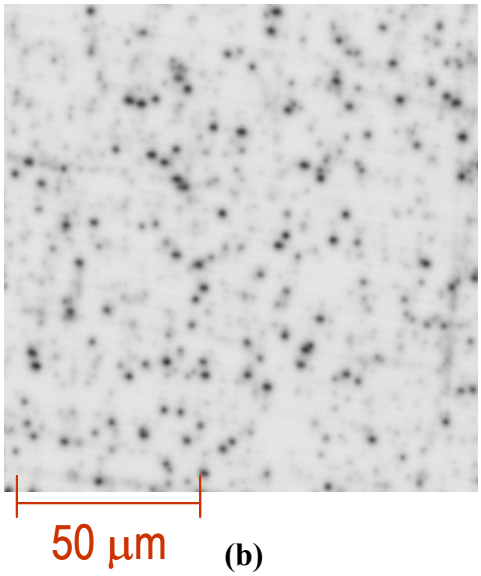

(b)

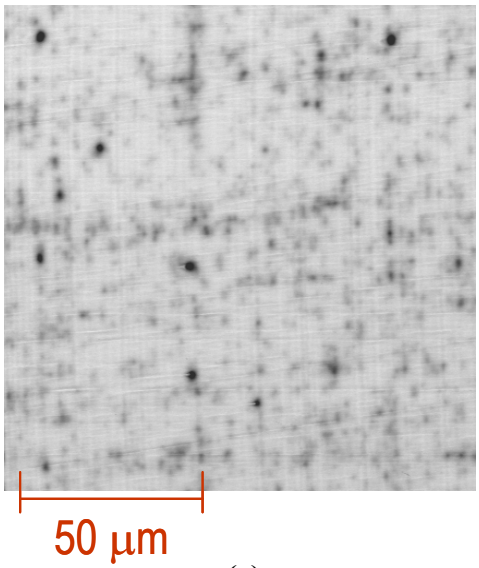

(c)

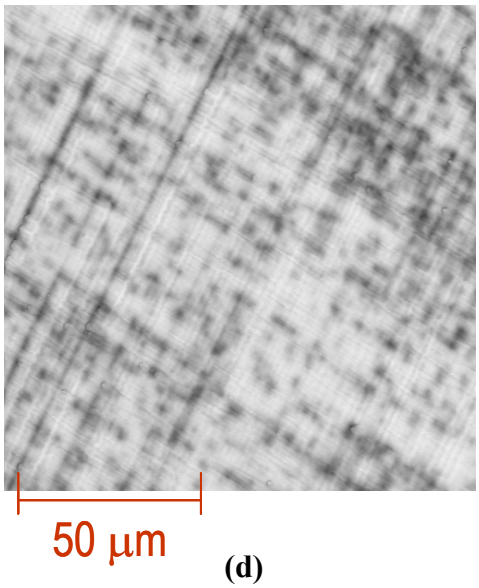

(d)

Fig. 2.15.7 Electron-beam-induced current (EBIC) images of dislocations in inverted metamorphic solar cells with band gaps of (a) 1.39 eV; (b) 1.10 eV; (c) 0.97 eV; and (d) 0.84 eV, as described in the text.

Figure 2.15.7 plots the band gap measured by EQE, Voc from illuminated I-V measurements at approximately one sun, and the band gap-voltage offset Woc ≡ (Eg/q) – Voc as a function of indium content and lattice mismatch for four different GaInAs inverted metamorphic solar cells. The band gap-voltage offset provides a measure of crystal quality and minority-carrier lifetime since it is a measure of how far the electron and hole quasi-Fermi levels are from their respective band edges [1], with smaller values of Woc indicating lower recombination. Woc shows some variation in the different inverted MM solar cell samples, but is roughly constant over a wide range of In compositions and lattice mismatches. Dislocation densities measured by EBIC are also plotted in Fig. 2.15.7, and show a nearly linear dependence on In composition and lattice mismatch with respect to the Ge substrate.

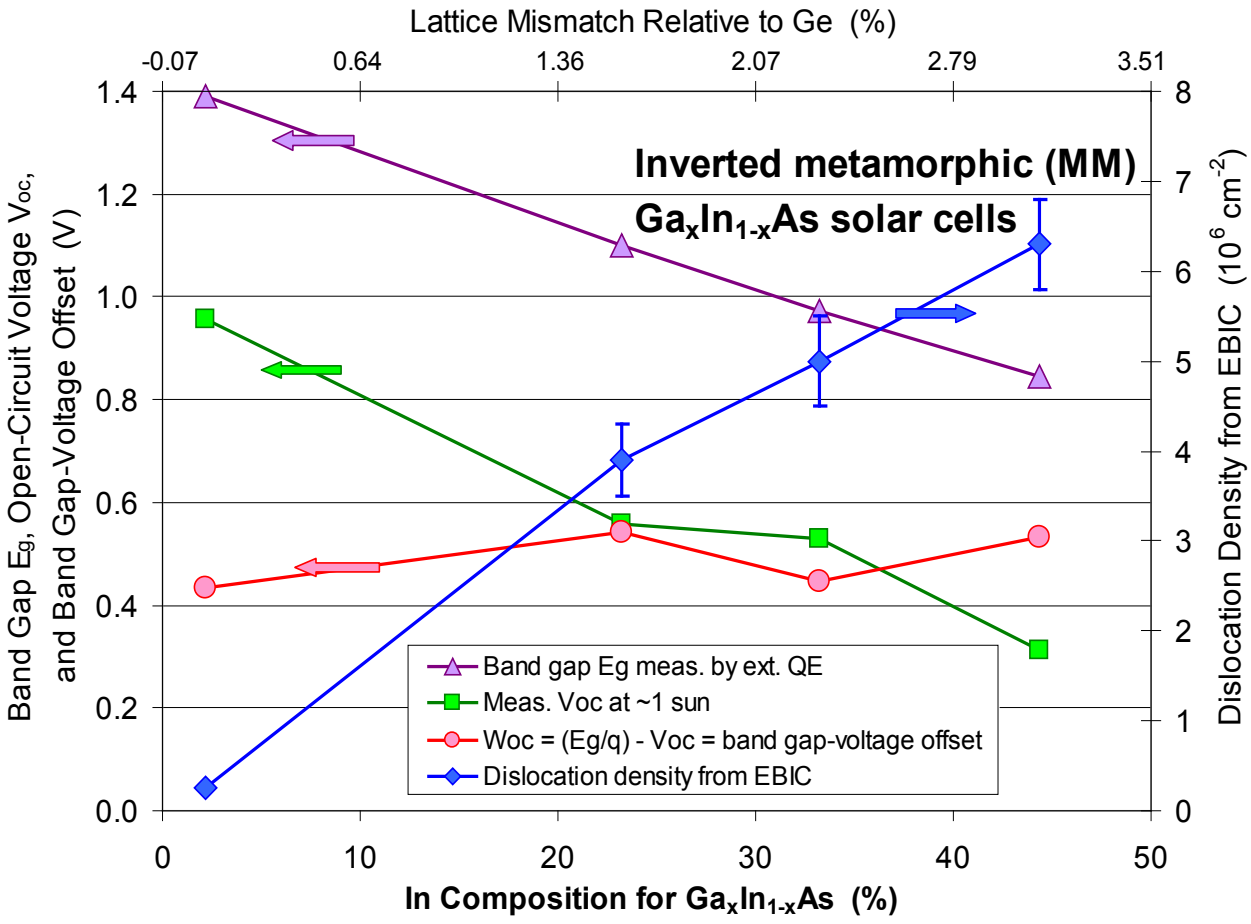

Fig. 2.15.7 Measured band gap, open-circuit voltage, and band gap-voltage offset for inverted metamorphic GaInAs solar cells as a function of In composition and lattice mismatch, and comparison to dislocation measured by electron-beam-induced current (EBIC) at NREL.

Figure 2.15.8 plots the cathodoluminescence photon intensity for a wide field of view including both dislocations and background regions of the samples. These measurements provide confirmation of the cell band gaps, and also show the lower photon intensity from increased recombination due to increased average recombination activity at each dislocation, as well as the higher dislocation density as lattice mismatch is increased.

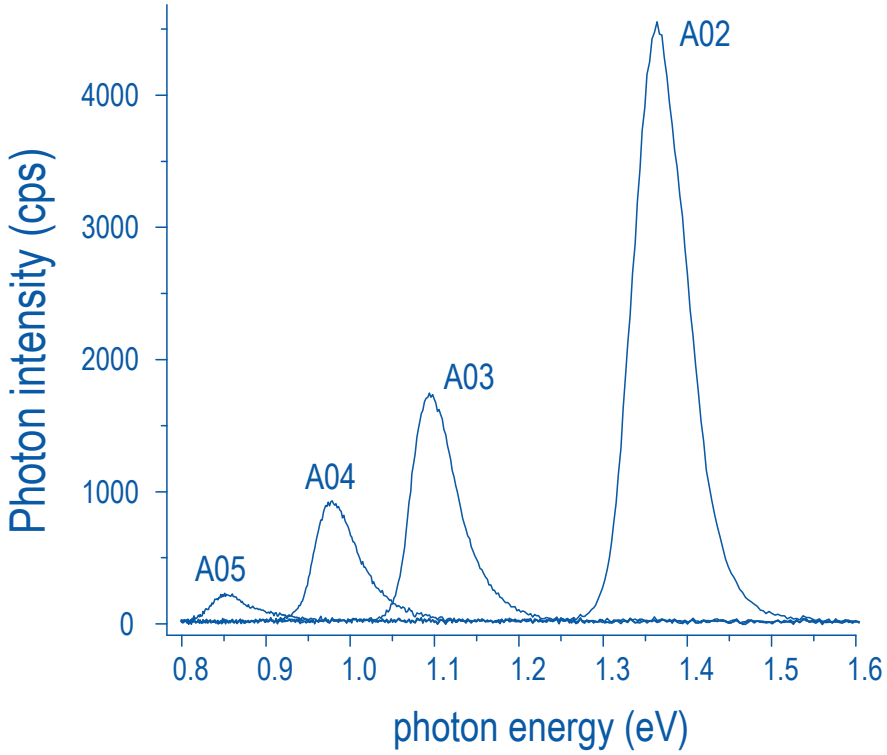

Fig. 2.15.8 Cathodoluminescence photon intensity as a function of photon energy for 4 compositions of inverted metamorphic GaInAs solar cells.

In Fig. 2.15.9, the dislocation density is plotted as before as a function of indium composition, along with the CL photon intensity. The measured CL photon intensity declines roughly linearly with increasing lattice mismatch to the Ge growth substrate. The average fraction of carriers lost at each dislocation is also plotted, as a relative measure of the recombination activity of each dislocation for the 4 different In compositions. The fraction of carriers lost at a dislocation is calculated from CL measurements by finding the difference between the background CL photon intensity I_{BG} and the minimum CL photon intensity right over the dislocation I_D , divided by I_{BG} :

(1) $$(I_{BG} - I_D)/I_{BG}$$

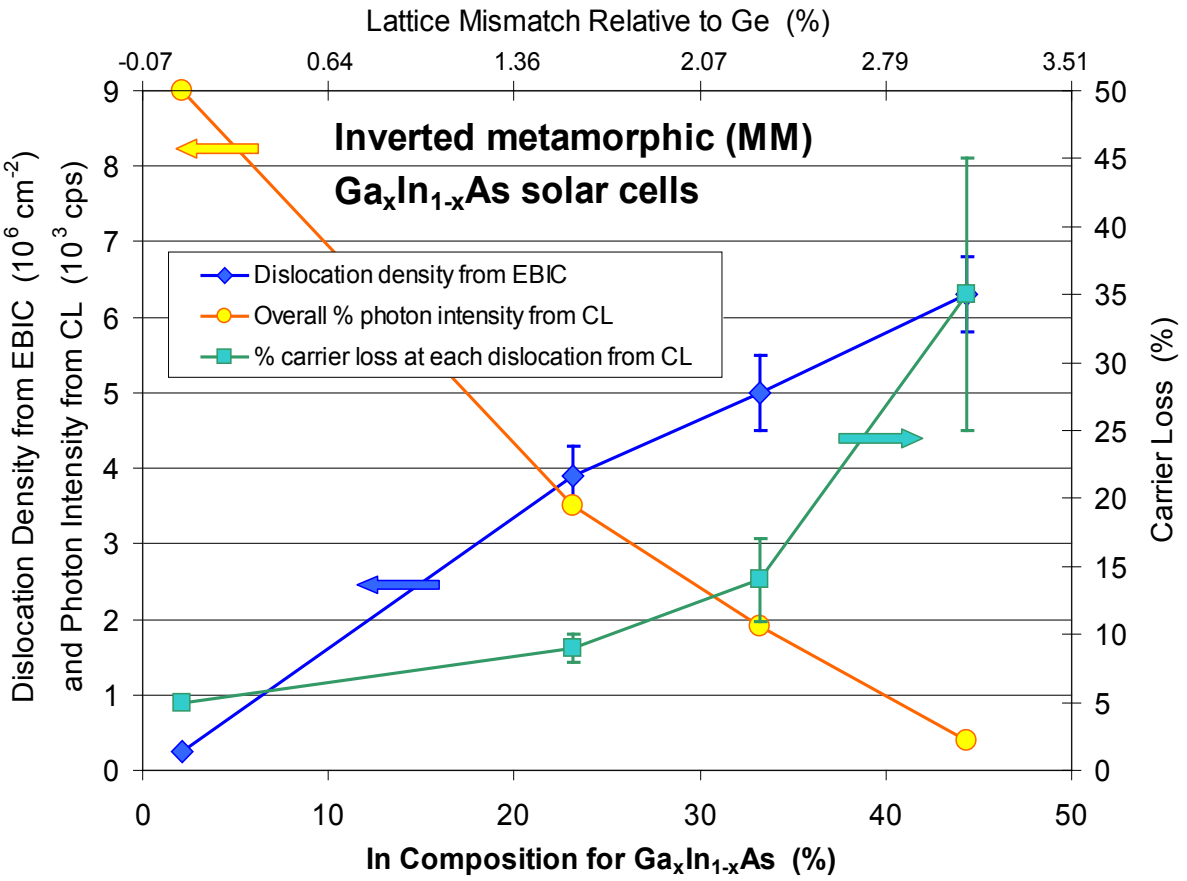

Fig. 2.15.9 Dislocation density measured by EBIC, overall photon intensity measured by cathodoluminescence (CL), and average carrier loss measured for dislocations as described in the text, for 4 GaInAs inverted metamorphic solar cell compositions.

The impact of this average recombination activity at dislocations in different GaInAs matrices can be roughly gauged by combining the dislocation density N_{disloc} measured by EBIC with the fractional carrier loss at dislocations f_{disloc} measured by CL, and assuming an approximate radius r_i over which a dislocation can influence recombination of carriers. Choosing an approximate radius of influence of ~1 μm, corresponding to the dark area surrounding each dislocation, allows one to calculate a total fractional carrier loss across the sample f_{total} :

(2) $$f_{total} = N_{disloc} \pi r_i^2 f_{disloc}$$

which reflects the recombination activity of dislocations as well as the dislocation density. This relative measure of total fractional carrier loss, plotted in Fig. 2.15.10, has a roughly exponential dependence on In composition and lattice mismatch. A more accurate analysis would include a measurement of the effective radius of influence of the dislocations on recombination from the CL data at each In composition.

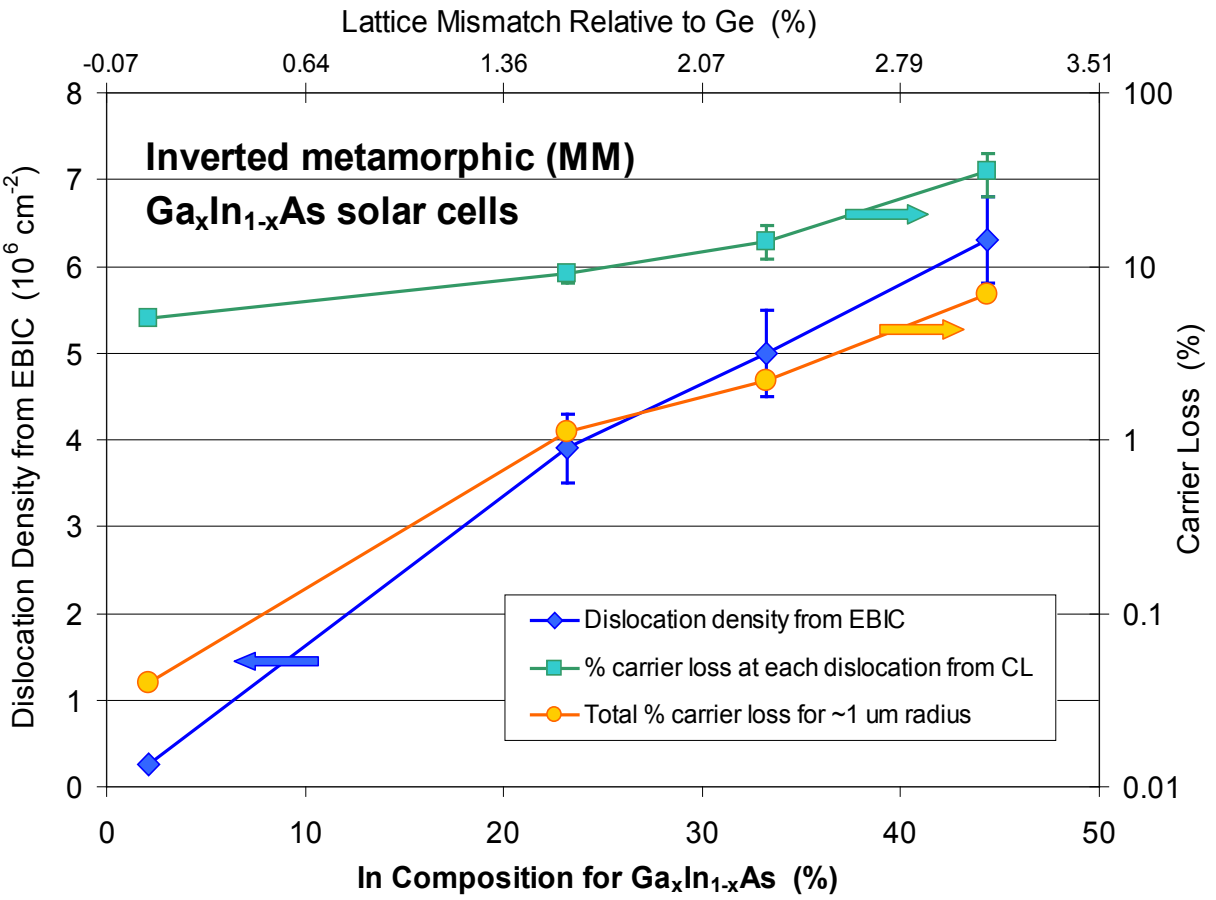

Fig. 2.15.10 Dislocation density, average carrier loss providing a measure of recombination activity of each dislocation, and relative total carrier loss from dislocations taking into account number of dislocations, average recombination activity for a single dislocation, and assuming an approximate radius of influence of ~1 μm surrounding each dislocation.

2.15.4 Inverted Metamorphic 3-Junction Solar Cell Development

The inverted-metamorphic (IMM) terrestrial triple-junction (3J) solar cell structure design aims to implement the near-optimal 1.9/1.4/1.0 eV band-gap combination by employing inverted growth of lattice-matched top and middle subcells followed by a metamorphic bottom subcell. Towards the goal of developing potentially high-efficiency devices of this type, we have performed MOVPE growth runs to prepare GaInP/ Ga(In)As/ GaInAs 3J-IMM terrestrial concentrator solar cell structures.

Selected wafers from these runs underwent a full IMM solar cell process which consists of metal-bonding onto a Ge handle substrate, removing the original Ge growth substrate, and fabricating into upright 1.0 cm^2-area devices with photolithographically-defined concentrator grid patterns. Current-voltage testing was then performed on the resulting cells, under simulated illumination calibrated to the AM1.5D terrestrial solar spectrum, for a range of intensities.

Figure 2.15.11 shows several examples of 3J-IMM cell LIV curves, measured using an XT-10 steady-state solar simulator for the low-level concentration range shown in panel (a), and a pulsed solar simulator for the higher intensities shown in panel (b). The measurements indicate that both tunnel junctions in the structure exhibit the desired ohmic behavior (no indication of negative resistance characteristics) for intensities up to ~85 suns.

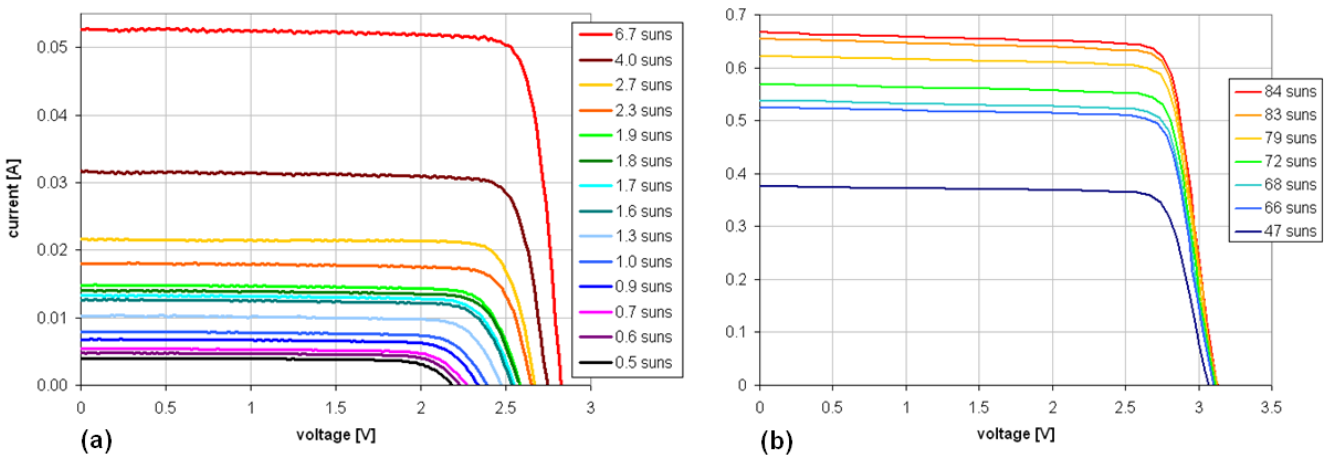

Fig. 2.15.11 Terrestrial concentrator 3J-IMM cell light I-V curves measured under (a) low, (b) moderate concentration.

The external quantum efficiency (EQE) of those devices was also measured, with a representative example shown in Fig. 2.15.12. One feature that stands out in these early runs is the sub-optimal behavior of subcell 1 (top subcell), especially in the blue 350-550 region of the spectrum. Therefore, the blue response of the top subcell was identified as an area of priority for further 3J-IMM work, as detailed in the next section. In contrast, subcell 2 (middle subcell) has excellent quantum efficiency, indicating that it generates enough current to support a high-efficiency triple-junction cell. Another noteworthy feature is the spectral response curve for subcell 3 (bottom subcell). This subcell is in closest proximity to the bonding interface for upright-processed devices, which makes it most susceptible to any bonding-induced defects or impurities. Therefore, the nearly-optimal quantum efficiency of the bottom subcell constitutes an important validation of the 3J-IMM process.

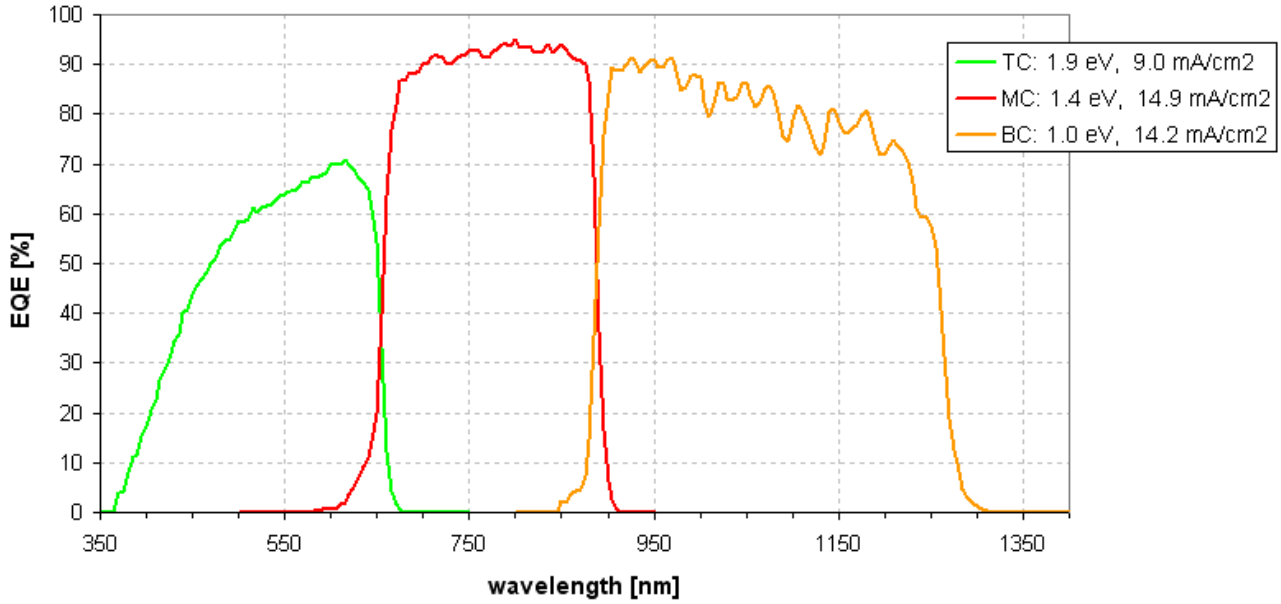

Fig. 2.15.12 Measured spectral response for each of the three subcells of an inverted metamorphic terrestrial concentrator 3-junction cell.

2.15.5 Inverted Lattice-Matched 1.9-eV Subcell Development

While the inverted growth of a 3J-IMM structure allows its top two subcells to benefit from the high crystal quality associated with lattice-matched layers, it also presents a significant challenge when it comes to bringing the device performance of those subcells to the level of their upright-grown counterparts.

In this study, we focused our subcell development work on the inverted lattice-matched 1.9-eV top component of the IMM 3-junction terrestrial concentrator cell structure. The experimental matrix included MOVPE runs to prepare top-subcell-only inverted-growth solar cell structures with: 1) two different base-layer thicknesses, differing from each other by a factor of 2×, which we will refer to as "thin" and "thick"; and 2) two different doping levels in the emitter layer, which we will label as "light" and "heavy". The thin-base, lightly-doped structure would be suitable for a solar cell intended for operation under the 1-sun AM0 space spectrum. By contrast, the lower short-wavelength intensity in the AM1.5D spectrum requires the top subcell of a terrestrial device to be nearly optically-thick; also, since such a cell is intended for operation under concentration, it will require low sheet resistance as enabled by a highly-doped emitter layer. Therefore, this experiment aims to compare the structure with a thin base and lightly-doped emitter, to the desired structure with a thick base and heavily-doped emitter needed for terrestrial concentrator cells.

Selected wafers from representative runs in each of the four structure types were processed into upright handle-mounted concentrator cells. Figure 2.15.13 shows the measured external quantum efficiency for representative cells from each of the four device structures. As compared to the structure labeled as "thin-light" in the figure (thin overall top cell thickness, light top cell emitter doping), all others show relatively poor response in the short-wavelength 350-550 nm region of the spectrum, a behavior indicative of minority-hole diffusion length in the emitter that is comparable to or less than the emitter thickness, rather than the desired case of a diffusion length many times the emitter thickness. This can be caused by inferior emitter crystal quality, excessive emitter doping, and other mechanisms.

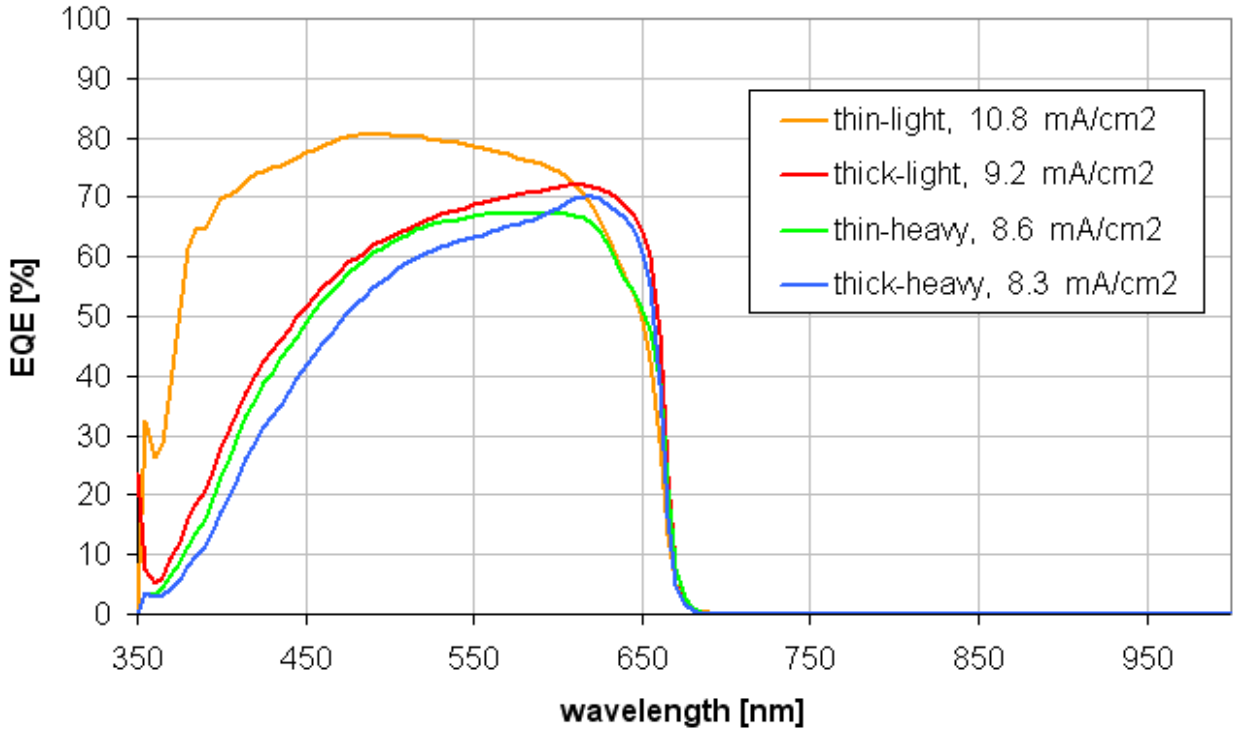

Fig. 2.15.13 Impact of device structure on the inverted 1.9-eV top subcell spectral response.

In the case of the highly-doped compositions (denoted by "thick-heavy" and "thin-heavy"), this behavior is presumably due to sub-optimal doping conditions, limiting the minority-carrier diffusion length and hence the current generation in the emitter. Another notable result is the increased response that both thick-base structures exhibit in the longer-wavelength 600-670 nm region of the spectrum, when compared to their thin-base counterparts. This is due to the intended effect of increasing the optical thickness of the top cell base, and allowing less light to pass through to the middle subcell, as demanded by the current-matching requirements of the terrestrial solar spectrum. Future work on the lattice-matched inverted 1.9 eV component development should include a doping-level optimization experiment, which is expected to significantly improve the blue spectral response of these devices.

References – Section 2.15

[1] R. R. King, D. C. Law, K. M. Edmondson, C. M. Fetzer, G. S. Kinsey, H. Yoon, R. A. Sherif, and N. H. Karam, "40% efficient metamorphic GaInP / GaInAs / Ge multijunction solar cells," *Appl. Phys. Lett.*, Vol. 90, No. 18, 183516, 4 May 2007.

[17] R. R. King, A. Boca, K. M. Edmondson, M. J. Romero, H. Yoon, D. C. Law, C. M. Fetzer, M. Haddad, A. Zakaria, W. Hong, S. Mesropian, D. D. Krut, G. S. Kinsey, P. Pien, R. A. Sherif, and N. H. Karam, "Raising the Efficiency Ceiling with Multijunction III-V Concentrator Photovoltaics," *Proc. 23rd European Photovoltaic Solar Energy Conference*, Valencia, Spain, Sep. 1-5, 2008

3 Receiver Package Technology Development

3.0 Introduction

Developing the reliability of the concentrator cell receiver package, also referred to as the concentrator cell assembly (CCA), under the thermally and electrically demanding operating conditions for concentrator solar cells, and reducing the significant costs associated with the receiver package, are crucial to the successful implementation of concentrator PV at the production scale of 1 GW/year or greater [19].

Some of the key results in terrestrial concentrator receiver package technology in this program include:

Demonstration of the first grid-connected application for a high-concentration system with triple-junction cells [20], together with Arizona Public Service (APS) using a robust high-concentration module built with Spectrolab's concentrator multijunction cells. This system had a nominal output power of 1 kW, also making this system at APS, built with Spectrolab multijunction concentrator cells, the first ever 1-kW grid-connected system with triple-junction solar cells.

A wide range of process parameters was explored for fabrication of the concentrator cell receiver package, or concentrator cell assembly (CCA), resulting in highly reliable performance of the cell receiver package under the severe light intensity, current conduction, and thermal conditions of normal concentrator cell operation.

Reliable performance of multijunction terrestrial concentrator solar cells in real-world, on-sun conditions was demonstrated with the 1-kW grid connected concentrator system at APS, using Spectrolab solar cells.

Steps were taken to thoroughly document production processes for Spectrolab terrestrial concentrator cells, in order to formally qualify Spectrolab terrestrial concentrator cells as a product.

High-efficiency terrestrial concentrator cells were delivered to Pyron and Amonix, as well as for the APS 1-kW system, in order to evaluate multijunction cells in these commercially important concentrator systems.

References – Section 3.0

[19] R. A. Sherif, R. R. King, N. H. Karam, and D. R. Lillington, "The Path to 1 GW of Concentrator Photovoltaics Using Multijunction Solar Cells," *Proc. 31st IEEE Photovoltaic Specialists Conf.*, Lake Buena Vista, Florida, Jan. 3-7, 2005, pp. 17-22.

[20] R. A. Sherif, S. Kusek, H. Hayden, R. R. King, H. L. Cotal, J. Peacock, M. Caraway, and N. H. Karam, "First Demonstration of Multijunction Receivers in a Grid-Connected Concentrator Module," *Proc. 31st IEEE Photovoltaic Specialists Conf.*, Lake Buena Vista, Florida, Jan. 3-7, 2005, pp. 635-638.

3.1 Receiver Development Progress Reports 1-4

3.1.1 Baseline Performance

Figure 3.1.1 shows the basic concentrator cell package that we used to obtain data on multijunction cells under high concentration. It consists of one solar cell that is soldered to a metallized ceramic substrate using a Spectrolab proprietary process that was developed to obtain a void-free solder joint. A bypass diode is also soldered to the substrate to provide protection from reverse bias in case of partial shadowing.

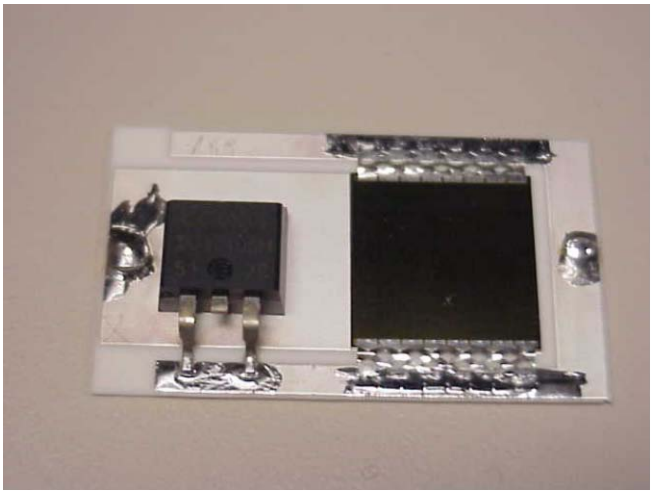

Fig. 3.1.1 A basic concentrator cell assembly (CCA).

We tested 6 cell assemblies at Spectrolab using an outdoor test station. The cells have 1cm x 1cm area, and are based on the low-band-gap (lo-Eg) GaInP top subcell technology. The test equipment is shown in Fig. 3.1.2. By changing the relative distance between lens and the cell, we obtain different concentration ratios. The cell assemblies are mounted on a cooling plate with a water chiller supplying active cooling to the cells. Light I-V data from these tests are shown in Fig. 3.1.3.

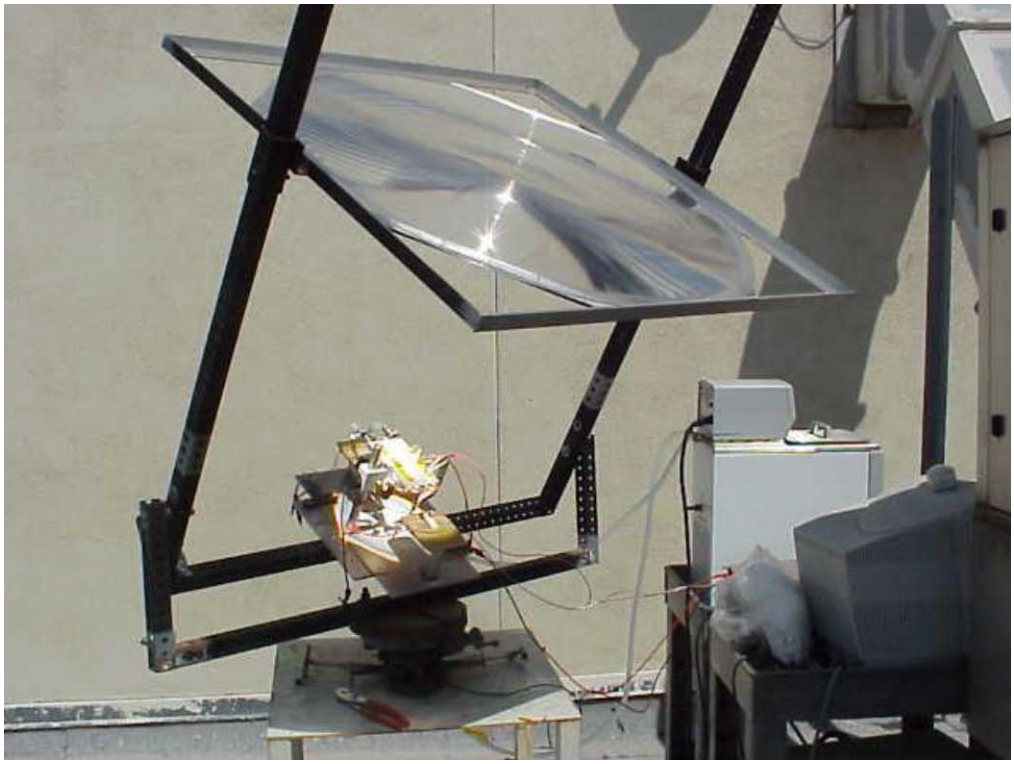

Fig. 3.1.2 Outdoor test station at Spectrolab.

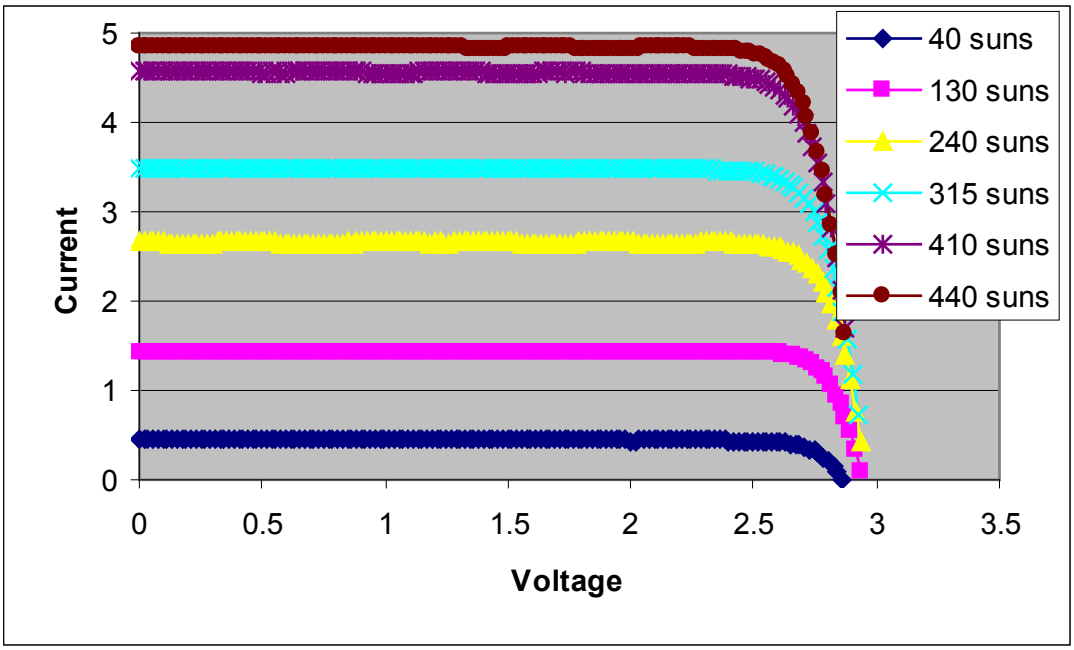

Fig. 3.1.3a Light I-V Data on 1cm x 1cm concentrator cell assemblies at Spectrolab outdoor test station.

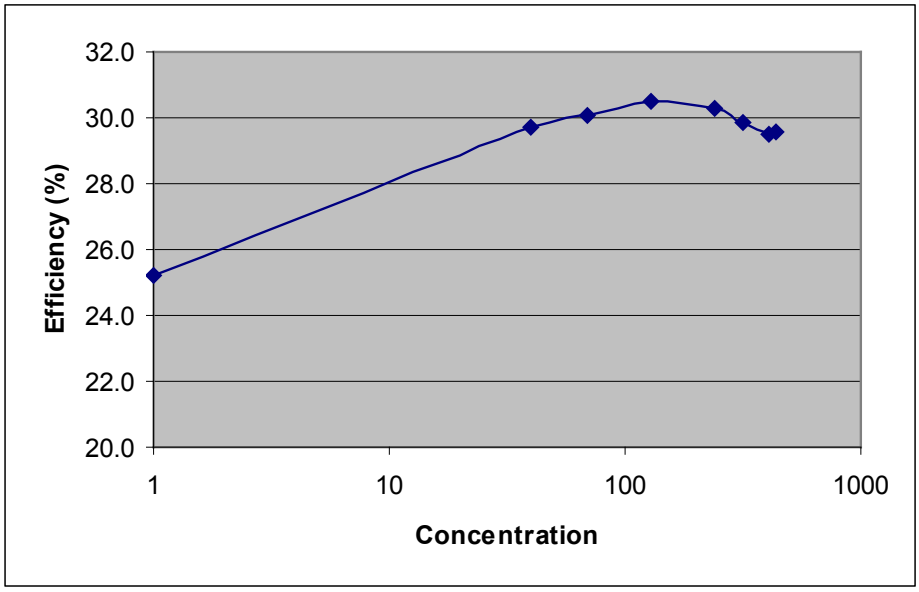

Fig. 3.1.3b Efficiency vs. concentration for 1cm x 1cm cell assemblies at Spectrolab outdoor test station.

It is interesting to note from the above data that the cells achieved their peak efficiency at concentration in the 200-sun range. These cells were designed to operate at 500-sun concentration. Also, the cells peak efficiency is just over 30%, which is far below what this cell technology has achieved in the past. At concentration >400 suns, the efficiency of the cell receiver from this particular batch of early in the course of cell and receiver development is below 30%. One reason is the effect of temperature; in this test the cells are operating at around 60-70 C at concentration in the 400-500 suns range. However, the elevated temperature does not seem to account for the full difference between expected and observed cell receiver efficiency at this stage of development.

3.1.2 Demonstrated Reliability in the Field

We worked with several customers to do a long-term high concentration test of multijunction concentrator cell receivers in the field. Of these customers, we will discuss the work with Arizona Public Service (APS) using the Concentrating Technologies (CT) micro-dish system in this report.

This work utilizes the basic assembly of Fig. 3.1.1, with a concentrator cell of 1.5cm x 1.5cm area. The concentration level received by the cells is around 450 suns and the cells are passively cooled via a heat sink attached to the back of the assembly. Figure 3.1.4 shows a picture of some of the cell assemblies receiving concentrated sunlight in the field. This system was developed over a period of 2 years and was used to test some of our triple-junction cells. Frequent interruptions were encountered early on due to electrical shorts. This was apparently caused by the thermal grease (used to bond the cell assembly and the heat sink), which would become electrically conductive when squeezed into very small gaps. This problem was addressed by using a conformal coating on the entire cell assembly. This coating provides electrical isolation even in the presence of water and moisture.

Fig. 3.1.4 Concentrator cell assemblies in the Arizona Public Service (APS) STAR facility.

At this stage in the cell receiver development, we had a complete unit of 52 cell assemblies operating in the field. The unit is connected to an inverter and is producing AC power that is feeding into the grid at the APS Solar Test and Research (STAR) facility in Tempe, Arizona. The unit was first operational on September 3, 2004, and is shown in Fig. 3.1.5. The typical AC power over a period of 3 days (September 11-13, 2004) is shown in Fig. 3.1.6a, and the corresponding irradiance and ambient temperature are shown in Fig. 3.1.6b.

Fig. 3.1.5 A prototype of a high concentration module at the APS STAR facility using triple-junction concentrator solar cells. This system was the first grid-connected solar concentrator system using triple-junction cells.

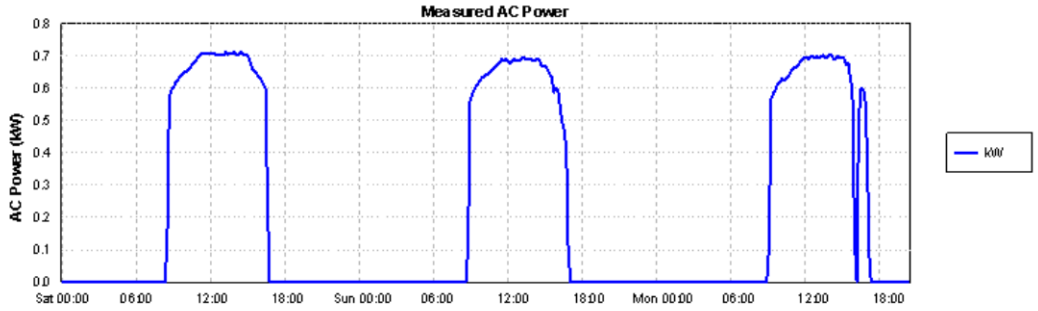

Fig. 3.1.6a Output of the system (AC power) over a 3-day period September 11-13, 2004.

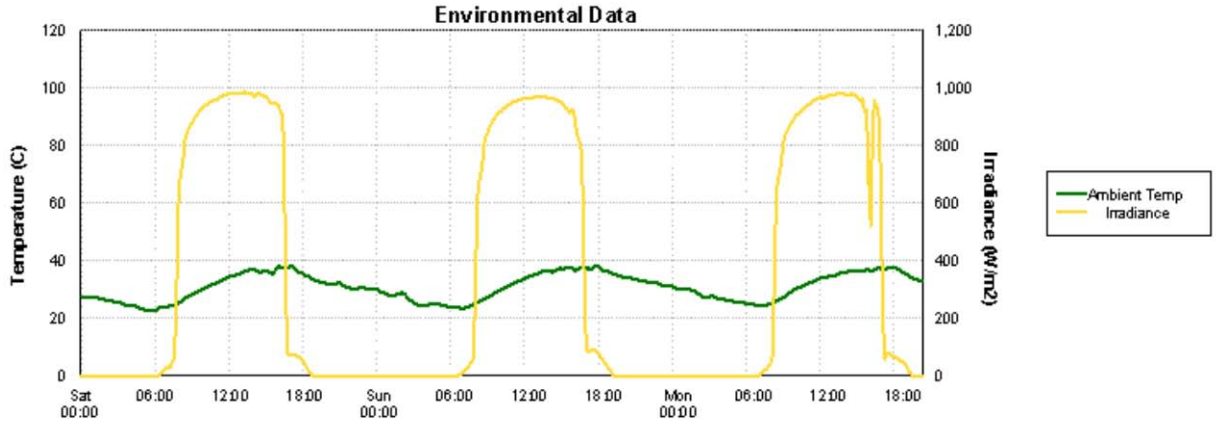

Fig. 3.1.6b Corresponding irradiance and ambient temperature for September 11-13, 2004.

The system of 52 cells is composed of two strings; each string consists of 26 cells in series and the two strings are connected in parallel. The performance of each string is shown in Fig. 3.1.7.

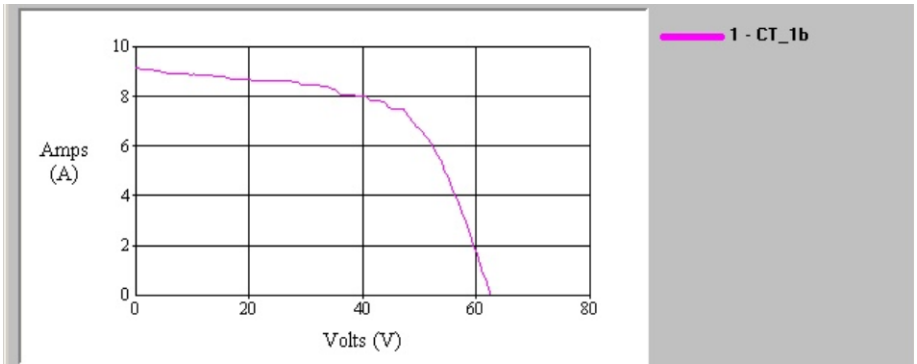

	Curve Name	Ppk	Fill Fact	Temp. #1	Voc	Isc
1	CT_1b	352.26	62	46.5	62.402	9.111

Fig. 3.1.7a Performance (DC power) of String #1 in the Concentrating Technologies (CT) unit.

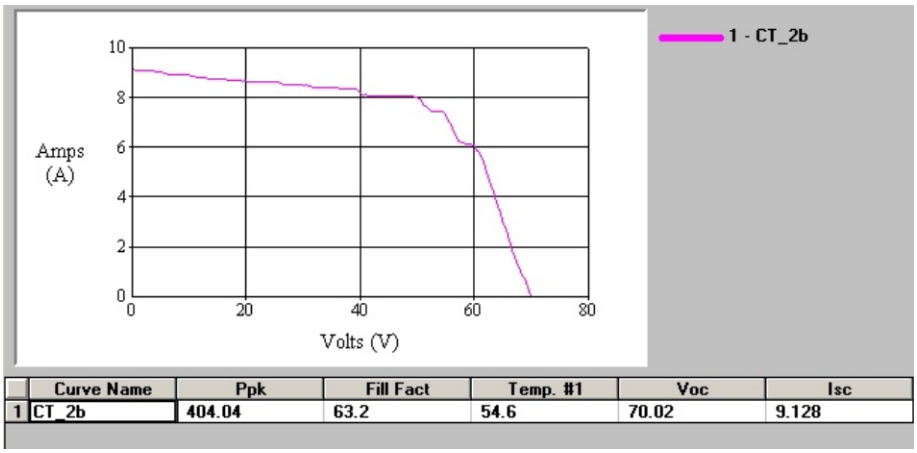

	Curve Name	Ppk	Fill Fact	Temp. #1	Voc	Isc
1	CT_2b	404.04	63.2	54.6	70.02	9.128

Fig. 3.1.7b Performance (DC power) of String #2 in the CT unit.

The I-V curves of both strings show that there is a large level of mismatch in each string. This is attributed mainly to the fact that the cells in the strings are getting different levels of flux (optical non-uniformity). Also, note that String 1 is about 8V less (in terms of open-circuit voltage) than String 2. This means that there are 3 cells in String 1 that are not active.

This is the first demonstration of a robust high concentration module using Spectrolab's multijunction cells. This is also the first ever grid-connected application for a high-concentration system with triple-junction cells [20].

In subsequent months, we populate the array with more triple-junction concentrator cells to increase the system output from 0.7 kW to 1 kW of AC power, to form the first 1 kW grid-connected concentrator system using triple-junction concentrator cells.

This system, though not optimized, was used to collect as much reliability data as possible. The intention was to show how much degradation to the cells will occur during their operation under continuous illumination, with real-world exposure to ultraviolet (UV) light, temperature cycling, and temperature/humidity.

3.1.3 Pyron Module

We provided Pyron with 110 cells assembled on their conduit to integrate into their modules. At this stage of development, Pyron had a module up and running and were collecting data on the performance. In the course of this work, however, they are learning a few things about their module. As such, they learned that the adhesive they used to connect the secondary optics to the solar cells did not have the required strength as the parts were exposed to temperature cycles during its operation in the field. Unfortunately, they lost about 60 cells because of that. Their corrective action was to use a primer to strengthen the adhesion. Preliminary data suggest this is working better. We decided to provide them with reject cells or mechanical cells to experiment with before providing them with replacement cells with good efficiency.

Some data on the cell assemblies operating in the field are shown below in Fig. 3.1.8. Additional data was collected on the module.

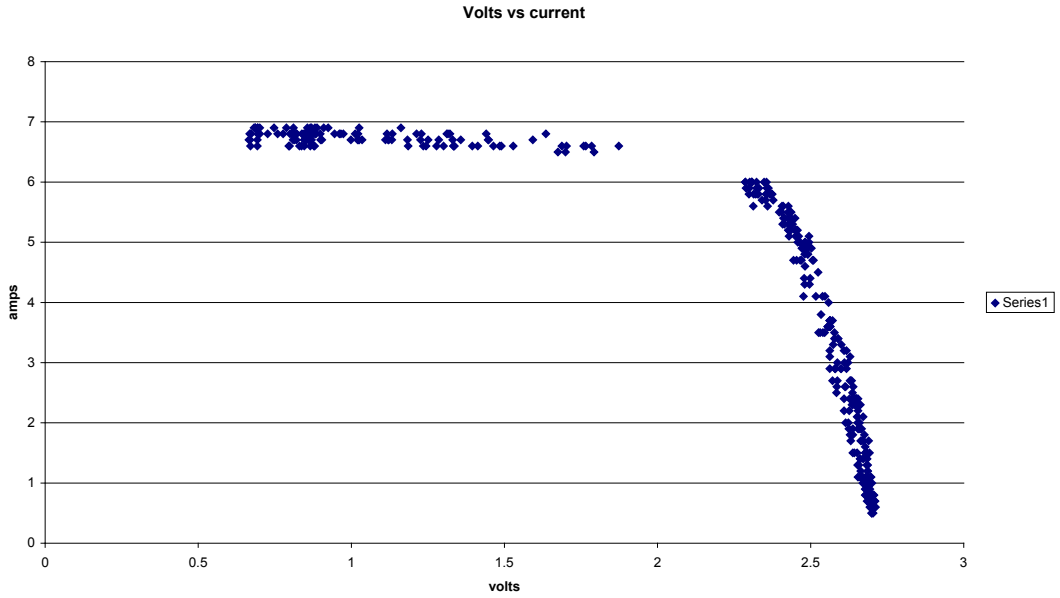

Fig. 3.1.8 Light I-V curve of one cell in the Pyron module.

Additionally, we delivered 21 cells to Pyron assembled on a new substrate (conduit) that they have re-designed. The cells are divided equally between different 3 J-ratios. Pyron is to test the cells in strings of 5 cells, trying to assess the performance difference between the different J-ratios in their system.

3.1.4 Characterization of Concentrator Receivers with Several Cell Sizes

We have fabricated different cell sizes for evaluation under different levels of concentration. Part of the NREL/Spectrolab HiPerf PV program calls for testing of our concentrator cells using different concentrator modules. For this, we have worked with Amonix to test some of our concentrator cells that have 1 cm x 1 cm aperture area.

Earlier, Amonix assembled cells of this type in their test set-up and measured the performance of the cells at concentration in the range of 500 suns. They have reported some good results on most cells, but later they reported that some cells shunted very rapidly under concentration. As we have demonstrated in Phase 1A of the HiPerf PV program, cell shunting is closely tied to the way the cells are packaged. We assembled 10 cells on Amonix substrates, 5 cells with conformal coating and 5 without. We tested all cells on the High Intensity Pulsed Solar Simulator (HIPSS) with none of the 10 cells showing any signs of shunting. A typical light I-V curve is for one of these assemblies is shown in Fig. 3.1.9. The 10 parts were shipped to Amonix for their evaluation. If the data looks good at Amonix, we will provide Amonix with enough solar cells to populate one full plate.

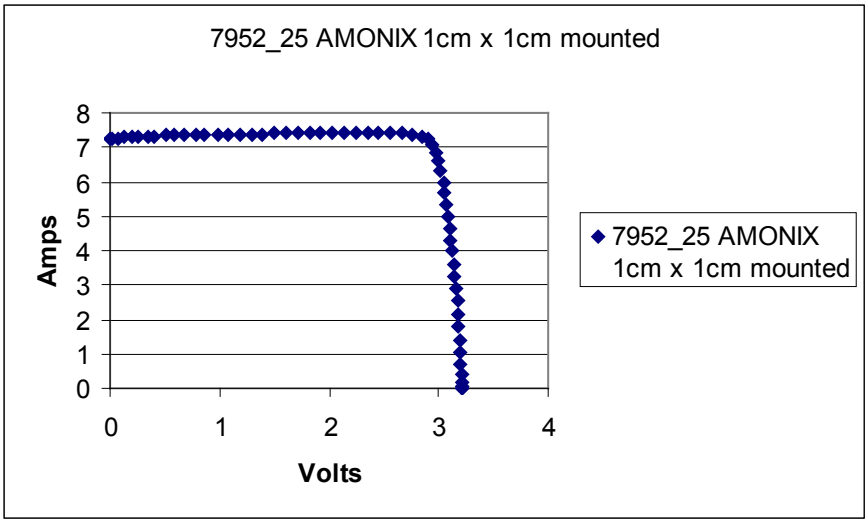

Fig. 3.1.9 Light I-V curve of a typical 1cm x 1cm cell, assembled on an Amonix substrate, and tested at Spectrolab.

To reduce concentrator cell area, thereby reducing cell cost, it is interesting to consider operation of solar cells at ultra-high incident intensities. In the regime of ultra-high concentration for solar cells (above 1000 suns) a key challenge is thermal management. At these concentration levels, cell areas need to be reduced to a few mm^2 rather than the cm^2 range. Figure 3.1.10 shows the results of a 3-dimensional finite element model to project the cell operating temperature in the ultra-high concentration regime. In this model, we assumed that the cells are soldered directly to a copper heat spreader, which is practical from the perspective of coefficient of thermal expansion (CTE) mismatch between cell (mostly Ge) and copper, given that the cells are very small.

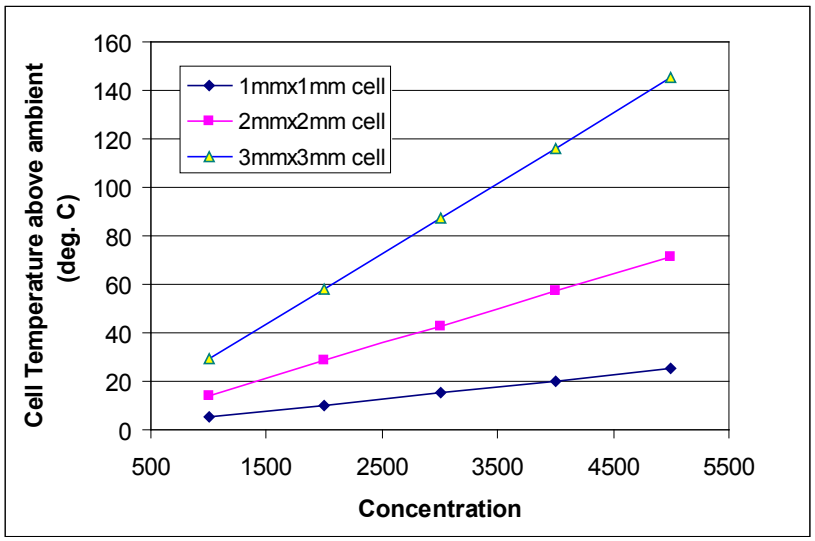

Fig. 3.1.10 Temperature projections for 3J cells in the ultra-high concentration regime.

The data in Fig. 3.1.10 suggest that reasonable operating cell temperatures are possible with concentration around 3000X, as long as the cell area is maintained below 4 mm^2. The EC-01 mask set and EC-01 build have cells that are 1 mm^2 and 4 mm^2 in area, in order to test the thermal properties under operation and series resistance performance of these small-area cells under ultra-high concentration.

References – Section 3.1

[20] R. A. Sherif, S. Kusek, H. Hayden, R. R. King, H. L. Cotal, J. Peacock, M. Caraway, and N. H. Karam, "First Demonstration of Multijunction Receivers in a Grid-Connected Concentrator Module," *Proc. 31st IEEE Photovoltaic Specialists Conf.*, Lake Buena Vista, Florida, Jan. 3-7, 2005, pp. 635-638.

3.2 Receiver Development Progress Reports 5-8

3.2.1 Qualification Plan for Terrestrial Concentrator Cells and Receivers

In Year 2 of this program, we shifted our attention to developing a qualification plan for commercial concentrator cells and receivers. The plan will follow the Concentrator Receiver & Module Qualification document that has been in the works for the last several years, led by NREL with participation from various university and industry groups (including Spectrolab). The objectives of the qualification tests will be to identify the projected performance degradation of MJ cells in concentrator modules. We believe that this will be one of the biggest issues facing commercialization of CPV modules.

In order to follow a structured qualification test program, it is necessary to freeze the concentrator cell and receiver design. We elected to consider two types of epitaxial structures. The first will be referred to as CITJ (which stands for Concentrator Improved Triple Junction). The second structure will be referred to as CUTJ (which stands for Concentrator Ultra Triple Junction). Both used lattice-matched structures, as we believe the metamorphic cells are not yet ready to go through qualification tests. The CITJ cells have a lower band gap (lo-Eg) top subcell. CITJ cells should have lower efficiency, but also will have less expensive epitaxial growth. Accordingly they are targeted for cost-performance applications (typical for on-grid application, *e.g.*, utility-scale electricity production). The CUTJ cells will be higher in performance, aimed at applications where a 1% absolute increase in cell efficiency is leveraging for system cost reduction (typical for off-grid, distributed energy markets). It is worthwhile mentioning that most of our experience, in terms of outdoor tests, has been obtained with the CITJ cells. Hence, these will be the first ones to go through qualification tests.

Once the epi structure is defined, the next step is to define the cell size. We have several cell sizes to choose from. These cell sizes were defined as part of our commercialization plans. They include cells as small as 1 mm^2 in area, to cells as large as 2.25 cm^2. In the subsequent test plans, we will focus on a cell size that is 1 cm^2, a popular size for most systems.

With this cell size in mind, we have re-designed our so-called CDO 1 x 1 (which stands for Concentrator Dual Ohmic 1 cm x 1 cm aperture area), shown in Fig. 3.2.1. We have fabricated about 1000 cells using CITJ wafers. These cells have been tested at 1 sun and are currently pending tests under concentrated sunlight using the High Intensity Pulsed Solar Simulator (HIPSS). We have also re-designed the ceramic substrate for use with this cell size in the concentrator cell receiver, or concentrator cell assembly (CCA).

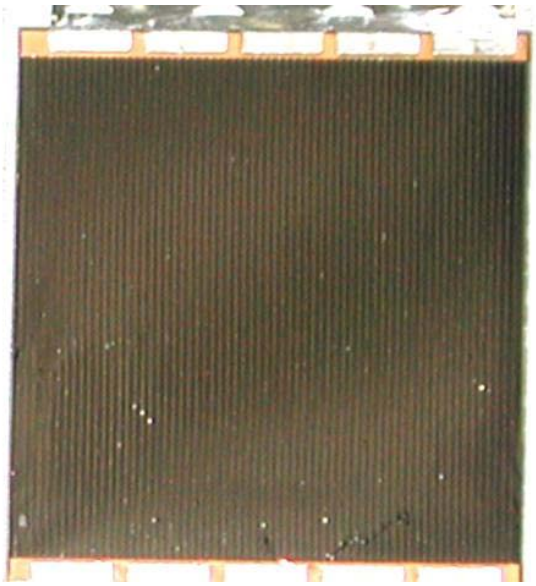

Fig. 3.2.1 CDO 1 x 1 cell with optimized metallization (<7% aperture coverage).

3.2.2 Deliveries of Cell Assemblies

As recent terrestrial multijunction concentrator cell efficiency has increased to 39.0%, approaching the 40%-efficiency mark, interest in commercializing these cells has grown considerably. As part of the NREL HiPerf PV program, a number of cell assemblies have been delivered to customers for evaluation and field testing in prototype multijunction concentrator systems. The resulting field performance data will be useful in determining whether further optimization of the cell, cell assembly, or concentrator system is required. Valuable information on the robustness of the current designs under variable environmental conditions (such as humidity and air mass) will be acquired.

In December 2005, fifty (50) bare, 1 x 1 cm^2 concentrator cells were tested and delivered to Amonix. An additional fifty (50) cells with welded interconnects were tested and delivered in the first quarter of 2006. These cells will contribute to the determination as to whether multijunction cells will be viable in replacing silicon cells on the Amonix MegaModule system.

During the first quarter of 2006, two-hundred and fifty-eight (258) 1.5 x 1.5 cm^2 cells were delivered to Pyron. These cells were assembled on copper heat sinks provided by Pyron, as shown in Fig. 3.2.2.

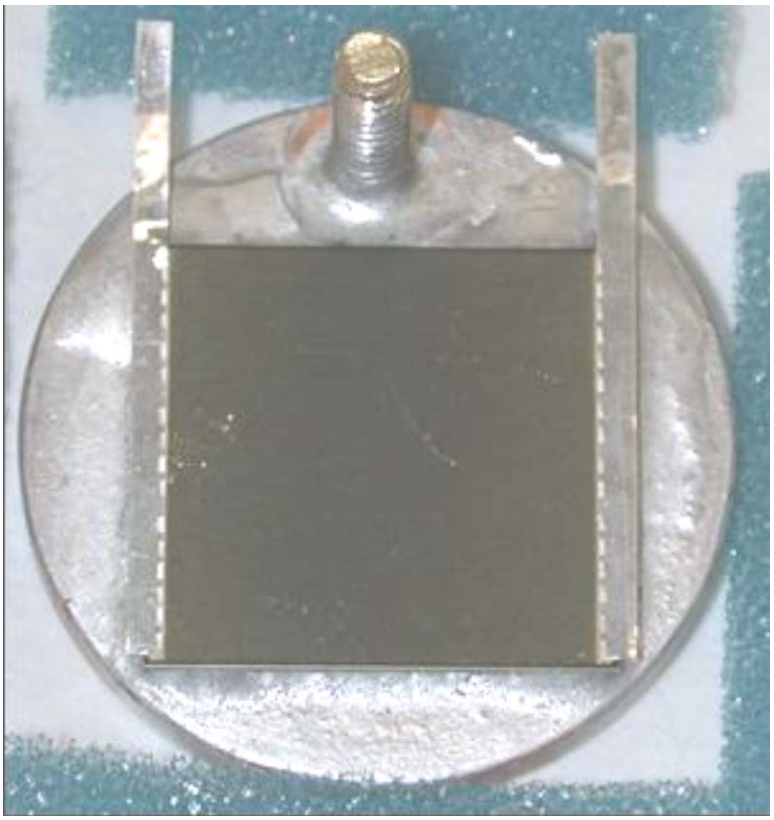

Fig. 3.2.2 1.5 x 1.5 cm^2 concentrator cell assembly (CCA) on a Pyron heat sink.

4 Summary

As described above, some of the key results in terrestrial concentrator cell technology in this program include:

A major program milestone, demonstration of solar cells with 41% efficiency, was met with the attainment of 40.7% conversion efficiency in a Spectrolab experimental metamorphic terrestrial concentrator cell in 2006. As described in King et al., *Appl. Phys. Lett.*, 2007 [1], this was the first solar cell of any type to reach over the 40% efficiency milestone. This efficiency result was independently confirmed as a world record by NREL.

Spectrolab received the R&D 100 Award for 2007, for its development of the metamorphic multijunction solar cell described in the last paragraph with up to 40.7% efficiency, in the High Performance Photovoltaics (HiPerf PV) program funded by NREL. NREL kindly nominated Spectrolab for the award.

Near the same time as the 40.7% metamorphic multijunction cell result was achieved, an experimental lattice-matched 3-junction terrestrial concentrator cell with 40.1% efficiency [1] was also produced by Spectrolab in the HiPerf PV program, a record for lattice-matched photovoltaic cells. This 40.1%-efficient lattice matched cell result was independently confirmed at NREL. Thus, although metamorphic multijunction cells have the highest efficiencies to date, lattice-matched cells are close behind. Another experimental metamorphic 3-junction cell produced by Spectrolab also reached 40.1% efficiency [18], as independently confirmed at NREL.

Prior to the 40.7% metamorphic and 40.1% lattice-matched record multijunction cell efficiencies above, Spectrolab achieved record cell efficiencies with 39.0% lattice-matched and 38.8% metamorphic 3-junction concentrator cells [4] in the NREL HiPerf PV program, which in turn broke the previous record efficiencies, also held by Spectrolab and established in the HiPerf PV program, for 37.3% lattice-matched and 36.9% metamorphic concentrator cells [2], which broke the still earlier Spectrolab record efficiency of 35.2% for a lattice-matched terrestrial concentrator cell [3]. Thus Spectrolab's work in the NREL HiPerf PV program was responsible for a high rate of advancement of the state-of-the-art in photovoltaic cell efficiency, sustained over many years, leading to the dominance of III-V multijunction cell technology in concentrator PV systems today, and contributing significantly to the rapid rise of the concentrator PV industry in recent years.

The efficiency benefits of high-band-gap, disordered GaInP top cells and wide-band-gap tunnel junctions under the terrestrial solar spectrum at high concentration were developed and demonstrated by Spectrolab in Phase 1A of the HiPerf PV program, for both metamorphic and lattice-matched 3-junction terrestrial concentrator cells, enabling the efficiency advances described above.

A large range of concentrator cell parameters were evaluated experimentally in multiple cell builds, including:

- differing types of wide-band-gap tunnel junctions
- different top subcell band gaps, and GaInP top subcell group-III sublattice disordering
- amount of current mismatch or J-ratio
- amount of lattice mismatch in metamorphic cells
- layer structure to reduce dislocation density in active cell regions resulting from the metamorphic buffer
- layer structure to result in high peak tunneling current density in tunnel junctions for high light intensities
- growth parameters in the metamorphic buffer layers
- subcell doping levels and doping profiles
- AR coating type
- gridline spacing and grid configuration
- gridline width and gridline definition process
- concentrator cell size, and
- other semiconductor device design parameters

contributing to the high experimental concentrator cell efficiencies achieved in the program.

A general multijunction solar cell modeling program was developed to calculate efficiency of cells with up to 10 subcells as a function of subcell band gap, concentration ratio, cell temperature, and other parameters [7]. The ideal efficiency limited by radiative recombination can be calculated, as well as efficiency including the effects of series resistance and metal grid shadowing, and the efficiency normalized to experimental concentrator cell results.

Four-junction (4J) terrestrial concentrator cells were modeled to determine the predicted efficiency as a function of subcell band gap, and 4J GaInP/ AlGaInAs/ GaInAs/ Ge concentrator cells were built and tested with efficiencies up to 35.7% in early prototype cells [7].

The energy production values of 3J, 4J, 5J, and 6J terrestrial concentrator cells were modeled and contrasted for varying sun angle over the course of the day, and for varying current balance among subcells in high-voltage, low-current device designs [7].

A large cell build was carried out incorporating high-efficiency cell structures (HECS) in lattice-matched as well as metamorphic multijunction cells, comparing the effects of HECS and metamorphic materials in high-efficiency terrestrial concentrator 3- and 4-junction cells.

Upright metamorphic GaInAs subcells were grown and characterized in terms of their band-gap-voltage offset, $(E_g/q) - V_{oc}$, with lattice mismatch to the Ge substrate up to 1.6% for 23%-In GaInAs with 1.1-eV band gap.

Inverted metamorphic (IMM) GaInAs subcells were grown and characterized in terms of band-gap-voltage offset, and by cathodoluminescence and electron-beam-induced current (EBIC) measurements, out to a high lattice mismatch of 3.1% with respect to Ge for 44%-In

GaInAs, with a band gap of 0.84 eV [17]. The dislocation density and recombination activity at a single dislocation was characterized as a function of subcell composition and lattice mismatch [17].

Inverted lattice-matched (ILM) cells such as inverted GaInP and inverted 1%-In GaInAs cells were grown and characterized, for incorporation into inverted metamorphic terrestrial concentrator multijunction cells.

Inverted metamorphic (IMM) GaInP/ 1%-In GaInAs/ 30%-In GaInAs 3-junction terrestrial concentrator cells were grown and processed, with tunnel junctions working well at over 80 suns for early prototype devices.

Single-junction component cells of high-efficiency 3-junction concentrator cells were built and tested at Spectrolab, representing a wide range of J-ratios for optimizing performance under fresnel lenses in actual field operating conditions. These single-junction component cells (also called "isotype" cells) were delivered June 19, 2008, for field testing at Amonix in their fresnel lens concentrator system, satisfying the deliverable associated with Task 30 of the revised statement of work for Spectrolab's HiPerf PV program with NREL.

High-efficiency 3-junction terrestrial concentrator cells were built and tested at Spectrolab, targeting improved efficiency and energy production under real-world operating conditions in the field in fresnel lens concentrator PV systems. Fifty (50) of these cells were delivered August 21, 2008, for field testing at Amonix in their fresnel lens concentrator system, satisfying the deliverable D3.7 associated with Task 31 of the revised statement of work for Spectrolab's HiPerf PV program with NREL. These high-efficiency Spectrolab cells have since been incorporated into a high-efficiency fresnel lens demonstration module by Amonix, for testing at NREL.

Some of the key results in terrestrial concentrator receiver package technology in this program include:

Demonstration of the first grid-connected application for a high-concentration system with triple-junction cells [20], together with Arizona Public Service (APS) using a robust high-concentration module built with Spectrolab’s concentrator multijunction cells. This system had a nominal output power of 1 kW, also making this system at APS, built with Spectrolab multijunction concentrator cells, the first ever 1-kW grid-connected system with triple-junction solar cells.

A wide range of process parameters was explored for fabrication of the concentrator cell receiver package, or concentrator cell assembly (CCA), resulting in highly reliable performance of the cell receiver package under the severe light intensity, current conduction, and thermal conditions of normal concentrator cell operation.

Reliable performance of multijunction terrestrial concentrator solar cells in real-world, on-sun conditions was demonstrated with the 1-kW grid connected concentrator system at APS, using Spectrolab solar cells.

Steps were taken to thoroughly document production processes for Spectrolab terrestrial concentrator cells, in order to formally qualify Spectrolab terrestrial concentrator cells as a product.

High-efficiency terrestrial concentrator cells were delivered to Pyron and Amonix, as well as for the APS 1-kW system, in order to evaluate multijunction cells in these commercially important concentrator systems.

These concentrator solar cell technology advances have taken terrestrial concentrator cell performance to new heights, resulting in the first solar cells of any kind to reach over the milestone efficiency of 40%. The research in this program has resulted in new understanding of concentrator solar cell design, and exploration of new architectures for terrestrial concentrator cells. Work in this program on the concentrator cell receiver package and concentrator PV system manufacturers has helped to establish high-efficiency terrestrial concentrator cell processes for mass production, and for implementation in commercial concentrator PV systems. The pioneering concentrator cell and receiver package advances in the Spectrolab/NREL High Performance Photovoltaics (HiPerf PV) program have led directly to the widespread acceptance of high-efficiency III-V multijunction cells as the dominant cell type in concentrator PV. The high efficiencies of terrestrial concentrator solar cells demonstrated in the HiPerf PV program have served as a catalyst for the explosive growth enjoyed by the concentrator PV industry over recent years, and have helped to pave the way to cost-effective solar electricity generation using concentrator photovoltaics.

5 References

[1] R. R. King, D. C. Law, K. M. Edmondson, C. M. Fetzer, G. S. Kinsey, H. Yoon, R. A. Sherif, and N. H. Karam, "40% efficient metamorphic GaInP / GaInAs / Ge multijunction solar cells," *Appl. Phys. Lett.*, Vol. 90, No. 18, 183516, 4 May 2007.

[2] R. R. King, C. M. Fetzer, K. M. Edmondson, D. C. Law, P. C. Colter, H. L. Cotal, R. A. Sherif, H. Yoon, T. Isshiki, D. D. Krut, G. S. Kinsey, J. H. Ermer, Sarah Kurtz, T. Moriarty, J. Kiehl, K. Emery, W. K. Metzger, R. K. Ahrenkiel, and N. H. Karam, "Metamorphic III-V Materials, Sublattice Disorder, and Multijunction Solar Cell Approaches with Over 37% Efficiency," *Proc. 19th European Photovoltaic Solar Energy Conference*, Paris, France, June 7-11, 2004 (WIP-Munich, Munich, Germany, 2004), ISBN 3-936-338-14-0, ISBN 88-89407-02-6, pp. 3587-93.

[3] R. R. King, C. M. Fetzer, P. C. Colter, K. M. Edmondson, D. C. Law, A. P. Stavrides, H. Yoon, G. S. Kinsey, H. L. Cotal, J. H. Ermer, R. A. Sherif, K. Emery, W. Metzger, R. K. Ahrenkiel, and N. H. Karam, "Lattice-Matched and Metamorphic GaInP/ GaInAs/ Ge Concentrator Solar Cells," *Proc. of the 3rd World Conference on Photovoltaic Energy Conversion*, Osaka, Japan, May 11-18, 2003, pp. 622-625.

[4] R. R. King, D. C. Law, C. M. Fetzer, R. A. Sherif, K. M. Edmondson, S. Kurtz, G. S. Kinsey, H. L. Cotal, D. D. Krut, J. H. Ermer, and N. H. Karam, "Pathways to 40%-Efficient Concentrator Photovoltaics," *Proc. 20th European Photovoltaic Solar Energy Conf.*, Barcelona, Spain, June 6-10, 2005, pp. 118-123.

[5] R. R. King, C. M. Fetzer, P. C. Colter, K. M. Edmondson, J. H. Ermer, H. L. Cotal, H. Yoon, A. P. Stavrides, G. Kinsey, D. D. Krut, N. H. Karam, "High-Efficiency Space and Terrestrial Multijunction Solar Cells Through Bandgap Control in Cell Structures," *Proc. 29th IEEE Photovoltaic Specialists Conf.*, New Orleans, Louisiana, May 20-24, 2002 (IEEE, New York, 2002), ISBN 0-7803-7471-1, pp. 776-781.

[6] R. R. King, P. C. Colter, D. E. Joslin, K. M. Edmondson, D. D. Krut, N. H. Karam, and Sarah Kurtz, "High-Voltage, Low-Current GaInP/GaInP/GaAs/GaInNAs/Ge Solar Cells," *Proc. 29th IEEE Photovoltaic Specialists Conf.*, New Orleans, Louisiana, May 20-24, 2002, pp. 852-855.

[7] R. R. King, R. A. Sherif, D. C. Law, J. T. Yen, M. Haddad, C. M. Fetzer, K. M. Edmondson, G. S. Kinsey, H. Yoon, M. Joshi, S. Mesropian, H. L. Cotal, D. D. Krut, J. H. Ermer, and N. H. Karam, "New Horizons in III-V Multijunction Terrestrial Concentrator Cell Research," *Proc. 21st European Photovoltaic Solar Energy Conference and Exhibition*, Dresden, Germany, Sep. 4-8, 2006 (Munich, WIP-Renewable Energies, 2006) (ISBN: 3-936338-20-5), pp. 124-128.

[8] R. K. Ahrenkiel, "Minority-Carrier Lifetime in III-V Semiconductors," Chap. 2, in *Semiconductors and Semimetals*, Vol. 39, Eds. R. K. Willardson, A. C. Beer, E. R. Weber (Academic Press, New York, 1993).

[9] R. N. Hall, *Proc. Inst. Elect. Eng.*, 106B, Suppl. 17, 983 (1960).

[10] S. Adachi, *GaAs and Related Materials*, (World Scientific, River Edge, NJ, 1994).

[11] F. Dimroth, U. Schubert, and A. W. Bett, "25.5% Efficient Ga0.35In0.65P/Ga0.83In0.17As Tandem Solar Cells Grown on GaAs Substrates," *IEEE Electron Device Lett.*, 21, p. 209 (2000).

[12] R. R. King et al., "Metamorphic GaInP/GaInAs/Ge Solar Cells," *Proc. 28th IEEE Photovoltaic Specialists Conf. (PVSC)*, Sep. 15-22, 2000, Anchorage, Alaska, pp. 982-985.

[13] M. W. Wanlass et al., "Lattice-Mismatched Approaches for High-Performance, III-V, Photovoltaic Energy Converters," *Proc. 31st IEEE PVSC*, Lake Buena Vista, Florida, Jan. 3-7, 2005, p. 530.

[14] M. W. Wanlass et al., "Advanced High-Efficiency Concentrator Tandem Solar Cells," *Proc. 22nd IEEE PVSC*, 1991, p. 38.

[15] R. R. King, D. C. Law, K. M. Edmondson, C. M. Fetzer, G. S. Kinsey, D. D. Krut, J. H. Ermer, R. A. Sherif, and N. H. Karam, "Metamorphic Concentrator Solar Cells with Over 40% Conversion Efficiency," *Proc. 4th International Conference on Solar Concentrators (ICSC-4)*, El Escorial, Spain, March 12-16, 2007 (ISBN: 978-84-690-6463-4), pp. 5-8.

[16] Richard R. King, Daniel C. Law, Kenneth M. Edmondson, Christopher M. Fetzer, Geoffrey S. Kinsey, Hojun Yoon, Dimitri D. Krut, James H. Ermer, Raed A. Sherif, and Nasser H. Karam, "Advances in High-Efficiency III-V Multijunction Solar Cells," *Advances in OptoElectronics*, Vol. 2007, Article ID 29523, 8 pages, doi:10.1155/2007/29523.

[17] R. R. King, A. Boca, K. M. Edmondson, M. J. Romero, H. Yoon, D. C. Law, C. M. Fetzer, M. Haddad, A. Zakaria, W. Hong, S. Mesropian, D. D. Krut, G. S. Kinsey, P. Pien, R. A. Sherif, and N. H. Karam, "Raising the Efficiency Ceiling with Multijunction III-V Concentrator Photovoltaics," *Proc. 23rd European Photovoltaic Solar Energy Conference*, Valencia, Spain, Sep. 1-5, 2008.

[18] R. R. King, D. C. Law, K. M. Edmondson, C. M. Fetzer, G. S. Kinsey, H. Yoon, R. A. Sherif, D. D. Krut, J. H. Ermer, P. Hebert, P. Pien, and N. H. Karam, "Multijunction Solar Cells with Over 40% Efficiency and Future Directions in Concentrator PV," *Proc. 22nd European Photovoltaic Solar Energy Conference*, Milan, Italy, Sep. 3-7, 2007, pp. 11-15.

[19] R. A. Sherif, R. R. King, N. H. Karam, and D. R. Lillington, "The Path to 1 GW of Concentrator Photovoltaics Using Multijunction Solar Cells," *Proc. 31st IEEE Photovoltaic Specialists Conf.*, Lake Buena Vista, Florida, Jan. 3-7, 2005, pp. 17-22.

[20] R. A. Sherif, S. Kusek, H. Hayden, R. R. King, H. L. Cotal, J. Peacock, M. Caraway, and N. H. Karam, "First Demonstration of Multijunction Receivers in a Grid-Connected Concentrator Module," *Proc. 31st IEEE Photovoltaic Specialists Conf.*, Lake Buena Vista, Florida, Jan. 3-7, 2005, pp. 635-638.

Acknowledgements

Spectrolab would like to thank Martha Symko-Davies, Bob McConnell, and Fannie Posey-Eddy at NREL for their leadership and encouragement as NREL Technical Monitors over the course of the HiPerf PV program at Spectrolab. A special acknowledgement is due to Martha Symko-Davies for her vision and energy in her role to launch the HiPerf PV program, and to make sure that high-efficiency concentrator PV research was an important part of the NREL HiPerf PV research portfolio. Raed Sherif did an excellent and inspired job as Program Manager and co-PI responsible for receiver package development in the crucial first years of the NREL HiPerf PV program, and we are grateful for all his contributions. We would like to thank the many people who worked hard to make the NREL HiPerf PV program a success over the years, including Keith Emery, James Kiehl, Tom Moriarty, and Manuel Romero at NREL, Yolanda Aguirre, Kent Barbour, Andreea Boca, Hector Cotal, Ken Edmondson, Chris Fetzer, Dennis Garcia, Moran Haddad, William Hong, Taka Isshiki, Monali Joshi, Mayk Kalachian, Nasser Karam, Geoff Kinsey, Dimitri Krut, Ed Labios, Daniel Law, Phat Le, Andrey Masalykin, Shoghig Mesropian, Hung Nguyen, Mark Takahashi, Dorothea Taylor, Steve Wallace, and Hojun Yoon at Spectrolab.

REPORT DOCUMENTATION PAGE

Form Approved
OMB No. 0704-0188

PLEASE DO NOT RETURN YOUR FORM TO THE ABOVE ORGANIZATION.

1. REPORT DATE *(DD-MM-YYYY)*	2. REPORT TYPE	3. DATES COVERED *(From - To)*
March 2010	Subcontract Report	05/13/05 - 12/10/08

4. TITLE AND SUBTITLE
Ultra-High-Efficiency Multijunction Cell and Receiver Module, Phase 1B: High Performance PV Exploring and Accelerating Ultimate Pathways

5a. CONTRACT NUMBER
DE-AC36-08-GO28308

5b. GRANT NUMBER

5c. PROGRAM ELEMENT NUMBER

6. AUTHOR(S)
R.R. King

5d. PROJECT NUMBER
NREL/SR-520-47602

5e. TASK NUMBER
PVA7.2001

5f. WORK UNIT NUMBER

7. PERFORMING ORGANIZATION NAME(S) AND ADDRESS(ES)
Spectrolab, Inc
12500 Gladstone Avenue
Sylmar, CA 91342

8. PERFORMING ORGANIZATION REPORT NUMBER
ZAT-4-33624-12

9. SPONSORING/MONITORING AGENCY NAME(S) AND ADDRESS(ES)
National Renewable Energy Laboratory
1617 Cole Blvd.
Golden, CO 80401-3393

10. SPONSOR/MONITOR'S ACRONYM(S)
NREL

11. SPONSORING/MONITORING AGENCY REPORT NUMBER
NREL/SR-520-47602

12. DISTRIBUTION AVAILABILITY STATEMENT
National Technical Information Service
U.S. Department of Commerce
5285 Port Royal Road
Springfield, VA 22161

13. SUPPLEMENTARY NOTES
NREL Technical Monitor: Fannie Eddy

14. ABSTRACT *(Maximum 200 Words)*

Spectrolab's High Performance Photovoltaics research program spanned seven years (August 2001 through December 2008) and was the main pathfinder research program for developing high-efficiency terrestrial concentrator solar cells and receivers at Spectrolab for many years when the efficiency and cost potential of these new types of cells were far from certain. The Spectrolab program was designed to achieve two primary objective in concentrator PV research and development: (1) to develop ultra-high-efficiency concentrator multijunction cells, in recognition of the tremendous leveraging effect that cell efficiency has on all area-related costs of the overall concentrator PV system; and (2) to develop a robust concentrator cell receiver package, enabling the reliable operation of concentrator cells in high-concentration modules.

15. SUBJECT TERMS
PV; HiPerf PV Program; concentrator solar cells; CPV; terrestrial PV; ultra-high efficiency; multijunction solar cell; cell receiver package; reliability; low cost

16. SECURITY CLASSIFICATION OF:			17. LIMITATION OF ABSTRACT	18. NUMBER OF PAGES	19a. NAME OF RESPONSIBLE PERSON
a. REPORT	b. ABSTRACT	c. THIS PAGE			
Unclassified	Unclassified	Unclassified	UL		19b. TELEPHONE NUMBER (*Include area code*)

Standard Form 298 (Rev. 8/98)
Prescribed by ANSI Std. Z39.18

F1146-E(10/2008)